Characterizing the transport of hydrocarbon contaminants in peat soils and peatlands

by

Behrad Gharedaghloo

A thesis
presented to the University of Waterloo
in fulfillment of the
thesis requirement for the degree of
Doctor of Philosophy
In
Geography (water)

Waterloo, Ontario, Canada, 2018

© Behrad Gharedaghloo

Examining Committee Membership

The following served on the Examining Committee for this thesis. The decision of the Examining Committee is by majority vote.

External Examiner	Dr. James Smith Professor, McMaster University
Supervisor(s)	Dr. Jonathan Price Professor, University of Waterloo
Internal Member	Dr. Maria Strack Associate Professor, University of Waterloo
Internal-external Member	Dr. Neil Thomson Professor, University of Waterloo
Other Member(s)	Dr. William Quinton Professor, University of Wilfrid Laurier

Author's Declaration

This thesis consists of material all of which I authored or co-authored: see Statement of Contributions included in the thesis. This is a true copy of the thesis, including any required final revisions, as accepted by my examiners.

I understand that my thesis may be made electronically available to the public

Statement of Contributions

This thesis is structured in accordance with the manuscript option.

Chapter two has been published as:

Gharedaghloo, B., & Price, J. S. (2017). Fate and transport of free-phase and dissolved-phase hydrocarbons in peat and peatlands: developing a conceptual model. *Environmental Reviews, 26*(1), 55–68. DOI:10.1139/er-2017-0002

B. Gharedaghloo wrote the first draft of the chapter. Dr. J. Price, who acted as the advisor of the thesis, provided editorial comments where required. Dr. J. Price also suggested revisions on the structure of the paper and the conceptual graphs of the manuscript.

Chapters three, four, and five have been submitted, and are under review in peer-review journals. Accordingly, these chapters will be subjected to the requests of the reviewers and may differ from the respective chapters presented here.

B. Gharedaghloo was the first author of all these chapters. B. Gharedaghloo designed the experimental instrumentation and procedures, and collected and analyzed the data. Dr. J. Price, as the thesis advisor, advised on the experimental designs and procedures, reviewed all the chapters/manuscripts, and provided technical and editorial comments.

Abstract

Widespread transportation corridors crossing Canadian peatlands make these landscapes vulnerable to hydrocarbon spills. After a spill happens, free hydrocarbon spreads in the peat layer forming a free-phase plume. Water soluble compounds of the free-phase plume then partition into the pore water and the flowing aqueous phase forming a dissolved-phase plume. These plumes threaten peatland ecosystem health and impose risk to aquatic systems located nearby the contaminated area. For this reason, environmental scientists should be able to predict the behavior of hydrocarbon contaminants and the temporal evolution of the hydrocarbon plumes. Properties of peat soils control the fate and transport of the spilled non-aqueous phase liquids (NAPL) and dissolved-phase hydrocarbon solutes in contaminated peatlands. Since the fate and transport of these contaminants in peat has received little attention, there is insufficient knowledge of parameters governing their mobility.

The cumulative effect of processes including dissolution, advection, and dispersion, diffusion into immobile water, adsorption onto soil matrix, volatilization, biodegradation, and other transformation processes determines the temporal evolution of contaminants in aquifers. The physical, hydraulic, and chemical properties of the aquifer soil and the hydrological, thermal, biological, and geochemical characteristics of the aquifer determine the rates and the relative dominance of abovementioned processes. It is well established that peat physical and hydraulic properties including its porosity, hydraulic conductivity, and average pore radius size vary systematically with peat depth. Also, peat decomposition and humification modifies the chemical composition of the peat matrix. However, the effect such systematic variations in peat has on the redistribution of hydrocarbon contaminants has not been investigated.

Multiphase flow characteristics of peat including capillary pressure-saturation-relative permeability (P_c-S-k_r) relations control the redistribution of free-phase hydrocarbon in a peatland. These relations will be functions of peat type and its physical properties. The functionality of P_c-S-k_r relations and residual NAPL (diesel) saturation (S_{Nr}) with peat type were examined in two types of peat in which S_{Nr} ranged between 0.3-17% and increased with peat bulk density. In a given peat, S_{Nr} was a function of saturation history and increased with increasing maximum diesel saturation. Irreducible water saturation, which is the saturation at which aqueous phase stops

moving, and the curvature of water k_r-S curves both were a function of peat type, and increased with peat bulk density. The results suggested that the k_r-S relations of water derived from unsaturated hydraulic conductivity of peat (in the presence of air) might be a good estimate of the water k_r–S relation in presence of NAPL.

Although the functionality P_c-S-kr relations to peat depth was not determined in this study, conceptually, it is expected that the reduction of pore radius typically taking place down the peat profile leads to 1) reduction of peat hydraulic conductivity with depth, 2) increase in NAPL-entry capillary pressure and water retention with depth, which cumulatively could cause a preferential migration of NAPL in shallower peat layers after a pressurized release of NAPL. In this condition, the exchange of gases between the source zone and the atmosphere happening due to wind or water table fluctuations may efficiently 1) drain contaminated soil-gas, and 2) promote aerobic conditions in the contaminated area. The water table fluctuation, however, might enhance the lateral redistribution of the free-phase plume.

The retardation of dissolved hydrocarbons is dominantly controlled by their adsorption onto the soil. The adsorption of benzene and toluene, as two of the most toxic and mobile dissolved organic compounds present in petroleum liquids, and their dependency on peat depth were explored. The linear adsorption isotherms for benzene and toluene were obtained with adsorption coefficients ranging from 16.2-48.7 L/kg and 31.6-48.7 L/kg, respectively. In the experiments, the benzene and toluene adsorption coefficients were not constant along the peat profile and varied with peat depth. The variations of toluene adsorption correlated with typical variations of cellulose and humic acid characteristic of a peat matrix. The organic carbon adsorption coefficient (K_{OC}) obtained for benzene in peat was equal and higher than the average benzene K_{OC} reported in literature for soils with low organic carbon content (f_{OC}). However, toluene K_{OC} was 10-50% less than the average value which suggests that using the average value might overestimate toluene retardation and underestimate its mobility down-gradient of the spill zone. The competition between benzene and toluene adsorption was insignificant, suggesting that individual adsorption coefficients could be used to study the adsorption of individual contaminants in a multi-solute problem.

The adsorption studies showed adsorption of benzene and toluene at the equilibrium condition. However, the adsorption model parameters that control the chemical equilibrium during contaminant transport remained unknown. Besides, the effect of mobile-immobile mass transfer, which takes place due to the dual-porosity pore structure of peat, on the retardation of dissolved hydrocarbons in the inactive pores, were not known. To address these, miscible (solute) transport experiments were conducted showing that the mass transfer rate between mobile and immobile zones of peat could be sufficiently high to establish physical-equilibrium between mobile and immobile zones of peat pore space. The results also showed that the relatively slow kinetics of adsorption could cause chemical non-equilibrium between the aqueous phase and adsorbed phase, leading to decreased adsorptive retardation in high discharge conditions. The retardation factor of benzene increased with depth and degree of peat decomposition. This coupled with the typical reduction of hydraulic conductivity with depth could cause a preferential redistribution of dissolved-contaminants in shallow peat layers in a contaminated peatland.

This study is the first study that characterizes the fate and transport of hydrocarbon contaminants in peat at the laboratory-scale and with specific focus on peat properties. Although scale-dependent phenomena such as field-scale heterogeneities might impose additional complexities to the fate and transport processes, the scale-independent parameters obtained in this study including adsorption partitioning coefficients and adsorption kinetics parameters, as well as residual NAPL saturation, irreducible water saturation, and water relative permeability relations have increased our understanding on the transport of free-phase and dissolved-phase hydrocarbons in in peat. The results can help predict the temporal evolution of the hydrocarbon plumes after a spill. The results also can help in assessing the risk after an oil spill accident and for evaluating the appropriateness of potential remediation plans.

Acknowledgement

First, I would like to thank my advisor, mentor, and wonderful friend Dr. Jonathan Price. I am grateful to you for giving me this opportunity and for believing in my capabilities. Through the last 4 years, you have always been there listening to me and guiding me with thoughtful advice; thank you for your time and patience.

I would also like to thank my examination committee members, Dr. William Quinton, Dr. James Smith, Dr. Maria Strack, and Dr. Neil Thomson for their invaluable advice and insightful feedbacks. Many thanks to the former and current colleagues in Wetlands Hydrology Laboratory at University of Waterloo, particularly James Sherwood, Eric Kessel, and Celeste Cameron for their help and support.

I am forever grateful to my parents, Parviz and Salemeh, who are the symbols of hard work and dedication to me, and my siblings Fatemeh, Elnaz and Behzad for their endless love and support. Also, countless thanks to my wife and my best friend Soheila; you have always been there for me holding my hands through all the moments of this journey; for sure, this thesis wouldn’t be completed without your help, support, and love.

Table of content

Examining Committee Membership ii
Abstract v
Acknowledgement viii
Table of content ix
List of figures xi
List of tables xiv
1 Introduction 1
1.1 Objectives 3
1.2 Organization of thesis 3
2 Fate and Transport of free-phase and dissolved-phase hydrocarbons in peat and peatlands: Developing a conceptual model 5
2.1 Introduction 5
2.2 Peat properties affecting NAPL movement 9
2.3 Dissolved-phase transport through the peatland 24
2.4 Volatilization and microbial decay of hydrocarbons 29
2.5 Summary and Conclusion 31
2.6 Acknowledgements 33
3 The role of peat depth and state of decomposition on benzene and toluene adsorption: Implications for their fate and transport in peatlands 34
3.1 Introduction 34
3.2 Materials and Method 37
3.3 Result and discussion 40
3.4 Conclusion 48
3.5 Appendix 49
4 Examination of the parameters controlling equilibria in the fate and transport of benzene in water saturated peat 51
4.1 Introduction 51
4.2 Materials and Methods 52
4.3 Results and Discussion 59
4.4 Summary and Conclusion 70
4.5 Acknowledgement 71
5 Characterizing the immiscible transport properties of diesel and water in peat soil 72

5.1 Introduction 72
5.2 Methods 73
5.3 Results 86
5.4 Discussion 95
5.5 Conclusion 100
5.6 Appendix A: Estimating diesel and water volumes in contaminated peat 101
5.7 Appendix B: mass balance in one dimensional peat column experiments 102
5.8 Appendix C. Preparing pressure transducers 103
5.9 Appendix D: Causes of the differences in the estimated S_{wirr} between BCM and PLM models 104
6 Conclusion and Recommendations 105
7 References 109

List of figures

Figure 2.1- Water/NAPL droplets sitting on a compressed peat surface in sessile drop experiments to establish water contact angles on the contact point of the water-NAPL interface and peat. (a) Water droplet on the peat surface in NAPL saturated conditions, illustrating the water contact angle during water advance (imbibition); (b) NAPL droplet on the peat surface in water saturated conditions, illustrating the water contact angle on peat during water recession (drainage). 13

Figure 2.2- a) Imbibition of NAPL into pore space, when the pore surface is water-wet and NAPL needs to overcome the capillary force to enter. In this example NAPL is lodged in the larger pores until it is able to exceed the sum of water pressure and pore entry capillary pressure; b) water displaces NAPL present in pore space. In this example, because of the NAPL-wet pore surface in NAPL-filled pores, water needs to overcome the sum of NAPL pressure and capillary pressure to be able to displace NAPL. 14

Figure 2.3- Bimodal pore size distribution of peat (Rezanezhad et al. 2012a; Weber et al. 2017) dominated by micro-pores, which have preference for retaining water. The shadings indicate the range of pore sizes the fluid is occupying. a) Hydrophilic and hydrophobic pore surfaces in the unsaturated zone of an uncontaminated peat layer; b) NAPL imbibes into the peat pore space through macro-pores with large radii, pore surface wettability changes to NAPL-wet in pores containing NAPL, resulting in a mixed-wet medium. The figure is inspired by Van Dijke et al. (2001). 16

Figure 2.4- a) The 3 to 5 orders of magnitude reduction in peat intrinsic permeability along top 50 cm of peat layer; b) systematic stratification in peat layer; highly permeable undecomposed layer at top and less permeable highly decomposed peat at depth; c) horizontal spread of free-phase plume in wet conditions when water table is shallow; d) horizontal spread of free-phase plume in dry seasons when water table is deep, causing preferential spreading in upper layers due to orders of magnitude higher permeability. It should be noted that NAPL saturation declines moving from plume center to its edge in the graphs. 17

Figure 2.5- Distribution of occupying fluids and pore surface chemistry between macro-pores and micro-pores of peat before and after free-phase contamination under a unique capillary pressure, and while the average pore radius and macro-pores frequency decline with depth due to macro-pore collapse. The graphs demonstrate that the capillarity, which is working against imbibition of air (a) and NAPL (b), increases with increasing depth and degree of decomposition. This causes smaller air/NAPL saturation in deeper peat. 19

Figure 2.6- Distribution of phases present in peat pore space before and during water percolation. a) Distribution of water and air within an uncontaminated unsaturated zone before water percolation; b) distribution of water in uncontaminated peat pore space during a water percolation event; c) distribution of water, air and NAPL within the unsaturated zone before water percolation for a NAPL-contaminated peat layer; and d) distribution of water and NAPL in peat pore space during water percolation event for a NAPL-contaminated peat layer. 22

Figure 2.7- Conceptual model of free-phase and dissolved-phase fate and transport through peatlands showing preferential spread of plumes in shallow peat horizons, and reduction of concentrations with distance from source zone in the dissolved-phase plume. Background image

of the figure is modified from http://www.gret-perg.ulaval.ca/fr/a-propos/tourbieres/hydrologie/acrotelme-et-catotelme/ 23
Figure 2.8- Schematic of the fate and transport of dissolved hydrocarbon solutes in peat soils showing advective-diffusive mass transport through the interconnected active porosity, and retardation of solute molecules due to diffusion into inactive porosity and adsorption onto the surface of interconnected and dead-end pores. Adsorption of hydrocarbon to the surface of DOC, which occurs naturally in peatland pore water, reduces the mass of hydrocarbon solutes available for adsorption to the pore surfaces; this leads to a reduction of the apparent adsorption coefficient. 26
Figure 3.1- Variation of benzene and toluene concentrations in feed solutions used in batch competitive adsorption experiments 40
Figure 3.2- Temporal variations of benzene (left) and toluene (right) concentrations in solutions during adsorption kinetics experiments while the adsorbent is moderately decomposed peat. 42
Figure 3.3- Adsorption of benzene and toluene onto peat of different depths and the linear model fitted to each isotherm. 43
Figure 3.4- Adsorption of benzene onto peat at a) 10-20 cm bgs and b) 20-30 bgs in the presence and absence of toluene. 44
Figure 3.5- Adsorption of toluene onto peat at a) 10-20 cm bgs and b) 20-30 cm bgs in presence and absence of benzene. 44
Figure 3.A.1- Schematic of water and solute discharge through a dual porosity porous medium with considerable mobile and immobile water contents 50
Figure 4.1- Variation of water retention curves with depth for peat soil samples obtained from core B (a) and core C (b) 60
Figure 4.2- Adsorption isotherms of benzene on peat of different depth at both cores B and C 62
Figure 4.3- Observed (obs.) BTCs of chloride (Cl) and benzene (BEN). Observed (grey and blue points) and simulated (grey and blue lines) breakthrough for peat of core B (left) and core C (right) at 0-10 cm (a, b), 10-20 cm (c, d) and 20-30 cm (e, f) below ground surface 65
Figure 4.4- Variation of pore size distribution with depth in core B (left) and core C (right). 68
Figure 5.1- Air bubble on peat in the water saturated condition (a), and diesel saturated condition (b), illustrating the water-air and diesel-air contact angles in gas imbibition, respectively. 74
Figure 5.2- Air inflow through top and liquid outflow through bottom of the separable column causing liquid drainage and air imbibition along the soil column (a); idealized vertical distributions of liquid and air saturation along the column at the end of the experiment (b). 76
Figure 5.3- (a) peat column is saturated with water and a diesel head is placed above the peat surface; (b) outflow valve is opened, diesel imbibes into the soil column and water flows out through column bottom due to gravity drainage; (c) three-phase flow begins when no diesel head is left above soil surface; (d) idealized variations of cumulative produced water and diesel through the two-phase flow period of the experiment 80
Figure 5.4- 2D peat box after the diesel spill; side well with diesel and water levels are evident; water and diesel pressure transducers with 10 cm spacing labelled N (for diesel) and W (for water). Hexagonal ports held electrodes enabling electrical resistance measurements through the experiment. 86

Figure 5.5- (a) unscaled height-saturation data for diesel-air and water-air column tests using milled peat; (b) unscaled capillary pressure-saturation relations for diesel-air and water-air drainage condition; (c) scaled diesel-air capillary pressure-saturation data (using Equation 5.1) compared to water-air capillary pressure-saturation data. 87
Figure 5.6- Variations of liquid saturation and water saturation with depth below ground surface (bgs) (top of each column) in the experimented columns of core A and core B..... 89
Figure 5.7- Measured and simulated cumulative production curves of water (black curves and circles) and diesel (grey curves and squares) in the experimened peat columns; note the different scales in the x- and y-axes of for the different peat types. 92
Figure 5.8- estimated water relative permeability (k_{rw}), diesel relative permeability (k_{rN}) and capillary pressure (Pc) curves using Brooks and Corey's model (BCM), and power-law model (PLM); grey circles illustrate diesel relative permeability measured using diesel outflow data. . 93
Figure 5.9- Spatial distribution of porosity in the peat box; value in each segment is (a) the porosity, (b) diesel saturation, and (c) water saturation of the segment; higher values in each figure are illustrated with more intense color. 95
Figure 5.10- Estimated relative permeability curves from two-phase diesel-water flow (curves) for core A (black curves) (A1, A2, and A3 columns) and core B (grey curves) (B2 and B3 columns), and measured water relative permeability in water-air system (grey circles) from Price et al. (2008), taken from the same peatland. 97
Figure 5.A.1- Actual and estimated volumes of water and diesel in peat pressing tests ... 102

List of tables

Table 2.1- Examples of physical and chemical properties of peat soils and mineral soils.... 6

Table 2.2- Variations of the measured water contact angle α_w in the presence of NAPL on peat during water drainage and imbibition; n=20. 14

Table 3.1- Summary of studies that have explored adsorption of BTEX onto peat soils; *L* and *F* respectively denote linear and Freundlich adsorption models; K_d is the linear adsorption coefficient [L^3M^{-1}]; K_F is Freundlich adsorption coefficient; K_{OM} is organic matter partitioning coefficient [L^3M^{-1}], and K_{OC} is organic carbon partitioning coefficient [L^3M^{-1}]. In the peat type column, HD is highly decomposed, MD is moderately decomposed, and UD is undecomposed.36

Table 3.2- Type of adsorption experiments carried out at each core..... 38

Table 3.3- Peat physical properties in both cores at different depths 41

Table 3.4- Summary of fitted linear model on benzene and toluene isotherms 43

Table 3.5- Linear adsorption coefficients for adsorption of benzene and toluene onto peat of different depths in presence and lack of the competing solute 45

Table 3.6- Variation of benzene and toluene retardation factors with depth in peat profile 47

Table 4.1- Ranges of uncertain parameters tested including ratio of active porosity to total porosity ($\phi_{active}/\phi_{total}$), first order mobile-immobile transfer coefficient (α_{MIM}), longitudinal dispersivity of the mobile zone (λ), fraction of instantaneous adsorption sites in both mobile and immobile zones (*frac*), first order kinetics adsorption coefficient (α_{kin}), and linear adsorption coefficient (K_d) considered in global search algorithm..... 59

Table 4.2- Physical properties of soil columns and discharge rate in BTC experiments; ϕ_{total} is total porosity, ρ_b is bulk density, and q is discharge through the soil column. 61

Table 4.3- Summary of linear isotherm model ($S=K_d \times C_e$) fitted to the data of benzene adsorption on peat..... 62

Table 4.4- Average (s.d.) soil properties in the experimental soil columns and summary of chloride and benzene errors in inverse modelling 66

Table 4.5- Retardation factor (R) and equilibrium retardation factor (R_{eq}) in the experimented soil columns 70

Table 5.1- Physical properties of peat columns in unsteady state immiscible transport experiments; *porosity of A1 is the average of A2 and A3..... 88

Table 5.2- Ranges of uncertain/unknown parameters in random search simulations..... 90

Table 5.3- Estimated parameters of P_c-S-k_r relations 90

Table 5.B.1- Summary of mass balance of diesel in the peat column experiments; where $V_{spilled}$ is volume of diesel initially placed above the water saturated peat column, $V_{outflow}$ is volume of diesel that flowed out of the column bottom by the end of the experiment, V_{column} is the estimated volume of diesel remaining inside the column; $Error_{volume}$ is the volumetric error of diesel mass that is missing due to assumptions, and *Error* is the percentage of missing to total volume. 103

1 Introduction

Peatlands cover more than 21% of Alberta, Saskatchewan, and Manitoba (Vitt et al. 2000). Peatland distribution in boreal northern Alberta, where petroleum hydrocarbon resources are extracted and transported, is even more widespread (Vitt et al. 2000). The transport of raw and processed petroleum hydrocarbons through pipelines or railroads crossing peatlands cause these landscapes to be vulnerable to petroleum hydrocarbon spills. However, very little attention has been paid to the fate and transport of these contaminants in peat and peatlands. There is a growing body of literature on transport of hydrocarbon contaminants in inorganic porous media; however, the results of these studies cannot be used directly in peatlands due to the systematic differences between the physical and chemical properties of peat soils and the inorganic porous material such as their porosity, pore structure, and wetting preferences, and the structural, hydrological, and geochemical character of peatlands. It is not clear how peat and peatland specific processes might influence the fate and transport of organic contaminants in different-scales from micro-scale to the field-scale. Therefore, there is a need for a conceptual model of the fate and transport of hydrocarbons that consider the specific properties and processes in peat and peatlands. The conceptual model can help identify the dominant processes after a hydrocarbon spill, and guide the response.

A spilled petroleum hydrocarbon liquid, as a non-aqueous phase liquid (NAPL) will spread in the groundwater system of a peatland after a spill accident (Moore et al. 2002; Gharedaghloo and Price 2017) forming a free-phase plume. As NAPL (hydrocarbon liquid) spreads, the soluble organic compounds present in NAPL dissolve into the pore water, forming dissolved-phase plumes (Soga et al. 2004). These free-phase and dissolved-phase plumes can potentially remobilize inorganic contaminants such as lead (Pb) that might be present in the peat matrix (Deiss et al. 2004). These organic and inorganic plumes impose threats to the health of the ecosystem and surrounding water bodies. To minimize the risk of the contamination, environmental scientists need to forecast the behavior of these plumes. Multiphase flow properties of the peat including capillary pressure-saturation-relative permeability relations *(Pc-S-kr*) determine the spatial

distribution and temporal variations of free-phase hydrocarbons. These relations have been examined for inorganic porous media and for the flow of water and NAPL together (e.g. Johnson et al. 1959; Leverett and Lewis 1941; Caudle et al. 1951). These relations have also been examined for water retention and flow in the presence of air in peat soils (e.g. Price et al. 2008; Price and Whittington 2010; McCarter and Price 2014). However, these relations for the two-phase flow of water and NAPL in peat soils are not available, although studies have indicated a preference of peat in the absorption of petroleum liquids (Zoltai and Kershaw 1995; Ghaly et al. 1999; and Adebajo et al. 2003), which potentially can impact the transport of free-phase hydrocarbons in peat pore space.

Peat is known to have a dual-porosity pore structure (Rezanezhad et al. 2016). Several studies have explored the transport of inorganic solutes in peat (Hoag and Price 1995, 1997; Ours et al. 1997; Baird and Gaffney 2000; McCarter and Price 2017) all showing the transport of solutes is controlled by the micro to meso-scale features of peat soils and peatlands. Despite the transport of inorganic solutes in peat, there are little data available on the effects of the peat matrix and pore structure on the transport of organic solutes such as dissolved-phase hydrocarbons. Among the dissolved-phase contaminants, benzene and toluene are compounds with higher mobility and less retardation in groundwater systems (e.g. Seagren and Becker, 2002). The adsorption of these contaminants varies with peat type (Cohen et al. 1991; Rutherford et al. 1992; Zytner et al.1994) which means the adsorption of organic contaminants onto peat could be a function of peat matrix composition. However, the variation of the adsorption of organic contaminants to peat within a peatland, as well as the effect of competition in the adsorption of an individual contaminant are not clearly known. In addition, it is not known if the average K_{OC} values reported for organic contaminants based on studies done using mineral soils are representative of adsorption onto peat organic carbon. Furthermore, since it could take more than a day to establish equilibrium between the dissolved phase contaminants and the adsorbed phase in peat (Rutherford et al. 1992; Zytner et al.1994), in conditions with high water discharge (for example after a heavy rainfall) the lack of equilibrium could reduce the total adsorbed mass; however, the parameters (e.g. adsorption kinetics rate) controlling the kinetics of adsorption reactions are not known for peat.

1.1 Objectives

The objectives of this study are 1) to assess the current state of knowledge regarding petroleum hydrocarbons in peatlands and to develop a conceptual model illustrating the behavior of free-phase and dissolved-phase plumes in a natural peatland setting; the model should consider the knowledge of organic contaminants' fate and transport and on peat and peatland characteristics in discussing the behavior of organic contaminants in peat and peatlands; 2) to determine the wetting tendency of peat toward water, NAPL (diesel), and air and different wetting scenarios. This could demonstrate the pore-scale distribution of water, air, and NAPLs (hydrocarbon liquids) in contaminated peat soil and help conceptualize the transport of NAPLs (hydrocarbon liquids); 3) to examine the adsorption of benzene and toluene, as two of the most soluble and mobile organic contaminants, onto peat, and to study the effect of competition between them on their individual adsorption; 4) to characterize the retardation of benzene and its adsorption kinetics model parameters, and to evaluate their variations down the peat profile; 5) to estimate the P_c-S-k_r model parameters (e.g. residual NAPL saturation, irreducible water saturation, and curvatures of relative permeability curves) of peat soils during transport of NAPL (diesel) and water, and to investigate the variations of these parameters with type of peat.

1.2 Organization of thesis

This thesis is composed of six chapters. Chapter one is the introduction which introduces the thesis topic, highlights the knowledge gap with respect to the topic of interest, and specifies the objectives of the research.

Chapter two (published manuscript) reviews the present state of knowledge regarding the fate and transport of free-phase and dissolved-phase hydrocarbons, which is well established for mineral soils, and contextualizes it for peat soils and peatlands with the inclusion of peat and peatland specific processes and experimentally observed wetting preferences of peat soil. A conceptual model is derived explaining how peat physical and chemical properties might influence the fate and transport processes of hydrocarbons, and could control the spatial distribution and

temporal variations of hydrocarbons mass in a contaminated peatland. This chapter addresses the first and second objective of the thesis.

Chapter three addresses the third objective of the thesis by examining the adsorption of benzene and toluene onto peat. This chapter, in addition, investigates the competitive adsorption of these compounds by comparing individual adsorption coefficients of benzene and toluene and their adsorption coefficients in binary solutions.

Chapter four examines the presence and the absence of equilibria in physical and chemical phenomena that govern the transport of benzene in peat; the chapter discusses how lack of chemical equilibrium might promote the redistribution of organic contaminants. The chapter also studies the variation of contaminant's retardation with peat depth, and discusses the field-scale implications of observations. This chapter specifically addresses objective four of the thesis.

Chapter five concentrates on the fifth objective of the thesis and discusses the transport of diesel, as an example of free-phase petroleum liquids, in peat soil. In this chapter the parameters of P_c-S-k_r models are estimated for the transport of diesel and water through peat soils. The residual diesel saturation is examined considering its variations with peat type and the antecedent moisture regimes of peat.

The summary of the conclusions and findings of each chapter is presented in chapter six. The chapter discusses primary findings of the thesis, makes some recommendations for spill response, and suggests potential experiments and studies that can expand our knowledge and fill the remaining data gap on the fate and transport of organic contaminants in peat and peatlands.

2 Fate and Transport of free-phase and dissolved-phase hydrocarbons in peat and peatlands: Developing a conceptual model

2.1 Introduction

Increasing hydrocarbon resource extraction activities and transportation in boreal ecozones, which are often dominated by wetlands, mostly peatlands (NWWG 1988), increase their susceptibility to hydrocarbon contamination. The processes governing the fate and transport of hydrocarbons in peatlands need to be better understood to effectively manage spills in wetland systems. Boreal peatlands include bogs, fens and swamps (NWWG 1998), which have different hydrological, hydrogeological, botanical, chemical and biogeochemical characteristics, each of which may influence transport behaviour. In this paper, the pore- to field-scale properties common to peat and peatlands, that affect the fate and transport of spilled hydrocarbons, is considered.

Due to its high water content, peat is highly compressible and can be subject to subsidence (Hobbs 1986; Price 2003). This instability can affect the integrity of pipelines (Jol and Smith 1995) and railroads routed across it, and can result in leakage (cf. TSB 2007; AER 2017a) or derailment (cf. TSB 2004; TSB 2006) and accidental spills. In the boreal zone, where peatlands are often the dominant landform (NWWG 1988; Vitt et al. 1996), the risk of spill and contamination by hydrocarbons or other industrial chemicals is concomitantly increased. Despite the spill risk, the transport of non-aqueous phase liquids (NAPLs) or dissolved contaminants in boreal peatlands has received little attention, compared to that in mineral aquifers (e.g., listed in Mercer and Cohen (1990) and Essaid et al. (2015)). Peatland systems have important differences in their structure, and the physical and chemical characteristics of their soils is distinct compared to those in mineral aquifers, including their active/total porosity, hydraulic conductivity, constituents, wetting behavior, and pore structure (Table 2.1). These factors can cause distinct differences in the distribution and mobility of NAPLs and solutes in groundwater systems, compared to their expected behaviour in mineral soil systems. Moreover, given the differences in the biological

origin of peat, the peat and pore-water chemistry, the structure of the soil profile and hydrological connectivity within and between adjacent ecosystems (Hobbs 1986), a range of hydrocarbon transport behaviours should also be expected among peatlands.

Table 2.1- Examples of physical and chemical properties of peat soils and mineral soils

Soil properties	in peat soil	in mineral soil (with low organic matter content)
Porosity	90%-95% (Schlotzhauer and Price 1999) *Sphagnum* peat: 92-94% (Landva and Pheeney 1980) Sedge peat: 86%-92% (Landva and Pheeney 1980)	Unconsolidated sand: 21%-49% (Wolff 1982) Unconsolidated clay: 14%-68.5% (Wolff 1982)
Effective porosity (total porosity)	*Sphagnum* moss: 53% (~90%) (Quinton et al. 2008) Lightly decomposed peat: 37% (87%) (Hoag and Price 1997) Humified peat: 10% (n.d.) (Siegel and Glaser 1987) Humified peat: 12% (75%) (Hoag and Price 1997)	Sandy sediment: 23% (32%) (Chapelle and Lovley 1990) Clayey sediment: 7.8% (43%) (Chapelle and Lovley 1990)
Hydraulic conductivity (m/s)	*Sphagnum* moss: 3×10^{-3}- 9×10^{-3} m/s (Quinton et al. 2008) Decomposed peat: ~1×10^{-5}(Quinton et al. 2008) Highly decomposed peat: ~1×10^{-8} (Whittington and Price 2006)	Unconsolidated sand: 4.2×10^{-8}-4.6×10^{-4} (Wolff 1982) Unconsolidated clay: 5.3×10^{-17}-6.1×10^{-6} (Wolff 1982)
Constituents	Organic compounds: lignin, cellulose, humic acids, fulvic acids, lipids, waxes, resin, and bitumen in which C, H, O, N, and S are the forming elements (Smith et al. 1958; Yonebayashi et al. 1994; Guignard et al. 2000; Bozkurt et al. 2001; Zaccone et al. 2007);	Minerals including quartz, feldspar, kaolinite, etc, where forming elements are Si, Al, Fe, K, etc (Nesbitt et al. 1997)
Wetting preference	Conditionally hydrophilic and hydrophobic (Valat et al. 1991; Michel et al. 2001)	Generally hydrophilic
Pore structure	Systematic dual porosity structure with an interconnected network of macro-pores and inactive dead end pores (Hoag and Price, 1997; Rezanezhad et al. 2012a)	Generally single porosity medium (in lack of fractures, vugs, etc)
Pore size distribution	Bimodal (Rezanezhad et al. 2012a; Weber et al. 2017)	Generally unimodal (Marshall 1958; Nimmo 1992)

In peatlands, the distinct hydraulic conductivities of the upper layer of soil (acrotelm) and the deeper, more decomposed peat (catotelm) promotes the shallow distribution of dissolved plumes (Hoag and Price, 1995). Hummock/hollow and ridge/pool microtopography common in peatlands (Ingram 1983; Tallis 1998) enhances solute dispersion (Balliston 2017; McCarter and Price 2017). In addition to the field-scale features, pore-scale properties of peat and particularly the dual-porosity pore structure of peat can even lead to retardation of conservative tracers (Hoag and Price 1997; Rezanezhad et al. 2012a). In addition, as adsorption of organic solutes on soils increase with organic carbon content of soils (Karickhoff 1984) and as peat has high organic carbon content (Andriesse 1988; Smith et al. 2004), it can adsorb dissolved hydrocarbons and retard their movement. The cumulative retardation, by both structural and chemical processes, determines the spatial distribution and temporal variation of dissolved hydrocarbon mass and concentration within a contaminated site.

In addition to solute retardation as noted above, the strong tendency of peat to absorb free-phase hydrocarbon can retard free-phase plume movement and control NAPL redistribution in a peatland. This tendency is caused by the surface chemistry of peat that imparts a preferential wetting tendency of peat to non-polar liquids, compared to water. This difference in wetting tendencies of peat controls the ability of NAPL and/or water to enter or drain from pore spaces. Zoltai and Kershaw (1995), Ghaly et al. (1999) and Adebajo et al. (2003) suggested using peat as an absorbent for removing free-phase product from open water because free-phase hydrocarbon liquids have higher affinity for peat, compared to water. This can cause profound differences in the permeability and retention capacity of peat toward water and NAPL, and can control the spatial distribution of NAPL, its fate and spreading velocity after a spill. For example Collins (1983) reported the high NAPL holding capacity of peat after its ingress caused NAPL to be absorbed, which limited its movement through the peatland.

While there is an emerging body of literature describing the behavior of various solutes in peat (e.g. Baird and Gaffney 2000; Holden 2005; McCarter and Price 2017) there is a paucity of knowledge regarding transport and fate of organic solutes and NAPLs in peat, and none of the parameters that control their fate and transport are well-characterized in peat soils and peatlands. Given the distinctive character of peat, e.g. its unique pore structure and wetting tendencies (Table

2.1), data on hydrocarbon behaviour in mineral soils, e.g. capillary pressure and relative permeability relations, are not necessarily applicable in peat. Because of this gap of knowledge, and due to the specific physical and chemical characteristics of peat soils, the consequences of oil spills and leakage into peatlands are poorly known. The failure to properly fill the data gaps and to understand the governing processes causes poor estimation of contamination behavior after a spill. This poor understanding can lead to the selection of inefficient clean-up strategies which can waste time, effort and money, and can impose additional strain on the health of the system. For example, it can lead to the application of remediation techniques (e.g. air-sparging, pump and treat, soil vapour extraction, in-situ chemical oxidation) designed and tested for mineral aquifers, while their successful application in shallow peatland aquifers has never been documented and justified. Filling the knowledge gap might help introducing new clean-up strategies that are less destructive than the current practice, which typically involves digging up and removing contaminated peat (Fitzhenry et al. 1992; ERCB 2011; AER 2017a) and severely disturbs the hydrology and ecology of the site that has taken thousands of years to develop (Clymo et al. 1998). If its mobility is restricted, and the peatland ecological function not notably impaired, it could be left in place, where peatland microbial processes can eventually degrade it (Kelly-Hooper et al. 2013).

The goal of this paper is to review the processes governing hydrocarbon mobility considering the properties of peat and peatlands. Peat properties control the fate and transport of both free- and dissolved-phase hydrocarbon plumes, as well as its volatilization. In this paper, respectively, the multiphase flow properties of peat, the transport of dissolved hydrocarbon, and hydrocarbon removal through volatilization and biodegradation are discussed in separate sections. In each section, contrasts to their behavior in mineral soils are made, along with the complexities that peat properties and peatland specific processes might introduce. After reviewing the fundamental governing processes, a conceptual model for hydrocarbon fate and transport in peatland systems is introduced. This is an important step in being able to make informed recommendations for spill management and remediation in peatlands.

2.2 Peat properties affecting NAPL movement

When hydrocarbon is released into a groundwater system, it can migrate below the surface, and then four distinct phases may be present in the subsurface including the NAPL, the aqueous phase, the air phase and the solid (soil) phase. Equation 2.1 (Faust, 1985) is the multiphase flow equation indicating the parameters controlling NAPL movement in groundwater systems. The equation is used to determine the spatial distribution of NAPL and its temporal variation below ground surface (Essaid et al., 2015):

$$\frac{\partial}{\partial t}\left(\phi S_f \rho_f\right) = \nabla.\left(\rho_f \frac{\kappa k_{rf}}{\mu_f}\left(\nabla p_f + \rho_f g \nabla z\right)\right) + Q_f \qquad \textbf{Equation 2.1}$$

where ϕ is porosity [L^3L^{-3}], S_f is fluid saturation [L^3L^{-3}], ρ_f is fluid density [ML^{-3}], Q_f is sink/source term [$ML^{-3}T^{-1}$], $\boldsymbol{\kappa}$ is the permeability tensor [L^2], k_{rf} is relative permeability (dimensionless), μ_f is fluid viscosity [$ML^{-1}T^{-1}$], g is acceleration due to gravity [LT^{-2}], z is elevation [L], p_f is fluid pressure [$ML^{-1}T^{-2}$], and f is fluid which can be NAPL, water, or air. Based on Equation 2.1, the distribution of NAPL in a groundwater system is a function of the physical and chemical characteristics of the NAPL, as well as that of the soil porous medium. The important characteristics of the soil that relate to the distributions of NAPL, aqueous phase, and air are capillary pressure-saturation (P_c-S) and relative permeability-saturation (k_r-S) relations, which both strongly depend on pore surface wettability. Relative permeability of NAPL (k_{rN}), which is the ratio of effective permeability of NAPL (k_{effN}) to the intrinsic permeability of porous medium (k), decreases as NAPL saturation declines (Mercer and Cohen 1990). As NAPL migrates into the groundwater system its spatial extent increases, causing average NAPL saturation to decline with time. k_{rN} decreases accordingly, hence NAPL migration velocity drops with time. NAPL eventually reaches a minimum saturation (residual saturation) where it ceases moving and its shape and extent stabilizes.

In addition to P_c-S-k_r relations, the field-scale characteristic of peatland systems will have a profound effect on NAPL movement. These properties include a dramatic reduction in peat intrinsic permeability with depth along the soil profile, shallow depth to water table (Zoltai and Kershaw 1995), and thickness of organic layer (Johnson et al. 1980), which is complicated by

microtopgraphic variability (e.g. hummock/hollow) (Rochefort et al. 2012). Beside, type of peatland (bog, fen or swamp) can control the NAPL movement. Bogs are *Sphagnum* moss dominated ombrotrophic (water and dissolved minerals received only from precipitation) and consequently acidic (pH<4) peatlands. Fens are bryophyte dominated (*Sphagnum* and brown moss) peatlands that typically receive base-rich minerals from surrounding uplands or from other wetlands, commonly via groundwater, and have a pH that ranges from ~4 to greater than 7 (Zoltai and Vitt 1995). Swamp peatlands are forested or wooded, and typically have a more widely fluctuating water table than bogs or fens (NWWG 1997). In addition to the type of peatlands and their specific hydrological settings, given the presence of permafrost or seasonal frost and the proximity of the water table to the surface in boreal peatlands, seasonal weather patterns likely have important effects on NAPL redistribution after a spill accident.

Although realistic P_c-S-k_r data are needed to successfully study the multiphase flow of NAPL, water and air in groundwater systems (Essaid et al. 2015) these data are not available for peat soils. These characteristics have been explored in mineral porous media (Dane et al. 1992; Dane et al. 1998; Demond and Roberts 1993; Demond et al. 1996; Hofstee et al. 1997; Lenhard and Parker 1988; Lenhard 1992), but have not been characterized for organic soils and peat. P_c-S-k_r relations of porous media are functions of wettability, pore size distribution, and pore structure (Burdine 1953; Joekar-Niasar et al. 2008). As discussed previously, since these factors differ between peat soil and mineral soils, P_c-S-k_r data available for mineral soils are not applicable to peat.

2.2.1 Peat pore surface chemistry and wettability

Wetting preferences of porous media influence the distribution of pore fluids in the pore space (Anderson 1986a), which means the distribution of pore fluids before and after a hydrocarbon spill is controlled by the peat wetting tendency toward NAPL, water, and air. The wetting behavior of a soil refers to the preference of the soil to increase the interface area between its pore surface and a fluid in presence other pore fluids (Bachmann et al. 2000a). Wetting tendency is a function of pore surface chemistry and soil wetting history. As an example, in peatlands, before a NAPL spill, water rises above the water table through capillarity, although water pressure is less than air

pressure in the vadose zone. This shows that peat wettability influences capillarity, and then capillarity controls the flow and storage of the aqueous phase and determines the vertical distribution of water in the unsaturated zone. Similarly, after NAPL intrusion into a peatland, as with other groundwater systems, the wetting tendency of the soil is the factor controlling the distribution of water and NAPL in the contaminated area (Newell et al. 1995).

Conditional hydrophilicity and water repellency observed in peat soil (Michel et al. 2001) can cause variable wetting tendencies of peat toward NAPL and water. The degree of soil water repellency and the wetting preference of a porous medium can be directly assessed by measuring contact angles of pore fluids (Adamson 1967). The contact angle is the angle that the interface of two facing fluids establish with the pore surface (Yuan and Lee 2013); its size illustrates the wetting tendencies of the porous medium toward fluids present in its pore space (Anderson 1986b). It has been observed that peat is water-wet when there is already water in its pore network, and it is air-wet (water repelling) when the water is drained from its pores. Valat (1991) demonstrated the hydrophobic behavior of dry peat by measuring contact angles higher than 110^{o}, which confirmed that the peat pore surface was water repelling and air-wet, when dry. Michel et al. (2001) and Michel (2009) observed peat surface changes from the hydrophilic to hydrophobic state as water drained from its pore space. Ketcheson and Price (2016) measured water droplet penetration time (WDPT) for peat soils at different moisture contents, and observed peat water repellency increased as peat water content decreased. At each level of water content the observed contact angle is the average of contact angles of all the pores. Due to capillarity, water in pores with smaller radii is drained only at high matric potentials. Therefore, the increase in contact angle with decreasing soil water content, observed in the scale of soil columns (Michel et al. 2001), occurs predominantly in pores with large radii, whose water drains first. These observations mean the peat pore surface can be conditionally water-wet and conditionally air-wet, and hysteresis in peat wettability occurs as a function of peat wetting history. The contact angle hysteresis can be due to heterogeneity of pore solid surfaces (Kwok and Neumann 1999) and is one of the causes of hysteresis in soil water characteristic relations (O'Kane 2005). For the same reason, peat may have conditional wettability and variable contact angle toward water and NAPL after NAPL intrusion into its pore space. Since the affinity of peat toward NAPL is unknown, it is essential to

characterize peat wetting preferences in the presence of NAPL and water during different peat wetting history scenarios.

2.2.1.1 Determining peat wettability

To quantify the contact angles of NAPL (diesel) and water on peat surface, we used the sessile drop method, which is a method commonly used for characterizing soil wetting tendency (Valet et al. 1991; Powers et al. 1996; Bachmann et al. 2000b; Shang et al. 2008; Leelamanie et al. 2008). Using this method, contact angles of the water-NAPL interface were measured on compressed wafers of *Sphagnum* peat in both (distilled) water saturated and NAPL (diesel) saturated conditions. A water droplet was placed on the surface of peat immersed in NAPL (Figure 2.1a). Alternatively, a NAPL droplet was released into a water saturated system and rose to contact the peat surface (Figure 2.1b). The contact angle of each droplet with respect to the peat surface was then obtained by analyzing droplet images (n=20). These images were captured using a high-resolution camera. Then the ratio of a droplet diameter to its base length was obtained from the captured images. Using geometrical rules and the aforementioned ratio, the contact angle of each droplet was calculated (cf. Yuan and Lee 2013). The former case (Figure 2.1a) represents the condition when NAPL is present in the pore space and water imbibes into the pore space by displacing NAPL. This takes place when soil water content rises in free-phase contaminated pores due to water infiltration or water table rise. The alternate condition (Figure 2.1b) represents the case when water is present in peat pore spaces and NAPL is introduced, displacing water. This happens immediately after a spill when NAPL is mobile and percolates into uncontaminated pores. The water contact angles obtained for the NAPL-saturated and water-saturated cases were assumed as contact angles during water imbibition and water drainage processes, respectively. Since in these wetting scenarios the aqueous phase is advancing on and receding from peat surface, the respective contact angles are a measure of the wettability of peat to water and NAPL in different wetting scenarios in a two-phase water-NAPL system.

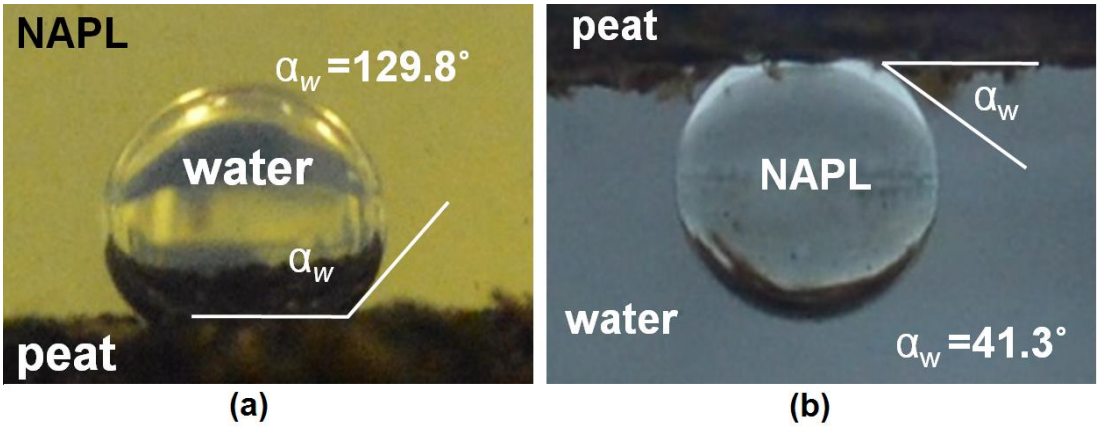

Figure 2.1- Water/NAPL (diesel) droplets sitting on a compressed peat surface in sessile drop experiments to establish water contact angles on the contact point of the water-NAPL interface and peat. (a) Water droplet on the peat surface in NAPL (diesel) saturated conditions, illustrating the water contact angle during NAPL drainage and water advance (imbibition); (b) NAPL droplet on the peat surface in water saturated conditions, illustrating the water contact angle on peat during water recession (drainage) and NAPL (diesel) imbibition condition.

The median contact angles, α_w, in water drainage and water imbibition processes (Table 2.2) were 41.3^o and 129.8^o, respectively. Porous media are water-wet when α_w is less than 70^o and are NAPL-wet when α_w is higher than 110^o (Anderson 1986b; Mercer and Cohen 1990). Therefore, α_w values imply that the peat pore surface is NAPL-wet in water imbibition (Figure 2.1a) and is water-wet during water drainage (Figure 2.1b). The results of contact angle experiments imply that prior to NAPL percolation into a pore, the pore surface is water-wet causing capillarity working toward keeping water in pore spaces. This means after NAPL is spilled into a peat layer, capillarity will work against NAPL percolation into water-containing pores. Therefore, NAPL pressure must be higher than pore entry pressure, which is the sum of water pressure and pore entry capillary pressure, to be able to displace water from pore space (Figure 2.2a). Thus NAPL preferentially enters larger pores as their pore entry capillary pressure is smaller than that of smaller pores. The same phenomenon takes place during NAPL intrusion into the water-wet mineral aquifers. On the other hand, as NAPL percolates into a pore, the pore surface chemistry is altered, and the pore surface becomes NAPL-wet. Afterward, water needs to overcome the capillary forces governing in favor of NAPL to be able to migrate into the NAPL-filled pores (Figure 2.2b). As an example, during snowmelt, rainfall or water table rise in peatlands when soil water content rises, water

pressure must be higher than the sum of NAPL pressure and capillary pressure, for water to imbibe into the contaminated pores and displace NAPL. This is different from mineral systems in which after a spill of petroleum products into a water-wet soil, the wetting tendency of the soil commonly stays water-wet (McCaffery and Mungan 1970; Powers et al. 1996), and water can imbibe into the NAPL containing pores with pressure less than NAPL pressure since capillarity works toward imbibing the water into the contaminated pores.

Table 2.2- Variations of the measured water contact angle α_w in the presence of NAPL on peat during water drainage and imbibition; n=20.

	Water drainage (diesel imbibition)	Water imbibition (diesel drainage)
Minimum	32.9	117.7
Median	41.3	129.8
Maximum	56.5	142.3

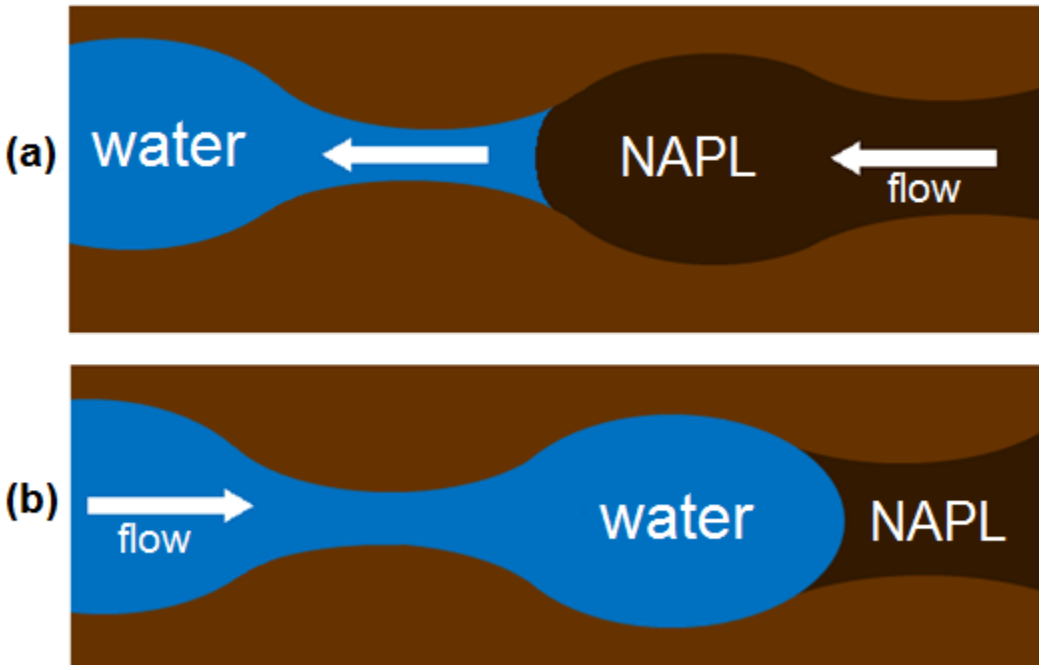

Figure 2.2- a) Imbibition of NAPL into pore space, when the pore surface is water-wet and NAPL needs to overcome the capillary force to enter. In this example NAPL is lodged in the larger pores until it is able to exceed the sum of water pressure and pore entry capillary pressure; b) water displaces NAPL present in pore space. In this example, because of the NAPL-wet pore surface in NAPL-filled pores, water needs to overcome the sum of NAPL pressure and capillary pressure to be able to displace NAPL.

Alteration of pore surface wetting tendency toward the imbibed fluid can cause peat to be a mixed-wet medium. In mixed-wet media, wettability of soil changes between pores. In the vadose zone of an uncontaminated peat layer, similar to in mineral aquifers, water drains from macro-pores prior to that in meso-pores and micro-pores (where the diameter of macro-pores are larger than 1 mm, the diameters of micro-pores are smaller than 10 microns, and the diameter of meso-pores are between 10 μm and 1 mm (Luxmoore 1981)). This causes peat to be partially hydrophilic (water-wet) and partially hydrophobic (air-wet) (Figure 2.3a). In a similar process, when NAPL is released onto peat it penetrates into the soil mainly through macro-pores and then through meso-pores. Consequently, the macro-pores and meso-pores containing NAPL become NAPL-wet and micro-pores containing water remain water-wet. This means the contaminated peat becomes a mixed-wet porous medium where pore surface wettability can be water-wet or NAPL-wet depending on that pore radius size (Figure 2.3b). Figure 2.3 highlights that the change in wetting tendency of pore surfaces is restricted to the pores with large radii. This must be noted that in the (large) pores in which the wetting tendency of pore surface is altered to hydrophobic or NAPL-wet (Figure 2.3) some of the rough corners might still hold water due to the capillarity; this can prevent the alteration of pore surface wetting tendency at those corners; however, this wouldn't be against the conceptual representation of the relation between pores' surface wetting tendency and their theoretical pore size (Figure 2.3) because those corners can be classified as individual pores with small theoretical pore radii.

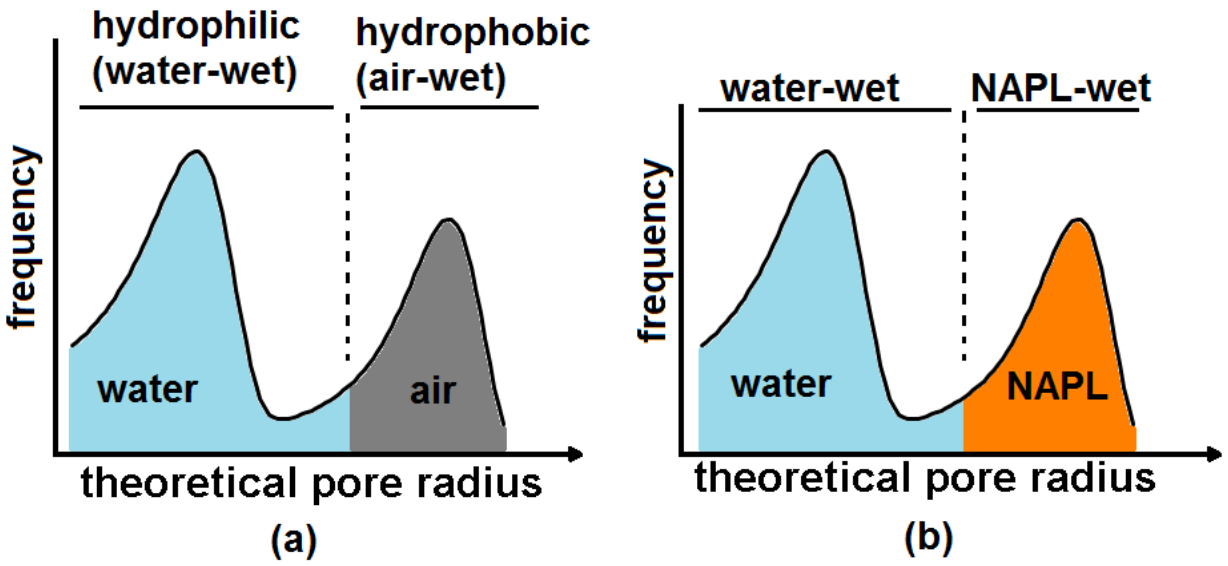

Figure 2.3- Bimodal pore size distribution of peat (Rezanezhad et al. 2012a; Weber et al. 2017) dominated by micro-pores, which have preference for retaining water. The shadings indicate the range of pore sizes the fluid is occupying. a) Hydrophilic and hydrophobic pore surfaces in the unsaturated zone of an uncontaminated peat layer; b) NAPL imbibes into the peat pore space through macro-pores with large radii, pore surface wettability changes to NAPL-wet in pores containing NAPL, resulting in a mixed-wet medium. The figure is inspired by Van Dijke et al. (2001).

2.2.2 Systematic layering and reduction in peat permeability

The characteristic decrease in intrinsic permeability of peat with depth, as well as capillary processes associated with smaller pores at depth restrict NAPL intrusion, and promote horizontal NAPL migration in shallow peat layers. Peat decomposition and its compaction by the overlying materials changes the peat pore structure and leads to less active porosity (Hoag and Price 1997), higher tortuosity (Rezanezhad et al. 2010) and smaller pore radius (Goetz and Price 2015) in more decomposed peat. This is why intrinsic permeability decreases with respect to depth and degree of decomposition (Figure 2.4a, b) in natural peat settings (Quinton et al. 2008). The reduction can be 3 to 5 orders of magnitude in fen and bog peatlands, respectively (e.g. Price and Maloney 1994; Hoag and Price 1995). In addition, the change in pore structure can result in anisotropy, such that at a given depth the horizontal intrinsic permeability (k_h) can be 10 times larger than the vertical intrinsic permeability (k_v) (Chason and Siegel 1986). Decreasing intrinsic permeability versus

depth and dominance of k_h over k_v in peat layers will contribute to the preferential lateral movement of NAPL in shallow subsurface layers. This is assuming NAPL effective permeability has variations similar to that of peat intrinsic permeability (no empirical data were found).

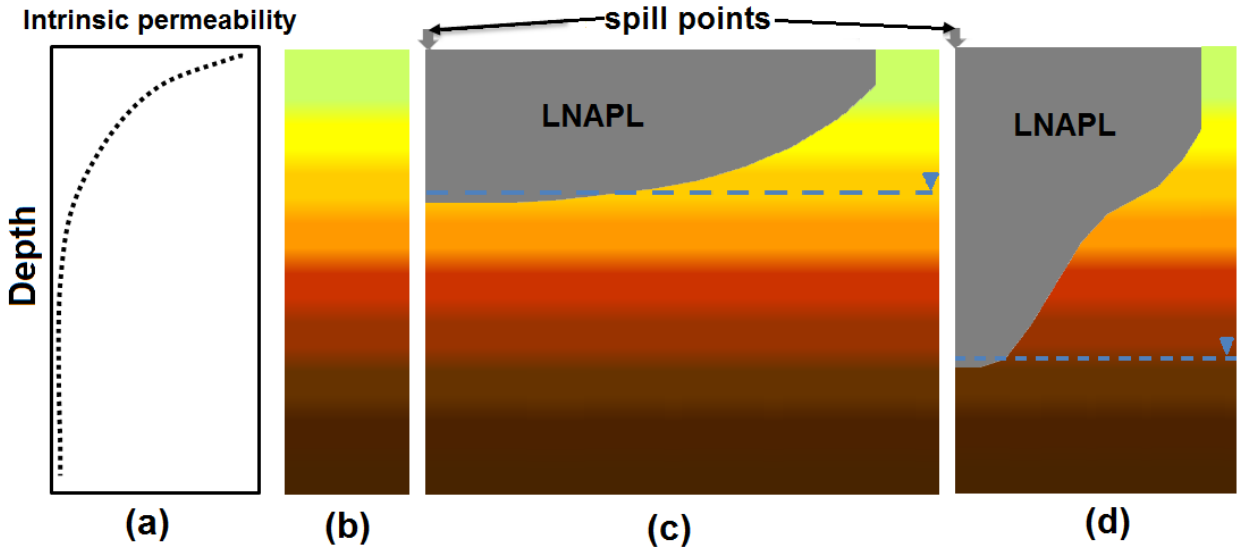

Figure 2.4- a) The 3 to 5 orders of magnitude reduction in peat intrinsic permeability along top 50 cm of peat layer; b) systematic stratification in peat layer; highly permeable undecomposed layer at top and less permeable highly decomposed peat at depth; c) horizontal spread of free-phase plume in wet conditions when water table is shallow; d) horizontal spread of free-phase plume in dry seasons when water table is deep, causing preferential spreading in upper layers due to orders of magnitude higher permeability. It should be noted that NAPL saturation declines moving from plume center to its edge in the graphs.

As a result of soil layering and the dominance of k_h over k_v, the influence of water table on redistribution of a spilled light non-aqueous phase liquid (LNAPL) will be depth-dependent. If a LNAPL spill occurs onto a peatland when the water table is high, occupying the zone of higher intrinsic permeability, LNAPL will readily move downward through the poorly decomposed upper peat layer and spread over the water saturated zone (Figure 2.4c), because the capillary fringe in this zone is typically small given the large pore-sizes (Goetz and Price 2015). However, if a spill occurs when the water table is relatively deep, occupying the zone of low intrinsic permeability, LNAPL will not necessarily move downward to spread over the water table. Instead, at a certain depth, lateral components of the LNAPL velocity vector become larger than the vertical component due to the higher permeability of the upper layers and the characteristic anisotropy,

causing preferential lateral movement of LNAPL above the saturated zone (Figure 2.4d). Johnson et al. (1980) reporting on a crude oil release onto a peatland found LNAPL stayed in the shallow organic layer and did not migrate vertically into deeper peat. Based on their observations where the peat was sufficiently thick, LNAPL migrated laterally within the upper moss layer and did not migrate to the underlying mineral horizon. However, where the organic layer was thin, LNAPL migrated through the peat but scarcely penetrated into the underlying mineral horizon. Although Johnson et al. (1980) did not report the permeability of soil layers, it is most likely that the absence of LNAPL in the mineral layer was because of its lower permeability compared to that of the overlying organic layer.

In addition to the low intrinsic permeability, the increasing pore entry capillary pressure with depth can prevent NAPL percolation into peat pore spaces of the saturated zone. As discussed earlier, during percolation, NAPL preferentially enters larger pores because pore entry capillary pressure is inversely proportional to the pore radius size. Adding this to the fact that maximum pore radius size typically decreases with depth in peatland soils (Goetz and Price 2015), a higher pore entry capillary pressure in deeper peat horizons is expected. This causes, under identical water tension, lower air saturation in deeper peat horizons (Figure 2.5a). Under a similar process, the capillarity preventing NAPL from percolating into water-saturated pores increases with increasing depth. Therefore, the range of pore sizes for which NAPL might have enough pressure to overcome their pore entry pressure and imbibe into, decreases with increasing depth (Figure 2.5b). This is an additional factor preventing downward movement of NAPL that promotes preferential horizontal migration in shallow layers. McGill and Nyborg (1973) reported 2.5 cm of NAPL infiltration into peat in wet conditions compared to ~30 cm of NAPL infiltration in dry conditions. The difference between wet season and dry season observations was due to the shallower water table in the wet season, which prevented light NAPL from percolating into deeper horizons and kept it within the top 2.5 cm of the soil profile. Both values were still small compared to the overall peat thickness at the contaminated site, reaffirming the tendency of NAPL to remain and migrate near the top of the peat layer (see Figure 2.4). The cumulative effect of these factors also leads to shallow NAPL redistribution, even when the spill is due to leakage of buried pipelines. In such cases, deeper releases will initially be constrained by the lower permeability of the deeper layers. Then, NAPL will accumulate and become over-pressured. In a controlled hydrocarbon spill study Kershaw

(1990) found that ~1m^3 of NAPL accumulated around the point of release because of the low permeability of peat at that depth, then moved to the surface whereupon it flowed laterally.

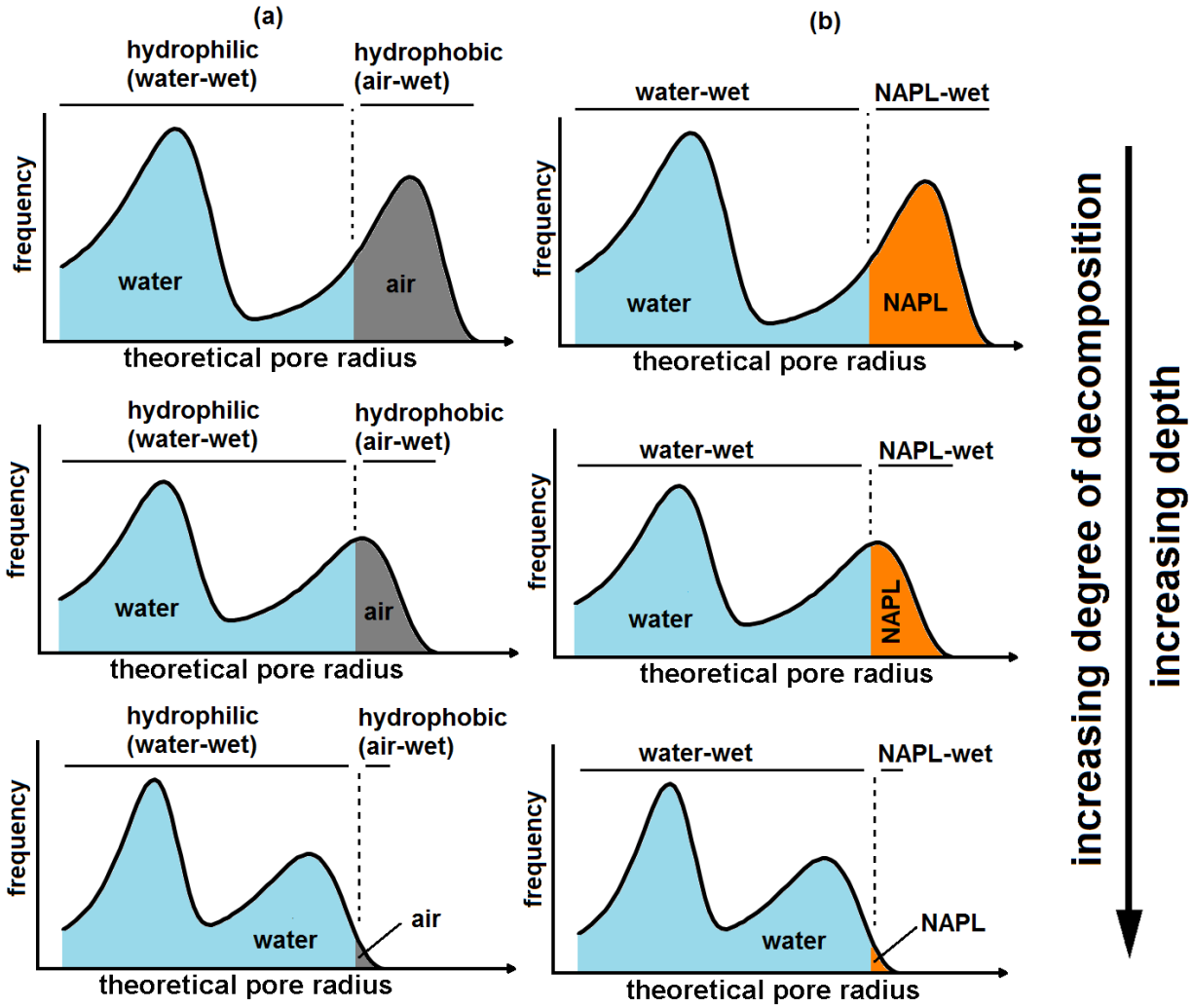

Figure 2.5- Distribution of occupying fluids and pore surface chemistry between macro-pores and micro-pores of peat before and after free-phase contamination under a unique capillary pressure, and while the average pore radius and macro-pores frequency decline with depth due to macro-pore collapse. The graphs demonstrate that the capillarity, which is working against imbibition of air (a) and NAPL (b), increases with increasing depth and degree of decomposition. This causes smaller air/NAPL saturation in deeper peat.

The preferential horizontal migration of NAPL will be favoured even for NAPL that is denser than water (DNAPL). Since DNAPL density is higher than that of water, it typically migrates

below the water table in mineral systems (e.g. Van Geel and Sykes 1994; Brewster et al. 1995). In a situation where DNAPL is released into a peatland when the water table is high, it may penetrate the water table through larger pore spaces. However, when the water table is low, or once it penetrates to a sufficient depth, DNAPL released onto a peatland will be subject to 1) the large systematic reduction in peat intrinsic permeability over a small vertical distance, 2) the anisotropy related to higher horizontal vs. vertical permeability, and 3) the reduced pore sizes in deeper peat associated with higher NAPL entry capillary pressure. These peat characteristics will limit downward migration of DNAPL and cause its preferential lateral movement through shallow peat horizons. In all these examples, NAPL partially occupying pore space influences the aqueous phase flow by reducing its pore-scale effective flow area and influencing its tortuosity.

2.2.3 Peat relative permeability relations and its residual NAPL saturation

The effective permeability of the aqueous phase, k_{effw}, can be dramatically reduced because of NAPL present in macro-pores of peat. This is because the intrinsic permeability of peat is mainly controlled by macro-pores (Baird 1997) and the NAPL present in macro-pores blocks the pore-scale water flow paths, reduces the effective water flow area, and increases the hydraulic tortuosity. Moore et al. (1999) measured the effective water hydraulic conductivity (K_{effw}) of a gas-condensate contaminated peatland and observed it was three to four orders of magnitude less than K_{effw} in an uncontaminated area. The reduction of K_{effw} in the contaminated area is not a surprising observation; however, the order of reduction seems high. To explain such dramatic reduction, consider that under drying conditions macro-pores in an uncontaminated peat layer tend to drain first (Figure 2.6a). These macro-pores can fill with water during a precipitation event and readily transfer the percolating water (Figure 2.6b). Following the release of NAPL onto a peatland, NAPL percolates into macro-pores and alters the wetting tendency of the surface of these pores to NAPL-wet (Figure 2.6c and Figure 2.6d). After this alteration, during a dry period, since air is the non-wetting phase for both water-wet and NAPL-wet pores, it will enter the pore space through largest pores of both water-wet and NAPL-wet pores (Figure 2.6c). In wet periods where water infiltrates into the pore space due to precipitation, water will be the non-wetting phase for NAPL-wet pores. Thus, water will percolate into the largest NAPL-wet pores (Figure 2.6d). Before NAPL

percolation, the majority of water flow in peat soils takes places through macro-pores (Carey et al. 2007; Quinton et al. 2008). However, after NAPL percolation, the alteration of macro-pore surface wetting tendency to the NAPL-wet state causes a higher residual NAPL saturation (S_{Nr}) in these pores (Fatt and Klikoff 1959; Donaldson et al. 1969; Owens and Archer 1971) during water imbibition. The residual NAPL restricts water flow through macro-pores (Figure 2.6d), leading to the substantial reduction of K_{effw}. It should be noted the reduction of K_{effw} due to residual NAPL also happens in water-wet mineral aquifers. However, it is less dramatic in mineral soils compared to peat. For example, k_{effw} of Torpedo sandstone is between 8%-80% of intrinsic permeability when S_{Nr} is ~20%-40% (Owens and Archer 1971) and k_{effw} of unconsolidated Houston sand is ~10%-55% of the intrinsic permeability at S_{Nr} ~ 25%-35% (Poston et al. 1970, Fig.10). In Berea sandstone k_{effw} is 11.7% of intrinsic permeability at S_{Nr} = 38% (Miller and Ramey 1985). The k_{effw} of Berea sandstone at 50% NAPL saturation is ~1% of intrinsic permeability (Brooks and Corey 1964; Lenhard and Parker 1987). These examples show that reduction of k_{effw} in mineral unconsolidated/consolidated porous media at residual NAPL saturation conditions or at NAPL saturation ~50% is less than two orders of magnitude, which is much less than the 3 to 4 orders of magnitude reduction observed in peat. However, observations have also shown that wettability alteration to NAPL-wet enhances k_{effw} at residual NAPL saturation (Owens and Archer 1971; Donaldson and Thomas 1971), which means the higher reduction of k_{effw} in peat soils compared to that in mineral soils is not necessarily because of the wettability alteration in peat; it might be either because of the higher S_{Nr} in macro-pores, or due to a different connectivity between larger pores and small pores in mineral soils versus peat soils. Further research is needed to clarify the cause-effect relationship between peat pore structure, wettability, and its k_{effw}.

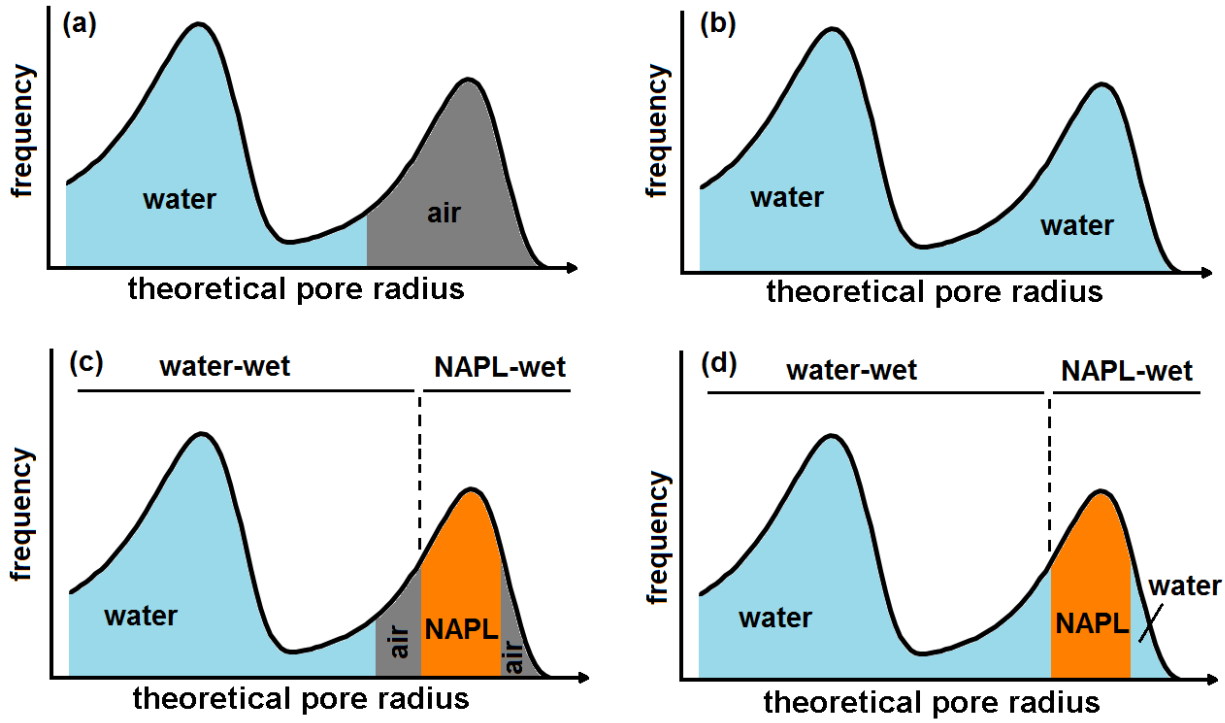

Figure 2.6- Distribution of phases present in peat pore space before and during water percolation. a) Distribution of water and air within an uncontaminated unsaturated zone before water percolation; b) distribution of water in uncontaminated peat pore space during a water percolation event; c) distribution of water, air and NAPL within the unsaturated zone before water percolation for a NAPL-contaminated peat layer; and d) distribution of water and NAPL in peat pore space during water percolation event for a NAPL-contaminated peat layer.

Under the conditions of reduced K_{effw}, water infiltration from above the contaminated peat layer is restricted. This was observed by Everett (1978), who attributed the reduction of water infiltration rate to the alteration of pore surface wettability, although s/he did not quantify it. The reduced water infiltration rate into NAPL contaminated peat can result in water accumulating at the peatland surface, ponding over LNAPL-contaminated peat soil (McGill and Nyborg 1973), which shows that in spite of the buoyant force of LNAPL and water pressure being higher than LNAPL pressure, LNAPL can remain below the water table. This illustrates the resistance to water flow into peat pore spaces occupied by NAPL, and to drainage of NAPL from it. It should be noted

that such high LNAPL saturation below the water table occurs when pore surfaces are preferentially wet by NAPL, rather than water (Al-Futaisi and Patzek 2004). Similar to the reduction of water infiltration, the groundwater discharge/recharge rate can decline in NAPL-contaminated peat due to the reduction K_{effw}. Alterations to infiltration and recharge via the groundwater flow regime could alter the peatland's water balance in the contaminated area.

S_{Nr} and K_{effw} control the maximum extent of the free-phase plume. As the finite volume free-phase plume grows, the average saturation of NAPL declines, causing gradual reduction of NAPL effective permeability (k_{effN}). Within a time period, which depends on several factors including P_c-S-k_r relations and might range between weeks to years and, NAPL saturation will reach- S_{Nr}, in which k_{effN} equals zero. At this state, the free-phase plume stops growing and its shape and extent stabilizes. The stabilized plume refers only to the condition of the free-phase product; at this stage it acts as a contamination source that releases soluble toxic hydrocarbon compounds into a dissolved-phase plume (Figure 2.7).

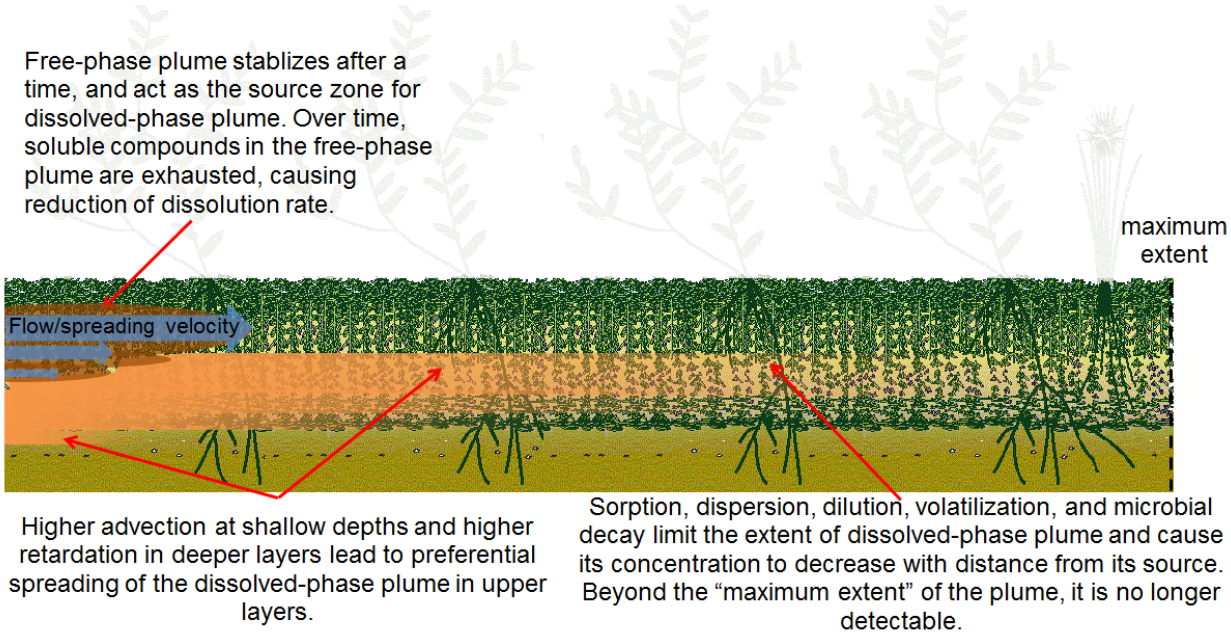

Figure 2.7- Conceptual model of free-phase and dissolved-phase fate and transport through peatlands showing preferential spread of plumes in shallow peat horizons, and reduction of concentrations with distance from source zone in the dissolved-phase plume. Background image of the figure is modified from http://www.gret-perg.ulaval.ca/fr/a-propos/tourbieres/hydrologie/acrotelme-et-catotelme/ with permission.

2.3 Dissolved-phase transport through the peatland

Dissolution is the partitioning of hydrocarbon contaminants from free-phase into aqueous phase in contact with liquid hydrocarbon (Kim and Corapcioglu 2003). After NAPL moves into a groundwater system, the free phase hydrocarbon plume establishes interfaces with the flowing aqueous phase, causing interfacial mass transfer between them. Due to the partitioning of water-soluble hydrocarbon molecules from NAPL into the aqueous phase, a dissolved-phase hydrocarbon plume is formed within the groundwater system (Newell et al. 1995). Consequently, the free-phase plume becomes the source for contamination of the aqueous phase by water-soluble hydrocarbon compounds (Kim and Corapcioglu 2003; Essaid et al. 2011; Essaid et al. 2015). The dissolution rate is a function of interfacial area between the aqueous phase and NAPL (Bradford and Abriola 2001), as well as the flow rate and Peclet number (Miller et al. 1990; Knutson et al. 2001; Dillard et al. 2001), temperature (Imhoff et al. 1997), and NAPL composition (Geller and Hunt 1993). Based on Raoult's law, more soluble compounds dissolve preferentially in the aqueous phase compared to less soluble compounds, thus are depleted earlier from the source (Geller and Hunt 1993). Therefore, the NAPL composition shifts toward less soluble hydrocarbon compounds, which can eventually lead to water-soluble organic compounds being completely depleted from the source, leaving non-soluble and very slowly dissolving compounds in the NAPL. The transport of dissolved organic hydrocarbon molecules through the groundwater system is controlled mainly by advection, dispersion, diffusion and sorption processes (Mackay et al. 1986; Roberts et al. 1986). The phenomena affecting the fate and transport of organic solutes in groundwater systems can be expressed by

$$\frac{\partial}{\partial t}\left(\varepsilon S_f C_{if}\right) = -\nabla.\left(q_f C_{if}\right) + \nabla.\left(\varepsilon S_f D_{if}.\nabla C_{if}\right) + K_{if} \qquad \textbf{Equation 2.2}$$

where C_{if} is concentration of compound i in phase f [ML^{-3}], q_f is specific /discharge [LT^{-1}], ε is porosity [L^3L^{-3}], S_f is saturation of phase f in the pore space [L^3L^{-3}], D_{if} is hydrodynamic dispersion [L^2T^{-1}], K_{if} is the rate of interface mass exchange processes [$ML^{-3}T^{-1}$] including volatilization, dissolution, biodegradation, and sorption (Pinder and Abriola 1986). By assuming saturated conditions, one dimensional transport, no variations of discharge rate, hydrodynamic dispersion

and porosity, and by considering adsorption as an inter-phase partitioning process, the equation for a solute simplifies to

$$\left(1+\frac{\partial S}{\partial C}\right)\frac{\partial C}{\partial t}=-\nabla.\left(vC\right)+\nabla.\left(D.\nabla C\right)+K \qquad \textbf{Equation 2.3}$$

where S is the adsorbed mass concentration [MM^{-1}], v is average linear flow velocity [LT^{-1}] and is equal to ratio of specific discharge and porosity, D is hydrodynamic dispersion [LT^{-2}], and K is the volatilization, biodegradation, and dissolution rate [$ML^{-3}T^{-1}$]. This equation is widely used to study the fate and transport of inorganic and organic solutes through groundwater systems (Gillham et al. 1984; Clement et al. 1998; Reeve et al. 2001; Guerin et al. 2002; Rubio et al. 2008). However, there are challenges in studying dissolved-phase hydrocarbon transport through peat and peatlands using this approach that leads to the inapplicability of Equation 2.3. The challenges arise from the dual porosity pore structure of peat soil (Hoag and Price 1997), the presence of dissolved organic carbon (DOC) in peat pore water (Freeman et al. 2001) and heterogeneity of peat pore surface (Cohen et al. 1991) in a vertical soil profile.

A primary challenge is the dual porosity pore structure of peat soils. Hoag and Price (1995; 1997) described *Sphagnum* peat as a dual porosity medium in which pore spaces are composed of a connected network of pores transmitting water and solute, which constitute the active porosity, and a group of dead-end pores characteristic of *Sphagnum*, forming inactive porosity. Retardation factor is the ratio of the average velocity of water to that of solute (Magee et al. 1991; Fry et al. 1995; Martin-Hayden and Robbins 1997). In peat, water flow and advective solute transport takes place through the active porosity; despite water flow, solute transport is influenced by the diffusive transport that occurs between active and inactive porosities due to a chemical gradient present between interconnected and dead-end pores (Hoag and Price 1995). Consequently, average linear velocity of water parcels, in peat pore space, is higher than the average linear velocity of solute parcels. This can lead to a retardation factor higher than 1, even without adsorption. Thus, for a non-conservative solute, the retardation is a lumped result of the solute adsorption onto pore surfaces and solute diffusion into inactive porosity (see Figure 2.8). Hoag and Price (1997) observed retardation of a non-reactive conservative tracer (Cl) through peat cores, which was

attributed to solute diffusion into the inactive porosity. The retardation of solute by this mechanism increases with the ratio of inactive to total porosity, thus in peatlands increases with depth (Hoag and Price 1997; Quinton et al. 2008). Since peat hydraulic conductivity typically declines with depth (Boelter 1965) and solute retardation caused by dead-end pores typically increases with depth (Hoag and Price 1997), a higher solute mass flux at the top of the saturated layer is favoured. This results in a preferential spreading of the dissolved-phase, such as hydrocarbon plumes, at and near the top of the saturated zone (Figure 2.7). The lack of a term for retardation of solutes in immobile zone (by diffusion), and inability of predicting solute concentration in dead-end pores, is why Equation 2.3 is inapplicable in some peat soils.

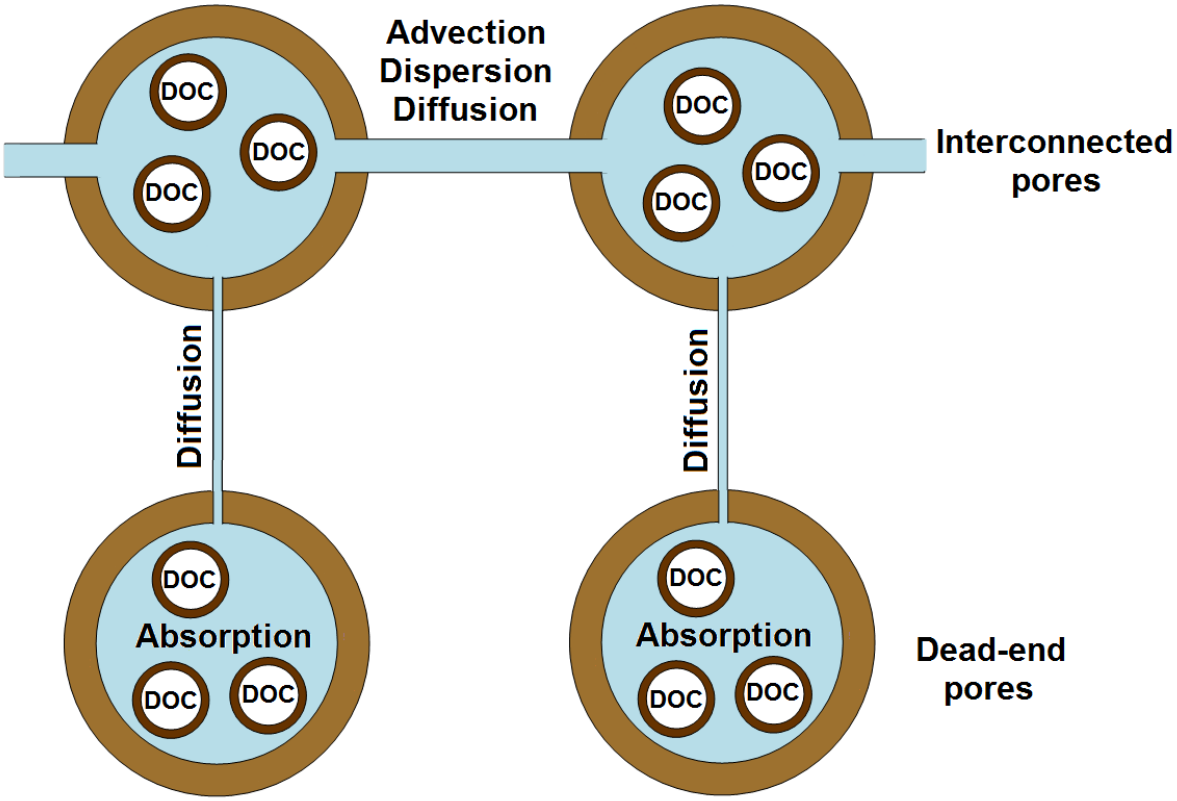

Figure 2.8- Schematic of the fate and transport of dissolved hydrocarbon solutes in peat soils showing advective-diffusive mass transport through the interconnected active porosity, and retardation of solute molecules due to diffusion into inactive porosity and adsorption onto the surface of interconnected and dead-end pores. Adsorption of hydrocarbon to the surface of DOC, which occurs naturally in peatland pore water, reduces the mass of hydrocarbon solutes available for adsorption to the pore surfaces; this leads to a reduction of the apparent adsorption coefficient.

The peat pore structure and the diffusive mass transfer between connected pores and dead-end pores necessitates adding another sink/source term to Equation 2.3, representing the rate of mass transfer between active and inactive porosities. Mobile-Immobile (MIM) models consider both solute transport through the mobile region (active porosity) and mass exchange between mobile and immobile (inactive porosity) regions (Van Genuchten and Wagenet 1989). Using these models in peat requires determination of parameters controlling solute mass exchange between mobile and immobile regions, as well as the proportion of these regions (Rezanezhad et al. 2012a). The mass exchange parameter remains a challenge for modeling dissolved-phase transport of hydrocarbons in peat soils, since it is not available for hydrocarbon solutes in peat.

First order solute mass exchange rate in MIM models is represented with a parameter α [T^{-1}], which is the coefficient of first order mass exchange between mobile and immobile zones. Several studies have characterized and reported α in mineral soils (Van Genuchten and Wierenga 1976; Gaudet et al. 1977; Jacobsen et al. 1992) showing that it is not unique and varies with soil type. Rezanezhad et al. (2012a) obtained different α values for chloride and sodium, and Hatfield et al. (1993) determined different values of α for benzene and toluene during transport studies in soil columns, both confirming that α, in addition to the type of soil, is a function of solute. Up to now, little attention has been paid to the transport of hydrocarbon solutes, especially monocyclic aromatic compounds such as benzene, toluene, ethylbenzene, and xylene (BTEX) through peat soils. Therefore, not surprisingly, values of the mass exchange parameter (α) for dissolved hydrocarbons in peat soils are not available. Apart from these dual-porosity challenges, adsorption is also an important phenomenon controlling the retardation of solutes during transport, being defined as the partitioning of a solute from an aqueous phase onto the soil solid surface (Calvet 1989). Adsorption of hydrocarbon solutes onto soil increases with increasing organic carbon content of the soil (Schwarzenbach and Westall 1981; Karickhoff 1984; Calvet 1989). Peat has a high organic carbon content around 50% (Andriesse 1988; Smith et al. 2004). Consequently, peat can exhibit a high adsorption partitioning coefficient toward dissolved hydrocarbon compounds compared to mineral aquifers, which have an organic carbon fraction around 2% (e.g. Kile et al. 1995), and can be an effective filter for removal of dissolved hydrocarbon from contaminated

water (Moore and Philips 1975; Moore et al. 1976; Zytner et al. 1989; Cohen et al. 1991; Guerin et al. 2002). For the sediments in which organic carbon mass fraction is higher than 0.1%, Schwarzenbach and Westall (1981) and Karickhoff (1984) described adsorption of organic solutes onto soil organic matter as

$$K_d = K_{OC} f_{OC} \qquad \textbf{Equation 2.4}$$

where K_d is the partition coefficient of the soil surface [L^3M^{-1}], K_{OC} is the partition coefficient of pure organic carbon [L^3M^{-1}], and f_{OC} is the mass fraction of organic carbon within solid phase [MM^{-1}]. Each organic solute has a K_{OC} value that increases as water solubility of the organic solutes decreases (Calvet 1989). Using Equation 2.4 requires the assumption that K_{OC} is constant, thus the organic matter in the medium must be homogeneous (Appelo and Postma 2004). This assumption is unlikely in a natural peat deposit. Peat is composed of several groups of organic substances including waxes, lignins, humic acids and cellulose (Smith et al. 1958). For a specific solute, K_{OC} of lignin and humic acid and cellulose are completely different (Garbarini and Lion 1986). Grathwohl (1990) observed as the ratio of hydrogen to oxygen in organic matter increases, K_{OC} of trichloroethylene (TCE) rises. Zytner et al. (1989) measured adsorption isotherms of perchloroethylene (PCE) for different soils and observed higher K_{OC} for peat compared to another type of organic soil. Cohen et al. (1991) also observed that humified peat soils have higher benzene and toluene K_{OC} compared to less decomposed peat soils. Since peat soil in different peatlands can have different fractions of lignin, cellulose and humic acid, and the fraction of these molecules in peat soil varies with increasing depth and humification (Delicato 1996), peat K_{OC} varies both within and between peatlands. Therefore, estimating peat K_d using Equation 2.4 can result in an error when calculating the total adsorbed mass and the solute retardation, and consequently its spreading velocity. It necessitates measuring the adsorption partitioning coefficient for peatland types and at depths corresponding to different degrees of humification. In addition to the heterogeneity of peat chemical properties, the dissolved organic carbon (DOC) present naturally in peat pore water influences the sorption of organic solutes onto peat pore surfaces.

DOC is an organic matter that can compete with pore surface adsorption sites for adsorption of organic molecules (Hassett and Anderson 1982) and can influence the solubility of hydrocarbon

solutes in the aqueous phase (Newell et al. 1995) facilitating the transport of these solutes. The process has been referred as cotransport of dissolved hydrocarbons and DOC (Kögel-Knabner and Totsche 1998; Tatalovich et al. 2000). This reduces the amount of solute available for mass adsorption onto peat solids (Figure 2.8) and thus decreases the apparent (effective) peat adsorption partitioning coefficient (Cram et al. 2004) by increasing the mass of hydrocarbon solute present in the aqueous phase. The effective peat partitioning coefficient is obtainable through correcting the K_{OC} value (Gschwend and Wu 1985) knowing the partitioning coefficient of hydrocarbon molecules on DOC, referred as K_{DOC} and considering that K_{DOC} is not necessarily the same as peat K_{OC} (Cram et al. 2004).

2.4 Volatilization and microbial decay of hydrocarbons

The release of hydrocarbons from the free-phase and dissolved-phase into a vapour-phase within the unsaturated zone is referred as volatilization (Mercer and Cohen 1990). Volatilization is the primary attenuating process immediately following NAPL percolation into a contaminated unconfined aquifer (Chaplin et al. 2002). The rate of volatilization is a function of the chemical composition of the plume, the pore-size distribution of the matrix and environmental conditions (Wilkins et al. 1995; Newell et al. 1995). With respect to chemical composition, short-chain hydrocarbon compounds have higher vapour pressure compared to long-chain hydrocarbons (Danesh 1998), and are therefore the primary volatilizing compounds after the spill (Essaid et al. 2011). Over time the volatile compounds become depleted within the free-phase plume (Newell et al. 1995), and the volatilization rate decreases (Chaplin et al. 2002). The volatilization rate is also controlled by the air (gas) phase permeability of the matrix, which is a function of pore-size (Grant and Groenevelt 1993) and air-filled porosity. Given the abundant large pores in near-surface *Sphagnum* peat of bogs and poor fens (Goetz and Price 2015) compared to mineral soils, coupled with the typically shallow depths to spilled hydrocarbon (Figure 2.7), volatilization losses could be large (Parker 2003). This will be amplified by turbulent surface wind that causes pore-air flow beneath surface and enhances gas exchange in coarse-textured soils (Ishihara et al. 1992). In boreal peatlands during the cold season, the low ambient temperature decreases the volatilization rate by reducing the vapour pressure of hydrocarbons, and the snow cover reduces free-air circulation in

the unsaturated zone, which also reduces vapour loss (Moore et al. 1999). During other seasons the rate of volatilization increases with increasing magnitude and frequency of water table fluctuation (Thomson et al. 1997). Given the presence of NAPL at shallow depths associated with the peat pore structure and the high water table, volatilization losses will likely be higher than in mineral groundwater systems with a deeper (and often more stable) water table, where NAPL migrates further below the surface. The magnitude and frequency of water table fluctuation varies between peatland types, so for a given spill volume and composition, the dominance of volatilization might vary between them.

Biodegradation also removes hydrocarbon mass and limits the spread of the dissolved-phase plume. Biodegradation refers to the biological degradation of organic molecules within the aqueous phase that is facilitated by soil microbial communities (Newell et al. 1995). Natural microbial communities present in boreal peat degrade peat organic matter by using it as a nutrient source and electron acceptor and donor in the biological reactions. Due to similar constituents of peat and crude oil, these microbes can efficiently biodegrade short- to long-chain alkane compounds of spilled crude oils (Kelly-Hooper et al. 2013). The rate of biodegradation depends on the type and availability of electron acceptors. In peatlands, the unsaturated zone is thin, but can contain a significant amount of hydrocarbon as noted above. The frequent episodic water table fluctuations and a seasonal draw-down of the water table, enhances the bulk flow and exchange of oxygen into the unsaturated zone (Limpens et al. 2008). This leads to a sustainable aerobic condition where biodegradation of hydrocarbon compounds, e.g. alkanes and BTEX, is relatively rapid compared to the anaerobic condition (Barker et al. 1987; Suarez and Rifai 1999; Salminen et al. 2004). In contrast, in mineral aquifers an aerobic condition is not sustainable, and anaerobic/methanogenic condition and oxygen depleted area might establish and grow in the unsaturated zone (Bekins et al. 1999; Chaplin et al. 2002; Essaid et al. 2011). Below the water table the pore-water has a low redox potential as oxygen is rapidly depleted by microbes (Andersen et al. 2013). Within this zone, microorganisms catalyze the redox reactions sequentially using different electron acceptors (nitrate, manganese, iron, sulphate, and organic matter), and grow biomass by metabolism of the contaminants (Essaid et al. 2015) and peat organic matter (Limpens et al. 2008). Thus, the water chemistry governs the presence and activity of the highly diverse heterotrophic microbes living in peatlands (Andersen et al. 2013), which oxidize organic matter

(including hydrocarbons; Moore et al. 1999) degrading it into CO_2, CH_4 and DOC (Limpens et al. 2008). In an ombrotrophic setting (i.e. bog) the limited input of base cations means their respective roles as a source of electron acceptors are more quickly depleted compared to minerotrophic peatlands like fens, thus methanogenesis may establish sooner. However, the low pH of bogs, which is due to the low capacity of these peatlands to buffer organic acids released by decaying vegetation (Zoltai and Vitt 1995), is less suitable for methanogenic archaea (Lai 2009). The sequential depletion of electron acceptors has been shown to be an indication of dissolved-hydrocarbon biodegradation in mineral aquifers (Bennett et al. 1993). Since degradation of naturally occurring organic compounds continuously takes place in peatlands, the sequential depletion of electron acceptors might be not a good indication for biodegradation of dissolved-phase hydrocarbon molecules. However, an increase in microbial population (Moore et al. 1999) and shift in the microbial community (Rezanezhad et al. 2012b) might be good indicators of hydrocarbon degradation in contaminated peatlands.

The cumulative effect of sorption, volatilization, and biodegradation of the dissolved hydrocarbon will eventually match the diminishing rate of dissolution from the free-phase product, and the dissolved-phase plume will stop growing, and will stabilize at a maximum extent in a steady-state condition (Figure 2.7). This distance in minerotrophic peatlands might be longer due to their typically higher water velocity (e.g. Price and Maloney 1994). However, due to the shallower water table enhancing both volatilization and aerobic biodegradation in the unsaturated zone, these peatlands might overcome the hydrocarbon contamination sooner than in ombrotrophic settings.

2.5 Summary and Conclusion

To understand the behavior of a free-phase plume it is critical to acquire the multiphase flow relations of the NAPL in the impacted peat soil. Unfortunately, this has received little attention. To fill this knowledge gap, it is essential to obtain realistic P_c-S-k_r relations for peat soils; not an easy task given the compressible and unconsolidated nature of peat soils, and the strong hysteresis in these relations. The cumulative effect of larger horizontal permeability and smaller pore entry

pressure near the peat surface will cause preferential horizontal migration of spilled NAPL at shallower, more permeable peat horizons (Figure 2.7). Over time free-phase will achieve residual saturation and will migrate no further (Figure 2.7).

With respect to dissolved hydrocarbons, the reduction of permeability associated with increasing inactive porosity with depth leads to stronger advection and weaker retardation of dissolved hydrocarbons near the peat surface, compared to that in deeper peat horizons (Figure 2.7). The influences of peat permeability and pore-structure variations on transport processes that promote plume migration in shallow peat horizons are similar in many respects for free-phase plume and solutes, including dissolved hydrocarbons and NaCl, for example. However, while dissolved plumes can be retarded by the inactive porosity commonly associated with peat, NAPL movement will be unaffected by this dual porosity because the strong capillarity of micro-pores prevents NAPL intrusion.

Solute retardation in a natural peat setting is controlled by various processes including solute diffusion into inactive porosity, their adsorption onto peat organic matter, and cotransport with DOC. The diffusion into inactive porosity necessitates the use of a mobile-immobile (MIM) transport model for peat. This requires a matrix diffusion mass exchange parameter, which has not been measured for hydrocarbon solutes in peat. In addition to matrix diffusion and adsorption, volatilization and biodegradation retard the migration of dissolved-phase hydrocarbon. Shallow spread of free-phase plume and frequent fluctuation of water table enhance aeration of shallow peat layers, which promotes both of these processes.

Depending on the rate of hydrocarbon dissolution from the free- to the aqueous phase, the aqueous phase discharge rate, and rate of solute retardation through the aforementioned mechanisms, the dissolved-phase plume could reach a steady-state condition and stop growing (Figure 2.7). Over time, the rate of hydrocarbon dissolution will decline due to the depletion of water-soluble compounds from free-phase plume, and the dissolved-phase plume will shrink. Given that both plumes stop growing after reaching their maximum extent, and then shrink with time, hydrocarbons spilled in sufficiently large and remote peatlands will likely be held within the peatland and not pose a risk to surrounding or down-gradient ecosystems. Consequently, managers will have the option to determine if the potential threat to downstream aquatic systems justifies

digging up the spill, and in the process destroying peatland function. Due to differences in geochemical properties like pH, availability of reductants, water table depth and fluctuation, and the physical character of the peat, the hydrocarbon flux and fate will be different between different types of peatlands, and even within peatlands. In fens, the water table is both higher and less variable (Price and Maloney 1994). This will keep spilled LNAPL closer to the surface where the horizontal element of the permeability tensor is greatest, and its transport rate will be relatively high. The more limited range of water table fluctuations in fens, compared to bogs and swamps, will lead to thinner smearing zone of the free-phase hydrocarbon in fens.

While this review has synthesized our understanding of the properties of peat and peatlands based on relatively scant information on the behavior of NAPLs and hydrocarbons within organic soils, empirical data are necessary to validate many processes and establish rates that govern their fate and transport. The gaps of knowledge in the empirical data are multiphase flow and P_c-S-k_r relations, S_{Nr}, K_{effw} in the zone impacted by NAPL, matrix diffusion coefficient (α) of hydrocarbon solutes, organic carbon partitioning coefficient (K_{OC}) of hydrocarbon solutes, partitioning coefficient of these solutes on DOC (K_{DOC}), and spatial variations of these parameters in peat soils and peatlands. Failing to address these data gaps will lead to poor estimation of NAPL and dissolved-phase plume distributions and transport rates in contaminated peatlands. Filling these data gaps is critical to manage hydrocarbon contamination and to predict the trajectory of their evolution in contaminated peatlands. The data are needed to better estimate the maximum extents of free-phase and dissolved-phase plumes, rates of free-phase and dissolved-phase plume growth after the spill, and the time until plumes start shrinking. This paper provides a conceptual model for hydrocarbon fate and transport in peatlands, and is a first step in providing information for regulators and land managers charged with assessing and remediating spills onto peatland systems.

2.6 Acknowledgements

We would like to thank Wetland Hydrology Lab, especially James Sherwood for assistance in the lab. Research was funded by a NSERC Discovery Grant to Dr. Price.

3 The role of peat depth and state of decomposition on benzene and toluene adsorption: Implications for their fate and transport in peatlands

3.1 Introduction

Peatlands located adjacent to hydrocarbon production areas or along ~800,000 km of transport pipelines in Canada (NRC, 2018), are at risk of petroleum hydrocarbon contamination. In the case of hydrocarbon spills onto peatland, the ability of water-soluble hydrocarbons in shallow groundwater to move to down-gradient aquatic systems, or to drinking water sources, is unknown. Canadian crude oils are composed of different hydrocarbon groups including saturates and aromatics (Westlake et al. 1974; Brooks et al. 1988; Yang 2011). Saturates represent alkanes and cycloalkanes, and aromatics are mono-cyclic and poly-cyclic aromatics (Garrett et al. 1998). The concentration of the mono-aromatics such as benzene, toluene, ethylbenzene, and xylenes (BTEX) in Canadian bitumen is more than 8% (w/w) (Selucky et al. 1977, 1978). The average concentration of aromatics in Canadian gasoline was more than 25% between 1995-2007, while the volumetric concentration of benzene, in 2007, was up to 2.97% (Environment Canada, 2008). These hydrocarbon compounds and groups have different solubilities in water. BTEX comprises monoaromatic hydrocarbons with relatively high solubility, so after a spill they readily dissolve and move in groundwater. BTEX concentration in dissolved-phase plumes depend on many factors including BTEX mass fraction in the spilled liquid, groundwater discharge rate, and physical and chemical properties of the aquifer material. The concentration can potentially exceed 65 mg/L (Kao and Wang 2000). Exposure to BTEX can cause severe health problems; benzene has been shown to be carcinogenic and cause leukemia in humans (World Health Organization 2004).

Among BTEX compounds, benzene and toluene have higher solubility in water (McAuliffe 1966) and lower adsorption tendencies to soil organic carbon compared to ethylbenzene and xylenes, thus experience weaker retardation in flowing groundwater (e.g. Seagren and Becker, 2002). Adsorption of benzene and toluene onto mineral soils has previously been studied (e.g.

Karickhoff et al. 1979; Rogers et al. 1980; Chiou et al. 1983; Seip et al. 1986). However, to date, the few studies that have investigated their adsorption onto highly organic natural soils, show that benzene and toluene adsorption vary in equilibration time, on the adsorption model used, and on adsorption model coefficients (e.g. Cohen et al. 1991; Zytner et al.1994; Rutherford et al. 1992). This variability is likely related to the chemical composition of peat organic matter, which varies with depth, since the degree of humification affects the fraction of cellulose, humic acid (HA), and lignin (Delicato 1996). These compounds have different affinities toward organic pollutants, consequently different adsorption coefficients. Chemical composition of peat may also be a function of its botanical origin, for example sedge- vs. moss-dominated peat. The combination of different affinities for peat type and state of decomposition (Table 3.1) implies that the adsorption of benzene and toluene is likely to vary within peat profiles, and within and between peatlands.

In addition to adsorption coefficients varying with peat type and degree of humification, competition for adsorption sites between BTEX compounds affects sorptivity. Very few studies have investigated this competition in organic or mineral aquifer material. Stuart et al. (1991) compared the results of competitive adsorption in a transport column experiment, to non-competitive batch adsorption tests for a sandy loam soil, with organic carbon content (f_{OC}) of 0.6%. They obtained significantly higher and lower adsorption coefficients, respectively, for benzene and xylenes, and attributed these variations to competitive adsorption. However, the mass fraction and the quality of organic carbon in such soils are not similar to those of peat; this may cause fundamentally different competitive adsorption behavior. To date, the competitive adsorption of organic pollutants, specifically BTEX compounds, has received little attention, and as it relates to highly organic soils, including peat, has received no attention. Using average K_{OC} values reported for benzene and toluene adsorption, based on mineral soils with low f_{OC}, can introduce error in estimating the adsorption of benzene and toluene in peat and peatlands. Therefore, given the importance and uncertainty associated with benzene and toluene behavior in organic soils, the specific objective of this study is to characterize benzene and toluene adsorption on *Sphagnum* dominated peat, including their competitive behavior, and assess these against the limited set of values reported in the literature. The results will provide new insights into the anticipated behavior of dissolved-phase hydrocarbon plumes in peatlands.

Table 3.1- Summary of studies that have explored adsorption of BTEX onto peat soils; *L* and *F* respectively denote linear and Freundlich adsorption models; K_d is the linear adsorption coefficient [L^3M^{-1}]; K_F is Freundlich adsorption coefficient; K_{OM} is organic matter partitioning coefficient [L^3M^{-1}], and K_{OC} is organic carbon partitioning coefficient [L^3M^{-1}]. In the peat type column, HD is highly decomposed, MD is moderately decomposed, and UD is undecomposed.

Study	Adsorbate	Peat type	model	Model coefficient(s)	Equilibrium time (h:hours, m:minutes, d:days)
Cohen et al. (1991)	Benzene	HD woody peat	L	K_{OC}=201****	24 h
		MD *Nyphia Sagittaria* peat	L	K_{OC}=91.7****	24 h
		MD spruce woody decot peat	L	K_{OC}=59.9****	24 h
		MD grass-sedge-fern peat	L	K_{OC}=73.5****	24 h
		MD *Nymphaea-Sagittaria* grass sedge peat	L	K_{OC}=65.4****	24 h
		UD *Sphagnum* Peat	L	K_{OC}=61.6****	24 h
	Toluene	HD woody peat	L	K_{OC}=107****	12 d
		MD *Nyphia Sagittaria* peat	L	K_{OC}=90.5****	12 d
		MD spruce-woody dicot peat	L	K_{OC}=98.7****	12 d
		UD *Sphagnum* Peat	L	K_{OC}=98.0****	12 d
Zytner et al.(1994)	Benzene	Peat moss	L	K_d=13.0L/kg (K_{OC}=28.9L/kg**)	92 h
	Toluene	Peat moss	F	K_F=74.06(mg/kg)(L/mg)$^{1/n}$*** 1/*n*=0.83	92 h
Rutherford et al. (1992)	Benzene	extracted peat	L	K_{OM}=20.8 L/kg (K_{OC}=41.6 L/kg*)	3-5 d
	Benzene	Peat	L	K_{OM}=12.5 L/kg (K_{OC}=25 L/kg*)	3-5 d
Rael et al. (1995)	Benzene	Peat	F	K_F=0.002(mg/g)(L/mg)$^{1/n}$*** (K_F=2 (mg/kg)(L/mg)$^{1/n}$*****) 1/*n*=1.78	72 h
Costa et al. (2012)	Benzene	Peat	F	K_F=0.077 (µg/g)(L/µg)$^{1/n}$*** (K_F=134.8 (mg/kg)(L/mg)$^{1/n}$*****) n=.925 (1/*n*=1.081)	2 h
	Toluene	Peat	F	K_F=0.172(µg/g)(L/µg)$^{1/n}$*** [K_F =217.7 (mg/kg)(L/mg)$^{1/n}$*****] *n*=0.967 (1/*n*=1.034)	2 h
Yerushalmi et al.(1999)	Benzene	Peat moss	L	K_d=10.1 L/kg (K_{OC}=22.4L/kg**)	~72 h
	Toluene	Peat moss	L	K_d=24.1 L/kg (K_{OC}=53.6L/kg**)	~72 h
Xing (1998)	Toluene	Peat	F	K_F=74.3(µg/g)(mL/µg)$^{1/n}$*** [K_F =74.3 (mg/kg)(L/mg)$^{1/n}$*****] 1/*n*=0.846	2 d

Calculated here assuming K_{OM}=0.5K_{OC}; **Calculated here assuming organic matter content (f_{OM}) is 0.9 (K_d=0.9K_{OM}), and K_{OM}=0.5K_{OC}; ***Units are determined here using units within corresponding study; ****Units are not available in the published work; ** Converted value in a converted unit.**

3.2 Materials and Method

3.2.1 Soil collection, preparation, and properties

Two peat cores (I and II) with 30 cm diameter and 40 cm length were extracted from a bog peatland in Southern Ontario (43.9° N, 80.4° W). Both cores were collected within 0.5 m of each other. The cores were frozen on the day of extraction, both to preserve them and to facilitate sectioning. Each core was sectioned into four 10 cm thick segments, to capture increasing degrees of decomposition with depth. The segments represent depth intervals of 0-10 cm, 10-20 cm, 20-30 cm, and 30-40 cm. Each segment was air-dried, and was ground until the peat particles passed a 1 mm sieve. This was intended to eliminate the effect of pore structure on adsorption time and adsorption capacity, and to homogenize the adsorbents, while preserving the variations of peat surface chemistry.

To predict the benzene and toluene retardation factors in peat, the mobile (θ_{mobile}) and immobile ($\theta_{immobile}$) water contents were estimated. McCarter and Price (2017) and Rezanezhad et al. (2012b) suggest that the drainable porosity at -100 cm soil water pressure represents mobile water in peat, Therefore, water retention measurements were made at ψ=-100 cm on "undisturbed" cylindrical samples (5 cm diameter, 5 cm length) taken from the remaining frozen peat segments. Samples were saturated, and then were placed in a pressure-plate extractor at ψ=-100 cm for 1 week, weighted then oven-dried at 80^{o}C for 72 hours. Sample weights in the drained and dried conditions were used to calculate bulk density (ρ_b) and $\theta_{immobile}$. Particle density of 0.9 g/cm^3 was used to determine the total porosity (θ_s). Finally, θ_{mobile} was calculated subtracting $\theta_{immobile}$ from θ_s. To determine the organic matter content of peat (f_{OM}), loss-on-ignition (LOI) tests were done in three replicates on peat samples taken from 4 depths.

The analyses of benzene and toluene concentrations were done in the *Groundwater and Soil Remediation Laboratory* at the University of Waterloo. The analyses of solution samples were done with a capillary gas chromatograph (Hewlett-Packard HP 5890) equipped with a flame ionization detector (FID), a Hewlett-Packard HP 7673A automatic sampler, and a DB1 capillary column.

3.2.2 Batch adsorption experiments

Batch adsorption experiments were done for benzene and toluene individually. Competitive adsorption batch experiments were also carried out. Table 3.2 illustrates the experiments carried out in each core and at each depth.

Table 3.2- Type of adsorption experiments carried out at each core

Core No.	peat depth	Benzene adsorption	Toluene adsorption	Competitive adsorption
Core I	0-10 cm	×		
	10-20 cm	×		
	20-30 cm	×		
	30-40 cm	×		
Core II	0-10 cm		×	
	10-20 cm	×	×	×
	20-30 cm	×	×	×
	30-40 cm		×	

3.2.2.1 Single solute adsorption

The feed solutions for adsorption experiments were prepared with benzene (EMD Millipore, GRgrade, purity>99%) and toluene (Alpha Aesar, HPLC grade, purity> 99.7%). Benzene and toluene were added to the solution bottle and stirred continuously for ~7 days to ascertain no free hydrocarbon remained. Samples were collected from feed solutions and were sent for analyses to determine the original concentration of benzene/toluene in the solutions.

Batch experiments were done in 120 mL amber glass bottles (Fisher Scientific) with PTFE lined caps. In each reaction bottle, 2-5 g (depending on peat depth) of air-dried peat were placed. The bottles then were filled with feed solutions having benzene concentrations ranging between 36-1503 mg/L or toluene concentrations ranging between 27-354 mg/L. The amount of peat soil added to each bottle was chosen to adsorb ~25-75% solute mass from the solution and to cause sufficiently large and detectable concentration reduction in the reaction bottles. The soil/water ratio was not identical but similar to that of saturated undisturbed peat. The batch adsorption experiments were run for four different depths and at four to five concentration steps, and for three

replicates in each depth-concentration combination. The equilibrium time reported in the literature for adsorption of benzene/toluene onto peat ranges from 2 hours to 12 days (Table 3.1), but generally less than 5 days. A limited set of kinetics experiments were done on 20-30 cm deep peat to obtain the equilibrium time for benzene and toluene for the peat used in this study. An equilibrium time of 4 days was used, which the kinetic adsorption experiments confirm was adequate (see Results). Reaction bottles were shaken for ~4-5 days to ascertain adsorption equilibrium had established. Before collecting solution samples, the bottles were settled for 6-8 hours allowing particles to separate from solution. Solution samples were extracted for each bottle using glass syringes, and then were placed in 11 mL vials (Pyrex®) with PTFE lined caps. The samples were preserved with two droplets of 30% hydrochloric acid and were stored at 4^{o}C in the dark for up to 1 week before analytical measurements. Ensuring no head-space in the reaction bottles minimized aerobic biodegradation. It is noted that dissolved oxygen could be still present in the original solutions. Maximum solubility of oxygen in water at 25 °C is 5.5 ml/L (Carpenter, 1966) which is equivalent of ~8 mg/L. Considering that the mass ratio of oxygen to benzene (and generally oxygen to BTEX) in aerobic degradation is 3 mg to 1 mg (Jindrova et al. 2002) the soluble oxygen might degrade ~2.6 mg/L of benzene and toluene. In case such aerobic degradation takes place through the experiment, it still would introduce insignificant error to the mass balance and the resulted adsorbed concentrations considering that original concentrations (36-1503 mg/l in case of benzene) were orders of magnitude higher than this possible error. Anaerobic biodegradation was assumed negligible considering the relatively short experiments (at most 5 days). Original and final equilibrium concentrations were determined by analytical measurements. The adsorbed concentrations were calculated using

$$q_e = \frac{V_{solution} \times (C_o - C_e)}{m_{soil}} \qquad \textbf{Equation 3.1}$$

where C_o is original concentration (mg/L), C_e is solution concentration at equilibrium (mg/L), $V_{solution}$ is the volume of solution in reaction bottles (mL), m_{soil} is the dry mass of peat soils (kg), and q_e is the concentration of adsorbed benzene/toluene in the solid phase (mg/kg).

3.2.2.2 Competitive adsorption

The batch adsorption experiments were repeated with the same procedure described earlier using feed solutions with varying concentrations of benzene and toluene (Figure 3.1). Peat at 10-20 cm and 20-30 cm depths were chosen as the adsorbent of this experiment. To ascertain adsorption equilibrium for both solutes in the competitive adsorption experiments, reaction vials were shaken for seven days. The final solutions of the reaction bottles were analyzed for both benzene and toluene giving the variations of q_e with C_e for each compound with and without the presence of the other compound.

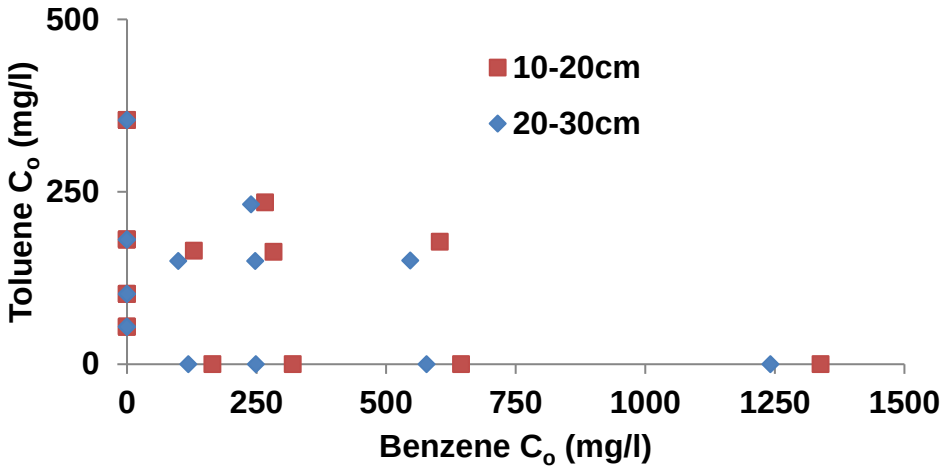

Figure 3.1- Variation of benzene and toluene concentrations in feed solutions used in batch competitive adsorption experiments

3.3 Result and discussion

3.3.1 Soil properties

Total porosity (θ_s) decreases with depth in core I and core II (Table 3.3). Conversely, ρ_b and $\theta_{immobile}$ increase with increasing depth in both cores. The downward increase of ρ_b and $\theta_{immobile}$ in peat profile has been attributed to *i*) peat decomposition, and *ii*) the compaction of peat by the weight of overlaying peat layers (Hobbs 1986; Hoag and Price 1997).

Loss on ignition tests showed that f_{OM} decreases with increasing depth. Several multiplying factors converting f_{OM} to f_{OC} have been suggested for different types of soils. The conversion factor for *Sphagnum* moss peat was assumed as 0.49 (Klingenfuß et al. 2014). f_{OC} in both cores is ~45%, slightly decreasing with depth.

Table 3.3- Peat physical properties in both cores at different depths

Core #	Core I				Core II			
Peat depth	0-10cm	10-20cm	20-30cm	30-40cm	0-10cm	10-20cm	20-30cm	30-40cm
θ_s(L/L)	0.96	0.95	0.87	0.87	0.93	0.93	0.88	0.86
$\theta_{immobile}$ (L/L)	0.20	0.24	0.42	0.42	0.40	0.37	0.36	0.46
ρ_b (kg/L)	0.035	0.044	0.11	0.12	0.067	0.063	0.11	0.13
f_{OM}	0.95	0.96	0.89	0.88	0.96	0.92	0.89	0.89
f_{OC} (f_{OC}=0.49×f_{OM})	0.47	0.47	0.44	0.43	0.47	0.45	0.44	0.43

3.3.2 Batch single solute adsorption

The results of kinetics experiments (Figure 3.2) showed that for both benzene and toluene the equilibrium established within four days. Kinetics data shows that more than 80% of the adsorption took place in first 24 hours, but still the full equilibrium established gradually through the following 3 days. The lack of instantaneous equilibrium in adsorption of benzene and toluene might have field-scale implications in area with high discharge regimes, such as after snowmelt or heavy rainfall, or in the areas with relatively high topographic gradient. In such conditions, the limited residence time of the solution could prevent chemical equilibrium and consequently promote down-gradient contamination.

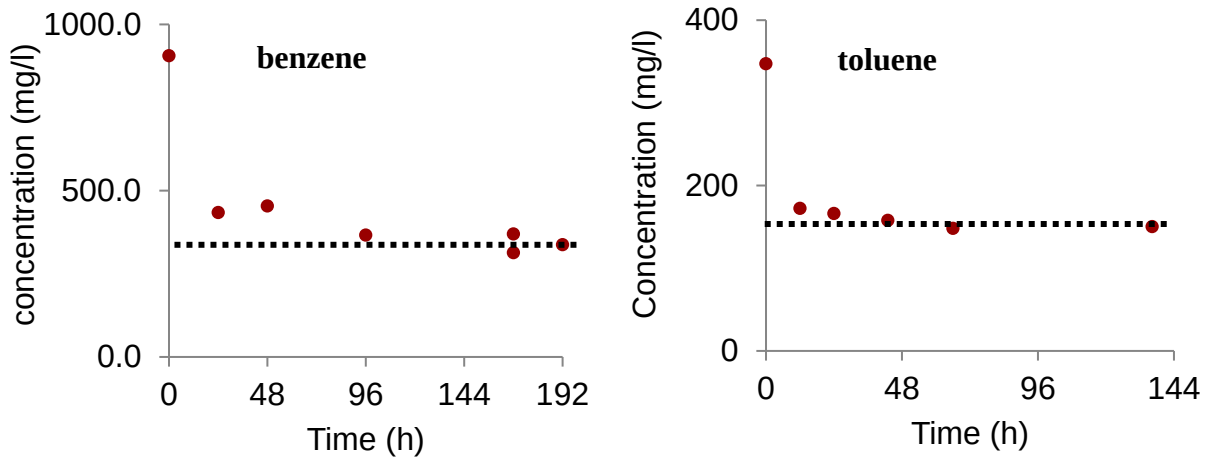

Figure 3.2- Temporal variations of benzene (left) and toluene (right) concentrations in solutions during adsorption kinetics experiments while the adsorbent is moderately decomposed peat.

The adsorption of benzene onto peat generally decreased with increasing peat depth and with increasing degree of decomposition (Figure 3.3a). Near-surface peat (0-10 cm bgs) had the highest adsorption partitioning coefficient and peat of 20-30 cm bgs had the lowest. In contrast, adsorption of toluene onto peat (Figure 3.3b) increased with increasing depth and degree of decomposition, where the partitioning coefficient was least at 0-10 cm bgs and maximized at 30-40 cm bgs. A linear adsorption model was fit to the benzene and toluene isotherms (Table 3.4) and the depth-specific variations of linear adsorption coefficients (K_d) were determined. Considering that the peat samples were ground and homogenized, we believe the variation in K_d was because of variations of peat chemical composition with depth, rather than surface area or texture. Cellulose, lignin, and humic acid (HA) are three major constituents of peat. Although, the variations of these with degree of decomposition are not fully understood for *Sphagnum* dominated peat soils, it is known that the fraction of lignin, cellulose, and HA in peat varies with peat depth and degree of decomposition (Delicato, 1996); the relative fraction of cellulose as a result of preferred decomposition decreases with depth, and consequently the relative concentration of humic acid as a product of decomposition increases with depth. These organic molecules have totally different affinities for adsorbing benzene and toluene; this difference may have caused the adsorption coefficient to vary down the peat profile.

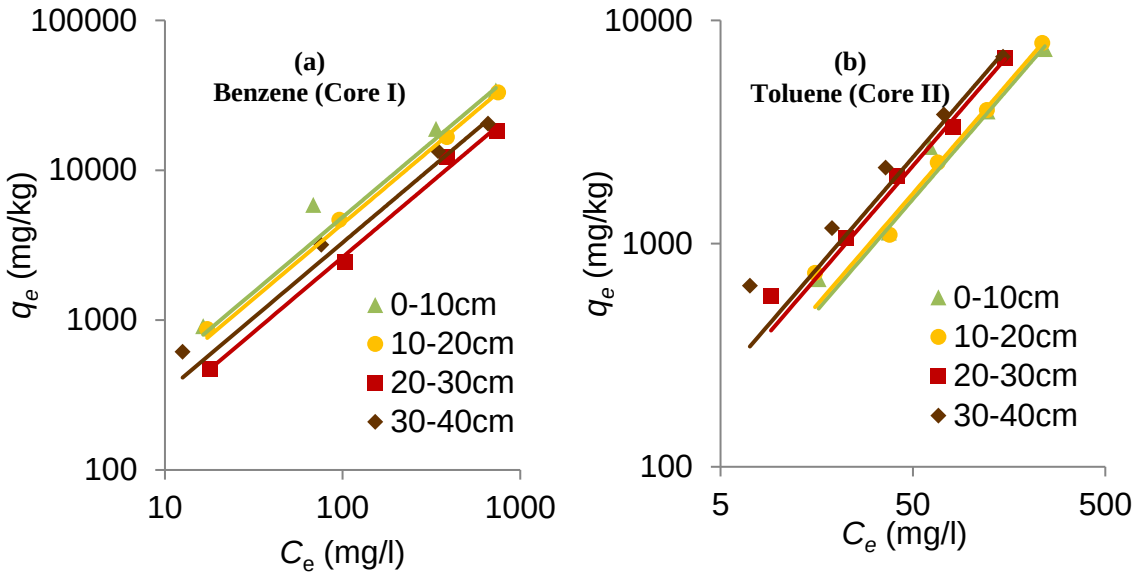

Figure 3.3- Adsorption of benzene and toluene onto peat of different depths and the linear model fitted to each isotherm.

Table 3.4- Summary of fitted linear model on benzene and toluene isotherms and 95% confidence intervals of the adsorption coefficients

Peat depth	Benzene (Core I)		Toluene (Core II)	
	K_d (L/kg)	r^2	K_d (L/kg)	r^2
0-10cm	48.7±8.9	0.98	31.6±4.1	0.98
10-20cm	44.0±1.3	1.00	33.5±1.5	1.00
20-30cm	26.3±5.0	0.98	44.6±2.8	1.00
30-40cm	32.9±6.1	0.98	48.7±5.8	0.98

3.3.3 Competitive adsorption

As illustrated in benzene adsorption isotherms (Figure 3.4) and the linear model parameters (Table 3.5), no significant reduction or increase were observed in benzene adsorption after adding toluene into the feed solution. This means benzene adsorption was influenced very little when toluene was present in the solution. Likewise, toluene isotherms (Figure 3.5) and linear adsorption coefficients (Table 3.5), with and without benzene present, were similar. These results indicate that, in the case of hydrocarbon contamination of a peatland, the competition for adsorption between benzene and toluene is likely insignificant, so using single-solute adsorption coefficients will introduce little error. This outcome is in agreement with observations of some previous studies

on other organic contaminants (Karickhoff et al. 1979; Schwarzenbach and Westall 1981). However, it is contrary to that of Stuart et al. (1991), who found benzene adsorption increased by ~90% when toluene and xylene isomers were present in a solution. The organic carbon content in Stuart et al. (1991) was 0.6%, which is nearly 2 orders of magnitude less than that of peat. The quality of organic carbon in their soil also could be different than that of peat soils considering that they dried their soil for 24 hours at 105°C, which could thermally treat the experimental soil and change its adsorption capacity.

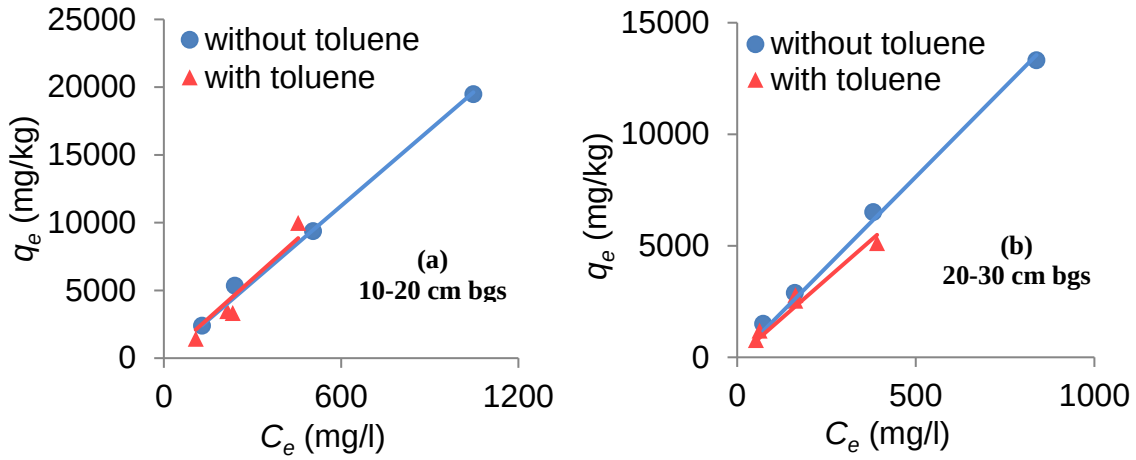

Figure 3.4- Adsorption of benzene onto peat at a) 10-20 cm bgs and b) 20-30 bgs in the presence and absence of toluene.

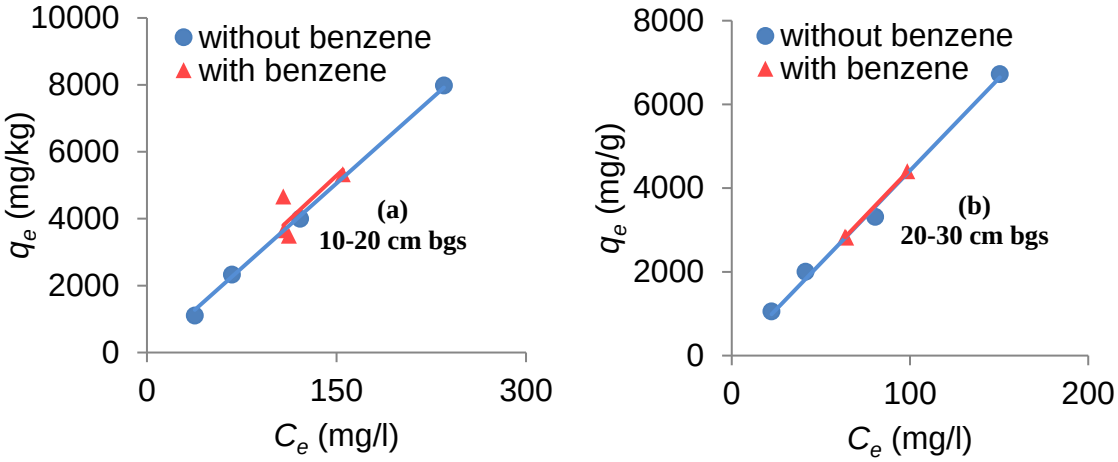

Figure 3.5- Adsorption of toluene onto peat at a) 10-20 cm bgs and b) 20-30 cm bgs in presence and absence of benzene.

Table 3.5- Linear adsorption coefficients±95% confidence intervals for adsorption of benzene and toluene onto peat of different depths in presence and lack of the competing solute

Peat depth	Benzene adsorption (Core II)				Toluene adsorption (Core II)			
	without toluene		with toluene		without benzene		with benzene	
	K_d (L/kg)	r^2	K_d (L/kg)	r^2	K_d (L/kg)	r^2	K_d (L/kg)	r^2
10-20 cm	18.7±1.3	1.00	19.5±6.2	0.91	33.5±1.5	1.00	35.2±7.5	0.55
20-30 cm	16.2±1.2	1.00	14.0±2.3	0.95	44.6±2.8	1.00	44.5±1.1	1.00

3.3.4 Organic carbon partitioning coefficient

Mackay et al. (1997) assembled a list of studies that have reported K_{OC} values for benzene and toluene adsorption, measured directly or predicted it using octanol/water partitioning coefficients. Their data listed adsorption of benzene and toluene onto untreated soils, treated media, and pure organic molecules (cellulose, HA, lignin, etc). Among those, the K_{OC} values determined through measurement for untreated aquifer soil (Karickhoff et al. 1979; Karickhoff 1981; Schwarzenbach and Westall 1981; Garbarini and Lion 1985; Garbarini and Lion 1986; Seip et al. 1986; Vowles and Mantoura 1987; Lee et al. 1989; Abdul et al. 1990; Walton et al. 1992; Xing et al. 1994; Dewulf et al. 1999) ranged from 22-83L/kg (average 55 L/kg) for benzene, and from 39-247L/kg (average 125 L/kg) for toluene. By comparison, K_{OC} values reported by EPA (1996) for benzene and toluene are respectively 66 L/kg and 145 L/kg.

Benzene K_d in this study ranges between 16.2-48.7 L/kg, and toluene between 31.6-48.7 L/kg. Since $K_{OC}=K_d/f_{OC}$ (from Table 3.3), benzene K_{OC} is 37.2-105 L/kg, and toluene K_{OC} is 66.9–113 L/kg, which is similar to the range previously reported for toluene in peat (Table 3.1) but ~10-50% less than the aforementioned average K_{OC}. The implications of using the higher values of K_{OC} reported for toluene in mineral soils, in a peatland setting, are that toluene adsorption and retardation may be overestimated, and thus its distribution velocity in a contaminated peatland underestimated. From a risk assessment point of view, underestimating adsorbed mass and retardation imposes less risk than overestimating, as the latter could result in unanticipated early

arrival of solute. Our results underscore the importance of using peat-based K_{OC} values, when studying or modeling BTEX contamination fate and transport in peatlands.

In addition, it is important to realize the depth-dependency of K_{OC} (Table 3.4); this may be explained by the changing proportions of cellulose, lignin and HA with peat decomposition, and their individual contribution to K_{OC}. Garbarini and Lion (1986) observed for toluene adsorption, K_{OC} of cellulose was over 1000 times smaller than those of HA and lignin. Since cellulose is more readily available for biodegradation than lignin (Waksman and Smith 1934), its proportion diminishes with depth, compared to lignin and HA (a product of peat decomposition), and the latter two have higher toluene K_{OC} than cellulose. The higher proportion of HA and lignin with depth, and their higher K_{OC}, relative to cellulose, results in deeper layers having higher K_{OC} for toluene than shallow peat. Unlike for toluene, the relative difference of benzene K_{OC} in cellulose, HA and lignin is unknown. Since the trend of benzene K_{OC} for depth is opposite to that of toluene, it is likely that benzene K_{OC} in the different organic fractions, differs from that of toluene.

While there is a clear trend in benzene and toluene adsorption with depth, spatial variation is also evident in different cores at similar depths. For example, K_d for benzene adsorption at 10 – 20 cm in core I was 44.0 L/kg, and core II was 18.7 L/kg (Table 3.4 and Table 3.5, respectively). Benzene K_d values at 20-30 cm bgs was 26.3 L/kg and 16.2 L/kg, respectively for core I and core II. Since f_{OC} at each depth are similar within each core (Table 3.3), the horizontal variation of K_d must be due to variation in K_{OC}. Such discrepancies between two cores might be due to differences in peat matrix composition between two cores. While this has been illustrated with regards to physical and hydraulic properties (Balliston, 2016; McCarter and Price, 2014), no literature on chemical differences could be found. The two *Sphagnum* moss peats were sampled within 0.5 m of each other, hosted, similar species, and similar depths might still have different adsorption affinities toward organic solutes.

3.3.5 Retardation factor

The retardation factor is defined as the ratio of water velocity to solute velocity in pore space (Magee et al. 1991; Fry et al. 1995; Martin-Hayden and Robbins 1997). The retardation factor, R_a, is a cumulative result of adsorptive retardation of reactive solutes, R_{ads}, and non-adsorptive

retardation caused by the diffusion of solutes into the immobile water of closed or partially closed pores ($R_{immobile}$). The latter includes conservative tracers (e.g., chloride and bromide), which has been shown to be important in peats (Hoag and Price, 1995; 1997). Given K_d (Table 3.4) and the appropriate soil hydraulic properties (Table 3.3), Equation 3.2 (derivations in the Appendix) describes the retardation of solutes in peat.

$$R_a = \frac{V_{water}}{V_{solute}} = R_{ads} + R_{immobile} = 1 + \frac{\rho_b \times K_d}{\theta_{mobile}} + \frac{\theta_{immobile}}{\theta_{mobile}} = 1 + \frac{\rho_b \times f_{OC} \times K_{OC}}{\theta_{mobile}} + \frac{\theta_{immobile}}{\theta_{mobile}} \qquad \textbf{Equation 3.2}$$

Based on equation 3.2, retardation factors are calculated for benzene and toluene at different depth intervals (Table 3.6). Benzene and toluene retardation factors increase with increasing depth. Benzene R_a is ~3.5 near the surface and increases to 10.7 at 30-40 cm depth. In a similar trend, toluene retardation is 5.8 at the surface layer and increases to 17.7 at 30-40 cm. These values are higher than those typically reported for transport in mineral aquifers, e.g. 1.4 (Chen et al. 1992) or 1.2 (Mackay et al. 2006) for benzene, and 1.6 (Chen et al. 1992; Mackay et al. 2006) or 2.8 (Da Silva and Alvarez 2002) for toluene. However, we note one study with similar retardation factors for benzene in mineral soils (10.0-14.3; Priddle and Jackson 1991). Based on Equation 3.2, R_a positively correlates with f_{OC} and ρ_b. Peat f_{OC} is high (>40%) whereas its ρ_b (0.035-0.127 g/mL) is an order of magnitude less than those of mineral aquifers. In peat, the positive effect of high f_{OC} on R_a is moderated by its small ρ_b; nevertheless, benzene and toluene retardation are still typically higher in peat compared to that in mineral aquifers.

Table 3.6- Variation of benzene and toluene retardation factors with depth in peat profile

Peat depth	Benzene adsorption and retardation (Core I)			Toluene adsorption and retardation (Core II)		
	$R_{immobile}=\theta_{immobile}/\theta_{mobile}$	$R_{ads}=1+(\rho_b K_d/\theta_{mobile})$	$R_a = R_{ads} + R_{immobile}$	$R_{immobile}=\theta_{immobile}/\theta_{mobile}$	$R_{ads}=1+(\rho_b K_d/\theta_{mobile})$	$R_a = R_{ads} + R_{immobile}$
0-10cm	0.26	3.24	3.51	0.75	5.03	5.78
10-20cm	0.33	3.70	4.03	0.66	4.76	5.42
20-30cm	0.93	7.67	8.59	0.69	10.53	11.23
30-40cm	0.94	9.75	10.69	1.15	16.53	17.68

3.4 Conclusion

Benzene and toluene K_d varied systematically with depth, the former decreasing with depth, while the latter increased. This was attributed to the different chemical affinities of cellulose, lignin and HA, whose proportions change with state of decomposition. However, benzene K_d also varied ~50% over a small horizontal distance (0.5 m), likely due to the high spatial variability in peat properties.

Competitive adsorption between benzene and toluene was not significant, meaning K_d derived from individual solutions of benzene or toluene can be used to predict their behaviour, notwithstanding the spatial patterns of K_d variability noted above. It must also be noted that competition between benzene and toluene was not observed in equilibrium adsorption reactions; however, it might be present when the adsorption reactions are rate-limited (kinetically controlled) and when equilibrium has not established in the adsorption reaction, such as when water discharge is high and the solute-solid contact time is not sufficient for chemical equilibrium. Rate-limited adsorption reduces solute retardation and enhances the contaminant's redistribution velocity. This can potentially happen in shallow peat layers and after a heavy rainfall event. In case the competitive adsorption governs in rate-limited adsorption process, and one of solutes restrains the kinetics rate of other solutes, the retardation of influenced solutes will be suppressed, leading to enhanced redistribution velocity.

Using literature K_{OC} values might cause considerable errors in estimating K_d of benzene and toluene in peat, especially when based on minor fractions of carbon in mineral soils. Considering toluene K_{OC} obtained here is smaller than average K_{OC} values reported in the literature, estimating K_d with an average value from previous literature values will underestimate the rate of toluene migration in peatlands. It must be noted that this error becomes more significant in the near-surface peat layer where the difference between peat K_{OC} and the average literature K_{OC}, is the most. Therefore, using non-peat-specific values will probably result in errors in assessing the risk of contamination and in calculating contaminant arrival time, when modeling the contaminant's behavior. Although this study does not cover the full range of peat type (sedge peat, woody peat, etc) and peatland types (bog, fen, swamp), it has addressed that of *Sphagnum* dominated peat and its degree of humification; in the case of hydrocarbon contamination in a peatland, it is more

relevant and likely less erroneous to use such peat-specific values for adsorption calculations, rather than values obtained for mineral aquifers. Further research is needed to elaborate on the effect of botanical origin of peat.

The retardation factors of benzene and toluene increased with depth and with degree of decomposition. In addition, the hydraulic conductivity in peat also decreases with increasing depth (e.g. Hoag and Price 1995, Quinton et al. 2008). These two cumulatively lead to smaller velocities of benzene and toluene in deeper layers compared to shallower ones in a peatland, thus preferential migration of these contaminants in shallow and poorly decomposed peat. It must be noted that benzene adsorption generally decreased with depth while its retardation increased with depth showing that the variations of benzene's adsorption with depth is reverse to the variation of its retardation with depth; this generally does not happen in mineral aquifers, and can arise in peat and along peat profile due to the systematic increase in its bulk density with depth.

3.5 Appendix

Assuming water is flowing into a peat soil sample having a cross sectional area of *Area* (L^2) and the rate of water flow is Q_{water} [L^3T^{-1}], where inflowing solute concentration is C [ML^{-3}]. The centre of the solute plume front moves the length Δx_{solute} [L] in period of *time* [T]. For a saturated peat soil, the pore space is divided to active and inactive zones, respectively having volumetric water contents of θ_{mobile} and $\theta_{immobile}$ [L^3L^{-3}]. Figure 3.A.1 shows the conceptual diagram of this process. The following equations discuss the retardation factor in this porous medium where R_a is the retardation factor, V_{water} is the average water velocity in soil [LT^{-1}], V_{solute} is the average velocity of solute in soil [LT^{-1}], R_{ads} is adsorptive retardation, $R_{immobile}$ is retardation due to solute diffusion into immobile water.

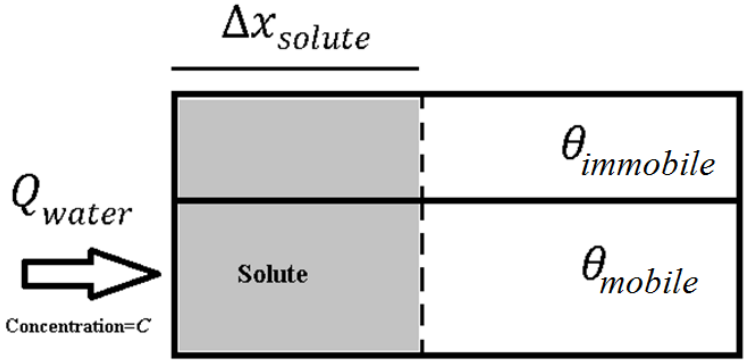

Figure 3.A.1- Schematic of water and solute discharge through a dual porosity porous medium with considerable mobile and immobile water contents

$$R_a = \frac{V_{water}}{V_{solute}} = V_{water} \times \frac{1}{V_{solute}} = \frac{Q_{water}}{Area \times \theta_{active}} \times \frac{time}{\Delta x_{solute}} = \frac{Q_{water} \times time}{\Delta x_{solute} \times Area \times \theta_{active}}$$
$$= \frac{Q_{water} \times time \times C}{\Delta x_{solute} \times Area \times \theta_{active} \times C} = \frac{m_{total}}{m_{solute_{active}}}$$

$$R_a = \frac{m_{total}}{m_{solute_{mobile}}} = \frac{m_{solute_{mobile}} + m_{solute_{immobile}} + m_{adsorbed_{mobile}} + m_{adsorbed_{immobile}}}{m_{solute_{mobile}}}$$
$$= 1 + \frac{m_{solute_{immobile}} + m_{adsorbed_{mobile}} + m_{adsorbed_{immoile}}}{m_{solute_{mobile}}}$$

If both adsorption and matrix diffusion processes reach instantaneous equilibrium, and $K_d = q/C$:

$$R_{total} = 1 + \frac{V_{bulk} \times \theta_{immobile} \times C + V_{bulk} \times \rho_{bulk} \times f \times q + V_{bulk} \times \rho_{bulk} \times (1-f) \times q}{V_{bulk} \times \theta_{mobile} \times C}$$
$$= 1 + \frac{V_{bulk} \times \theta_{immobile} \times C}{V_{bulk} \times \theta_{mobile} \times C} + \frac{V_{bulk} \times \rho_{bulk} \times q}{V_{bulk} \times \theta_{mobile} \times C} = 1 + \frac{\theta_{immobile}}{\theta_{mobile}} + \frac{\rho_{bulk} \times K_d}{\theta_{mobile}} =$$
$$= 1 + \frac{\rho_b \times f_{OC} \times K_{OC}}{\theta_{mobile}} + \frac{\theta_{immobile}}{\theta_{mobile}}$$

where f is the fraction of adsorption sites in contact with mobile water content, V_{bulk} is the bulk volume of soil segment [L^3], ρ_{bulk} is the bulk density of soil [ML^{-3}], q is the adsorbed concentration [MM^{-1}], and K_d is adsorption partitioning coefficient [L^3M^{-1}]. In this case, the retardation factor is formed by two terms which the latter ($\rho_b K_d/\theta_{mobile}$) is due to adsorption and the first term ($\theta_{immobile}/\theta_{mobile}$) is due to diffusion into inactive porosity.

4 Examination of the parameters controlling equilibria in the fate and transport of benzene in water saturated peat

4.1 Introduction

Petroleum products in Canada and elsewhere are extensively transported across peatlands, where pipeline leakage or train derailment can cause extensive spills (Alberta Energy Regulator 2017b). After a hydrocarbon spill, water-soluble hydrocarbons are dissolved in pore water forming dissolved-phase plumes. The plumes impose risk on ecosystem health and local populations. To predict plume behavior, it is crucial to use representative values for the parameters controlling their migration. However, very few have studied the fate and transport of organic contaminants in peat (e.g. Rezanezhad *et al.* 2012) or adsorption of mono-cyclic aromatics like benzene onto peat (e.g. Cohen *et al.* 1991; Rutherford *et al.* 1992; Zytner *et al.*1994). So far, the transport of these contaminants in peat and the parameters that control their adsorption onto peat have remained unclear.

It can take more than a day to establish equilibrium between the solution of organic contaminants and its adsorbed phase on peat (adsorption) (Rutherford *et al.* 1992; Zytner *et al.*1994; Chapter 3). This means at high water discharge (e.g. after a heavy rainfall) when the residence time is shorter, the inability to achieve chemical equilibrium will reduce the ability of peat to trap organic contaminants in the peatland. However, parameters (e.g. adsorption kinetics rate) controlling the chemical equilibrium are not known for peat, and it is possible that adsorption is partially instantaneous and partially kinetically-controlled. A two-site first-order (TSFO) adsorption model that can represent this type of adsorption process has been used to describe adsorption of organic solutes onto mineral aquifer material (e.g. Cameron and Klute 1977; Brusseau *et al.* 1991a, 1991b) and potentially could be used to describe the adsorption of organic contaminants onto peat soils.

In addition to the adsorptive properties of peat, the specific pore structure of peat soils influences the fate and transport of dissolved contaminants. Peat is a dual porosity medium (Hoag

and Price 1997; Rezanezhad *et al.* 2012; 2016) in which solute diffusion into the immobile zone affects the fate and transport of organic contaminants (Chapter 2; Gharedaghloo and Price, 2017). However, so far there has been little discussion on the mass transfer rate between mobile and immobile zones in peat. Furthermore, the dispersivity of peat, which controls the length of the mixing zone of contaminated and clean pore water has not been fully characterized. While dispersivity is known to be a result of the variations of pore size and pore tortuosity (Fetter 2000) the influence of pore size variations of peat on its dispersivity has not been closely examined. The pore size distribution in peatlands varies systematically with the state of decomposition and compaction of peat (Carey et al. 2007), as well as with the botanical origin of the peat (McCarter and Price, 2014).

The main objectives of this study are to 1) characterize the retardation of benzene in peat and to explore its functionality in relation to peat depth and state of decomposition; 2) to explore how adsorption kinetics rates and the fraction of instantaneous adsorption sites vary in the peat profile, and 3) determine how peat dispersivity relates to peat depth and pore size distribution. Results of this study are essential for groundwater managers and modellers to predict the fate and transport of organic solutes in a hydrocarbon contaminated peatland.

4.2 Materials and Methods

4.2.1 Soil extraction and handing

Two cylindrical peat cores (core B and C) (length 35 cm and diameter 25 cm) were extracted from a bog peatland in Ontario. The peat cores were frozen and then cut into segments representing 0-10 cm, 10-20 cm, and 20-30 cm below ground surface (bgs). One cylindrical sample (7.1 cm diameter, 15 cm length) was cut from each segment to be used in a flow-through-reactor (FTR) for miscible displacement experiments. From the same segment, two samples (7 cm diameter, 5 cm length) were also cut for water retention studies. The remaining portion of each segment was kept frozen to be used in adsorption experiments.

4.2.2 Soil characterization

In the soil cores a woody root layer was evident between 20-30 cm bgs in both cores, but more so in core B. The roots were up to ~6 mm diameter. A water retention cell was used to determine the soil-water characteristics of peat samples. Peat samples and retention disks were saturated for 48 hours, and then were placed in the pressure cells for water retention experiments. Retention experiments were done with matric potentials (ψ) ranging from -20 to -700 cm using a pressure plate apparatus (Soil Moisture Inc.). Each pressure-potential step was maintained for 1 week to allow water drainage until physical equilibrium between air and water phases within the peat samples was achieved. After the final step, the samples were oven-dried at 80^{o}C for 72 hours. The dry weight and the bulk volume of each sample was then used to calculate the bulk density (ρ_b) of the sample and its volumetric water content (θ) at the pressure steps. With increasing matrix potential, the samples shrunk and their bulk volume decreased up to ~10%. The field volume of the peat samples was used to calculate soil properties.

Since solute dispersion in porous media is controlled by pore-scale variations of pore radii, the variations of pore size distribution (PSD) in peat samples might correlate with the variations of peat dispersivity in the miscible displacement experiments. PSDs were calculated using the water retention data and the method of Ritter and Drake (1945). Using this method, the corresponding theoretical pore radius (r) [L] of each pressure step was obtained using Equation 4.1 in which σ is water/air interfacial tension (71.99 N/m), p is water pressure [M $L^{-1}T^{-2}$], and θ_{wa} is the water/air contact angle on peat. The contact angle was assumed as 51.3^{o} (Chapter 5; Gharedaghloo and Price 2015).

$$p = \frac{2\sigma \cos\theta_{wa}}{r} \qquad \textbf{Equation 4.1}$$

Next, the frequency of pores of radius of r was calculated using Equation 4.2 (Ritter and Drake 1945) where V_0 is the initial water volume in the unit volume (1 cm^3) of soil sample, and V is the volume of water remaining in the unit volume of soil sample at capillary pressure of p.

$$D(r) = \frac{p}{r}\frac{d(V_0 - V)}{dp}$$ **Equation 4.2**

where $D(r)$ [L^2] is the total cross-sectional area of pores of radius r, in 1 cm^3 of soil; it is a measure of the frequency of pores of radius r.

4.2.3 Miscible displacement experiment

Breakthrough curves (BTCs) were obtained by injecting solutions into peat columns in a series of miscible displacement experiments. Flow-through-reactors (FTRs) (ID: 7.1 cm, length: 15 cm) were constructed with PTFE material to prevent adsorption of organic solutes to the FTRs. Barry (2009) suggested a soil column with the ratio of length to radius >3 is sufficient to ensure uniform flow; the ratio in this study was ~4.2. The additional length reduces the effect of stagnant zones at the corners. Undisturbed partially frozen peat samples were placed in the FTRs, ensuring a snug fit. Soil columns were saturated through the bottom to minimize air trapping. Initial testing showed the effluent was not colorless, indicating the presence of dissolved organic carbon (DOC). Since DOC itself can adsorb organic solutes (Cram et al. 2004), thus influence the estimation of solute adsorption onto the peat matrix, the columns were flushed with deionized (DI) water (TOC< 4 parts per billion) for 3.5 days (>30 pore volumes) resulting in colorless effluent presumed to have negligible DOC concentration. At the end of flushing, chloride concentration and electrical conductivity of the effluent were also both negligible (Chloride concentrations was less than 0.6 mg/L).

Feed solutions containing benzene (EMD Millipore, GR grade, purity>99%) and NaCl were prepared. The addition of chloride, assumed to be a conservative tracer (Rezanezhad et al. 2012; Simhayov et al. 2018), along with benzene reduces the number of unknown parameters to match benzene BTCs, using inverse modelling. The feed solutions were stored in tedlar bags to avoid benzene volatilization and the variations of benzene concentration in the feed solutions. Prior to injection, samples from feed solutions were taken and placed in 11 mL glass vials (Pyrex®) with PTFE lined caps. To preserve the samples, two HCl droplets were added to each vial before storing them. The vials were stored at 4^{o}C for up to 1 week before benzene analytical measurements. The

concentrations of chloride and benzene in feed solutions were, respectively, between 602-1020 mg/L and between 293-449.7 mg/L, ranging between columns.

The experiments started by injecting the feed solutions into peat column with a discharge rate of 1.1-3.9 m day^{-1} (varying between columns and decreasing with increasing depth of peat) using a peristaltic pump (Longerpump WT600-3-J). Samples of effluent were taken for chloride and benzene every ~7 and ~15 minutes, respectively. The volumetric flow rates were monitored as the effluent samples were collected and were steady during all the experiments. At the end of each experiment, the soil column was oven-dried and the oven-dry weight was used to determine its bulk density and total porosity.

Chloride analysis was done on feed and effluent samples using an Orion chloride combination electrode (9617BNWP, Thermo Fisher Scientific Inc.). Probes were calibrated and handled using the procedure described in the user guide. The effluent sample for benzene analyses were preserved and stored using the same method as discussed above. The analyses of benzene concentrations in the feed and effluent samples were carried out in the *Groundwater and Soil Remediation Laboratory* at the University of Waterloo with a capillary gas chromatograph (Hewlett-Packard HP 5890) equipped with a flame ionization detector (FID), a Hewlett-Packard HP 7673A automatic sampler, and a DB1 capillary column.

4.2.4 Adsorption experiments

Batch adsorption experiments were carried out using solutions with varying concentrations of benzene. The experiments were done in 120 mL amber glass bottles (Fisher Scientific) with PTFE lined caps. Approximately 20 grams of wet peat samples remaining from the frozen segments were used for each batch adsorption test; a smaller portion was used to estimate the dry mass of the wet peat samples used in the experiment. Wet peat was placed in each reaction bottle, which was then filled with benzene solutions (concentration ranging in 187-1193 mg/L) and were shaken for ~5-6 days to assure equilibrium adsorption had occurred (Rutherford et al. 1992; Zytner et al. 1994;

Chapter 3). From each bottle, solution samples were collected using glass syringes and placed in 11 mL vials, preserved and stored with the same procedure as outlined above.

The dry mass of the wet peat was estimated by oven-drying three samples of the remaining peat. The oven-dried weight of the peat samples were then compared to their wet weight giving dry/wet weight ratio for the peat used in batch experiments. Using this ratio and the weights of wet peat added to the reaction bottles, the dry mass of peat and the volume of water associated with the wet peat were calculated. The original concentrations of the mixtures in the bottles were adjusted for the associated water content of the peat.

The procedure was repeated for samples from 0-10 cm, 10-20 cm, and 20-30 cm depth bgs. The adsorbed concentrations were calculated as

$$S = \frac{V_{solution} \times (C_o - C_e)}{m_{soil}} \qquad \textbf{Equation 4.3}$$

where C_o is the original concentration (mg/L) adjusted to the initial moisture of wet peat, C_e is solution concentration at adsorption equilibrium (mg/L), $V_{solution}$ is the volume of solution in the reaction bottles (mL), m_{soil} is the dry mass of peat soils (kg), and S is the concentration of benzene adsorbed onto peat matrix (mg/kg). The ratio of S to C_e then was assumed as the adsorption coefficient.

4.2.5 Numerical modelling

Solute transport equations for dual-porosity media including peat are:

$$\frac{\partial}{\partial t}(\theta_m C_m) + \frac{\partial}{\partial t}(f \rho_b S_m) = \frac{\partial}{\partial z}\left(\theta_m D \frac{\partial C_m}{\partial z}\right) - \frac{\partial}{\partial z}(qC_m) - \alpha_{mim}(C_m - C_{im}) \qquad \textbf{Equation 4.4}$$

$$\theta_{im} \frac{\partial C_{im}}{\partial t} + (1 - f)\rho_b \frac{\partial S_{im}}{\partial t} = \alpha_{mim}(C_m - C_{im}) \qquad \textbf{Equation 4.5}$$

where C_m is solute concentration in the mobile zone [ML^{-3}], S_m is concentration of solute sorbed to soil in the mobile zone [MM^{-1}], θ_m is the volumetric water content in mobile zone [L^3L^{-3}] and

equals the active porosity (ϕ_{active}), f is the fraction of adsorption sites in contact with solution in the mobile phase, ρ_b is soil bulk density [ML^{-3}], q is discharge [LT^{-1}], and α_{mim} is mobile-immobile transfer coefficient [T^{-1}] (Van Genuchten and Wierenga 1976). In this mobile-immobile (MIM) model adsorption was assumed to be instantaneous. However, as discussed earlier, a TSFO adsorption model is needed describe the benzene adsorption onto peat. This means S_m and S_{im} in Equation 4.4 and Equation 4.5 are determined as the sum of adsorption onto instantaneous and kinetically-controlled sites. Equation 4.6 to Equation 4.8 demonstrate the parameters controlling the adsorption process in a two-site adsorption model, where S is total adsorbed concentration [MM^{-1}], S_{eq} is adsorbed concentration onto equilibrium sites [MM^{-1}], S_{kin} is adsorbed concentration onto kinetically-controlled sites [MM^{-1}], K_d is adsorption coefficient [L^3M^{-1}], *frac* is fraction of instantaneous sorption sites, and α_{kin} is adsorption kinetics rate [T^{-1}] (Van Genuchten and Wagenet 1989).

$$S = S_{eq} + S_{kin} \qquad \textbf{Equation 4.6}$$

$$\frac{\partial S_{eq}}{\partial t} = frac \times K_d \frac{\partial C}{\partial t} \qquad \textbf{Equation 4.7}$$

$$\frac{\partial S_{kin}}{\partial t} = \alpha_{kin}\left(\left(1 - frac\right) K_d C - S_{kin}\right) \qquad \textbf{Equation 4.8}$$

HYDRUS-1D (Simunek *et al.* 2005) has frequently been used to numerically solve these equations and to model the fate and transport of organic and non-organic solutes in porous media (e.g. Dontsova et al. 2009; Casey et al. 2000; Gidley et al. 2012; Mark et al. 2017). The dual-permeability module of HYDRUS-1D was used as the solver recognizing the dual-porosity structure of peat and two-site adsorption in the active and inactive porosities (i.e., in the mobile and immobile pores). It must be noted that both dual-porosity and dual-permeability solvers of HYDRUS-1D simulate physical non-equilibrium. However, the dual-porosity solver was not selected since it only recognizes the two-site adsorption in the mobile zone, while this form of adsorption could happen in both active and inactive pores of peat. Since, in peat, there is no water flow within the immobile zone and between mobile and immobile zones, minimum hydraulic conductivity values were assigned to the numerical elements of immobile zone and to the hydraulic

conductivity of mobile-immobile water transfer term. This modified the dual-permeability module for modelling water and solute transport through the mobile zone, MIM solute transfer, and TSFO adsorption in both mobile and immobile zones.

4.2.6 Inverse modelling and parameter estimation

To estimate the values of unknown parameters that control the behavior of solutes in peat, and to avoid converging to local minima, which might happen using gradient-based optimization schemes of HYDRUS, a global search algorithm was programmed in MATLAB, linking MATLAB to HYDRUS. The program randomized unknown parameters including the ratio of active porosity to total porosity ($\phi_{active}/\phi_{total}$), first order mobile-immobile (MIM) transfer coefficient [T^{-1}] (α_{mim}), dispersivity [L] of mobile zone (λ), fraction of instantaneous adsorption sites in both mobile and immobile zones (*frac*), and first order kinetics adsorption coefficient [T^{-1}] (α_{kin}) assuming uniform distributions for the parameters. The upper and lower limits of these parameters assumed in the global search are presented in Table 4.1.

The program prepared HYDRUS input files using randomized parameters and called HYDRUS-1D to simulate chloride and benzene transport through soil columns and to calculate their BTCs for each randomized set of parameters. Residual mean square error (*RMSE*) of BTC data were calculated comparing simulated and observed BTCs and using Equation 4.9, in which $Y_{i\_measured}$ is the measured relative concentration (C/C_0), $Y_{i\_simulated}$ is the simulated C/C_0, i is the index of a measured point, and n is the number of measured points; repeating this procedure 1000 times, 2-4 realizations with minimum *RMSE* for both chloride and benzene were selected for each column as the realizations with representative parameters.

$$RMSE = \sqrt{\frac{\sum_{i=1}^{n}\left(Y_{i\_observed} - Y_{i\_simulated}\right)^2}{n}} \qquad \textbf{Equation 4.9}$$

Table 4.1- Ranges of uncertain parameters tested including ratio of active porosity to total porosity ($\phi_{active}/\phi_{total}$), first order mobile-immobile transfer coefficient (α_{MIM}), longitudinal dispersivity of the mobile zone (λ), fraction of instantaneous adsorption sites in both mobile and immobile zones (*frac*), first order kinetics adsorption coefficient (α_{kin}), and linear adsorption coefficient (K_d) considered in global search algorithm

Core (Depth)	B (0-10 cm)	C (0-10 cm)	B (10-20 cm)	C (10-20 cm)	B (20-30 cm)	C (20-30 cm)
$\phi_{active}/\phi_{total}$	0.8-0.95	0.85-0.95	0.8-0.85	0.8-0.88	0.67-0.77	0.85-0.95
α_{mim} (day^{-1})	15-1500	15-1500	30-3000	30-3000	0.3-3	0.3-30
λ (cm)	0.3-3	0.1-1	1.2-1.6	0.1-2	8-12	0.2-1
frac	0-0.5	0-0.5	0-0.5	0-0.5	0-0.5	0-0.5
α_{kin} (day^{-1})	1-100	1-100	1-10	0.1-10	1-10	1-10
K_d (cm^3/g)	5-15	5-15	20-35	20-40	35-55	35-60

It must be noted that the first order coefficient governing solute transfer into an immobile zone is linearly proportional to the molecular diffusion coefficient (D_m) of the solute (Appelo and Postma, 2004). This means the MIM transfer coefficients of chloride and benzene are not independent parameters and both of them cannot be randomized simultaneously. To incorporate their relation, the ratio of their molecular diffusion coefficients was used as the correlating factor. The molecular diffusion coefficient (D_m) of sodium chloride solution at 25°C is ~1.5×10^{-9} m^2/s (Vitagliano and Lyons 1956). D_m of benzene in water at 20°C and 40°C is 1.02×10^{-9}e-9 m^2/s and 1.6×10^{-9} m^2/s, respectively (Witherspoon and Bonoli 1969); D_m of ~1.15×10^{-9} m^2/s at 25°C was estimated for benzene using these data points. This means the diffusion coefficients of sodium chloride in water at 25°C and consequently the MIM transfer coefficient of chloride are ~1.3 times of that of benzene. This ratio between chloride and benzene MIM transfer coefficients was maintained in the parameter randomization step of the global search program.

4.3 Results and Discussion

4.3.1 Water retention

Water retention curves (Figure 4.1) show that in core B retention increased with depth, while in core C there was comparatively little difference between depths. The retention curves of core B

were typical of peat layers in which compaction and decomposition of peat leads to enhanced water retention with peat depth (Price et al. 2008; Golubev and Whittington, 2018). However, core C did not show the typical increase in water retention with depth, and the variations of bulk density with depth in core C was less than that of core B (Table 4.2). These cores were sampled from the same hummock, both had a distinct colour change with depth indicative of decomposition, but the structure of core C had evidently not collapsed as it had in core B. This marked spatial variability underscores the need for comprehensive sampling. The water retention data of peat were used to estimate the active porosity (pore volume that actively contributes to water and solute transport, forming the mobile phase) and inactive porosity (that retains the solutes and form the immobile phase). McCarter and Price (2017) suggested that water released from a sample, between saturation and a matric potential (ψ) of -100 cm, approximates the mobile water content and thus active porosity (ϕ_{active}) of peat. Assuming this and considering that the saturated volumetric water content equals total porosity (ϕ_{total}) the water retention data were used to estimate the ratio of active to total porosity ($\phi_{active}/\phi_{total}$) in the peat columns. A ~±5% error was considered in the estimated value to obtain the upper and lower limits of $\phi_{active}/\phi_{total}$ *i*n the soil column in the inverse modelling simulations (Table 4.1).

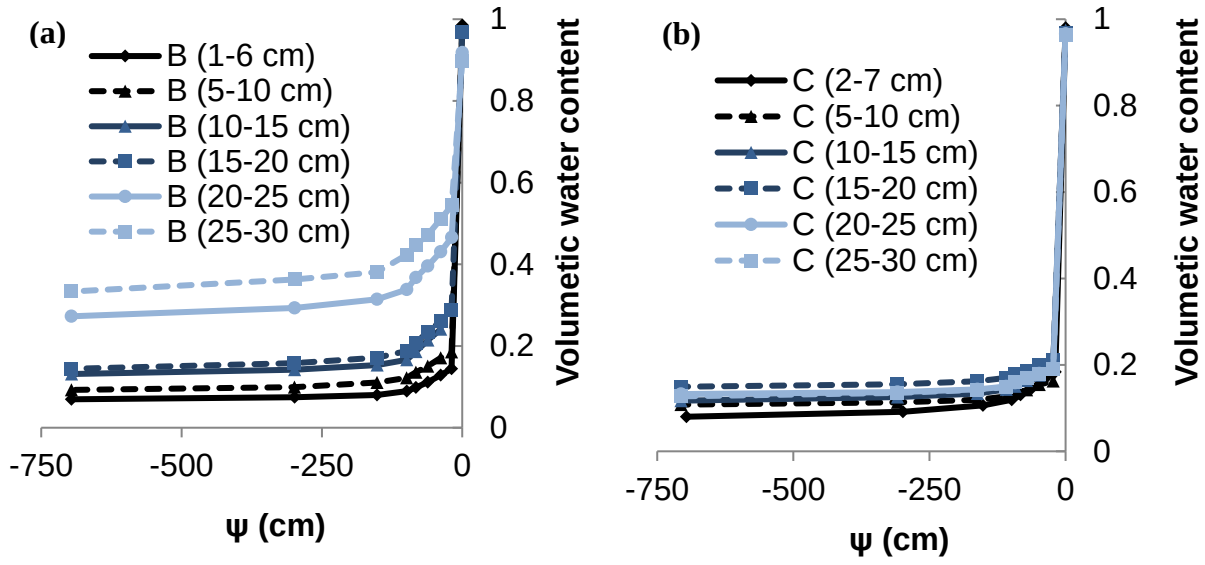

Figure 4.1- Variation of water retention curves with depth for peat soil samples obtained from core B (a) and core C (b)

Table 4.2- Physical properties of soil columns and discharge rate in BTC experiments; ϕ_{total} is total porosity, ρ_b is bulk density, and q is discharge through the soil column.

core	Depth	ϕ_{total}	ρ_b (g/cm^3)	q (cm/min)
B	0-10 cm	0.95	0.041	0.27
	10-20 cm	0.95	0.043	0.098
	20-30 cm	0.9	0.089	0.082
C	0-10 cm	0.97	0.027	0.27
	10-20 cm	0.95	0.043	0.094
	20-30 cm	0.96	0.04	0.078

4.3.2 Benzene adsorption experiment

A linear isotherm model was fit to the peat adsorption data (Figure 4.2) to determine the linear adsorption coefficients (K_d) (Table 4.3). The results show that K_d increases with depth down the peat profile in both cores B and C. The variation of benzene K_d with peat type and state of peat decomposition has been observed in previous studies (Cohen et al. 1991; Chapter 3). This coupled with the results of batch adsorption experiments suggest that peat surface chemistry and its adsorption capacity varies as chemical weathering changes the peat chemistry along peat profile. The linearity of the trends is also in agreement with previous studies (e.g. Chiou et al. 1983; Rutherford et al. 1992) and suggests that adsorption sites are not limited for benzene adsorption (Huang et al. 2003).

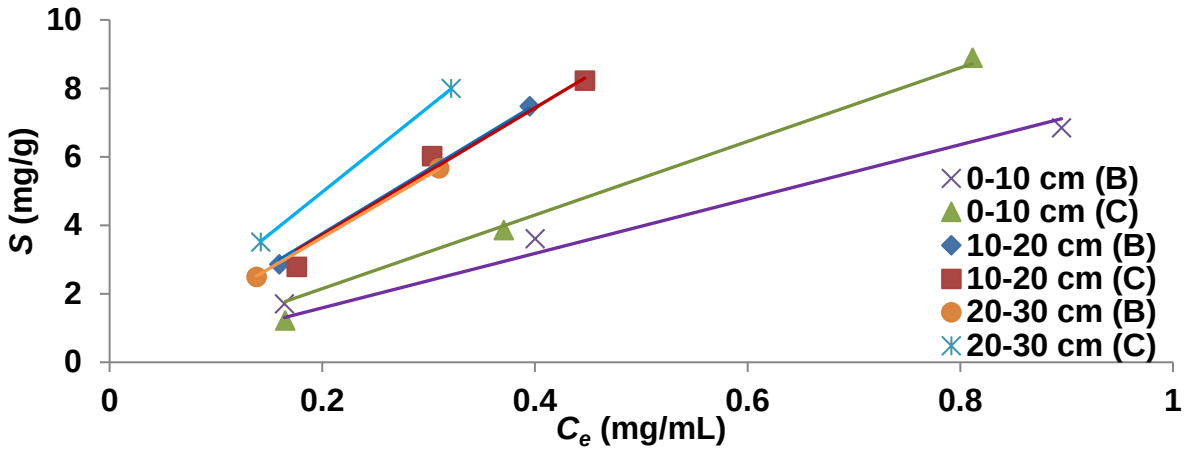

Figure 4.2- Adsorption isotherms of benzene on peat of different depth at both cores B and C

Table 4.3- Summary of linear isotherm model ($S=K_d \times C_e$) fitted to the data of benzene adsorption on peat

core	Depth bgs	K_d (mL/g)	R^2
B	0-10 cm	7.95	0.97
	10-20 cm	18.57	0.97
	20-30 cm	18.24	1.00
C	0-10 cm	10.75	0.99
	10-20 cm	18.79	1.00
	20-30 cm	24.86	1.00

4.3.3 Chloride and Benzene BTC

The observed chloride BTCs were generally symmetrical (Figure 4.3); asymmetry was only observed in core B at 20-30 cm bgs (Figure 4.3e). The symmetry in chloride BTC indicates physical equilibrium between mobile and immobile zones of a dual porosity media. For situations with specific discharge rates less than or equal to those used in these BTC experiments, physical equilibrium between active and inactive pores is likely for all solutes, including chloride as well as benzene. This is because at slower discharge rates, the residence time of solutes in the mobile zone are equal or longer than the residence time of the experiments conducted here. The longer residence time reduces the differences between concentrations in mobile and immobile zones and maintains the physical equilibrium. It should be noted that although physical equilibrium established in most soil columns in the laboratory experiments, field-scale heterogeneities

including significant difference in hydraulic conductivity down the peat profile can cause a physical non-equilibrium in larger scale studies and can lead to long tails in chloride breakthrough (Hoag and Price 1995). Given that physical equilibrium was achieved in (all but one) peat core, asymmetry in the benzene BTCs (Figure 4.3) must be due to chemical non-equilibrium occurring as a result of rate-limited adsorption. The BTCs are stretched out because peat retained capacity to adsorb more benzene since the solid phase (adsorbed benzene) had not reached equilibrium with the solution. In contrast, benzene BTCs were symmetrical for peat 0-10 cm bgs (Figure 4.3a,b). This suggests that the adsorption rates here were sufficiently high to reach chemical equilibrium, preventing long tails in benzene BTCs. That chemical equilibrium was achieved in this layer, in spite of the higher solute flow rate, testifies to notably different surface chemistry that favours rapid adsorption. The absence of chemical equilibrium in the adsorption of benzene and other dissolved hydrocarbons has been observed in other aquifer material (Pignatello and Xing 1995; Maraqa et al. 1999).

4.3.4 Parameter estimation

Total porosity, bulk density, and the water discharge rate of the columns (presented in Table 4.2) were used as known inputs for HYDRUS modelling. For each soil column, three to four realizations of the simulated BTC with minimum *RMSE* values for both chloride and benzene transport were selected. For each soil column, unknown/uncertain parameters and the average *RMSE* of chloride and benzene simulations obtained from representative realizations were calculated. Parameters estimated from the inverse modelling include MIM transfer coefficient (α_{mim}) dispersivity (λ), first order adsorption kinetics rate (α_{kin}), fraction of instantaneous adsorption sites (*frac*), and linear adsorption coefficient (K_d).

4.3.4.1 MIM transfer rates (α_{mim})

The first order MIM transfer coefficient, α_{mim}, at 0-10 and 10-20 cm bgs ranged from 18.8-955 day^{-1}, demonstrating high MIM transfer rates; physical equilibrium occurs considerably faster at these depths. However, α_{mim} decreased to 1-1.7 day^{-1} at 20-30 cm bgs; as a comparison, to decrease the difference between solute concentration in active porosity and inactive porosity to less than 5% with α_{mim} of 18.8 day^{-1}, 955 day^{-1}, and 1.7 day^{-1} respectively, 0.69 hr, 0.012 hr, and 11.04 hr would be needed. The reduction in MIM transfer rate at 20-30 cm depth could be due to a higher frequency of closed and isolated pores that decrease the rate of mass exchange with the mobile zone. $\phi_{active}/\phi_{total}$ decreased to 0.71 at 20-30cm bgs in core B (Table 4.4) indicating that the inactive porosity of this soil column was the highest of the experimental columns. The increase in inactive porosity could also be an indication of the higher frequency of isolated pores of core B at 20-30 cm bgs. Isolated pores have lower rates of solute exchange with active porosity compared to partially closed pores, therefore, the rate of MIM transfer into the isolated pores is less than that of partially closed pores. The isolated pores might belong to the roots that were primarily distributed in 20-30 cm bgs layer in both cores, reducing the relative frequency of partially-closed pores at this depth, thus the MIM transfer coefficients. In contrast, partially closed pores are distributed in the matrix of *Sphagnum* moss (Dickinson and Maggs 1974), which were dominantly distributed at the surface and near surface layers of these cores, and led to a higher MIM transfer rate in surface and near surface peat layers.

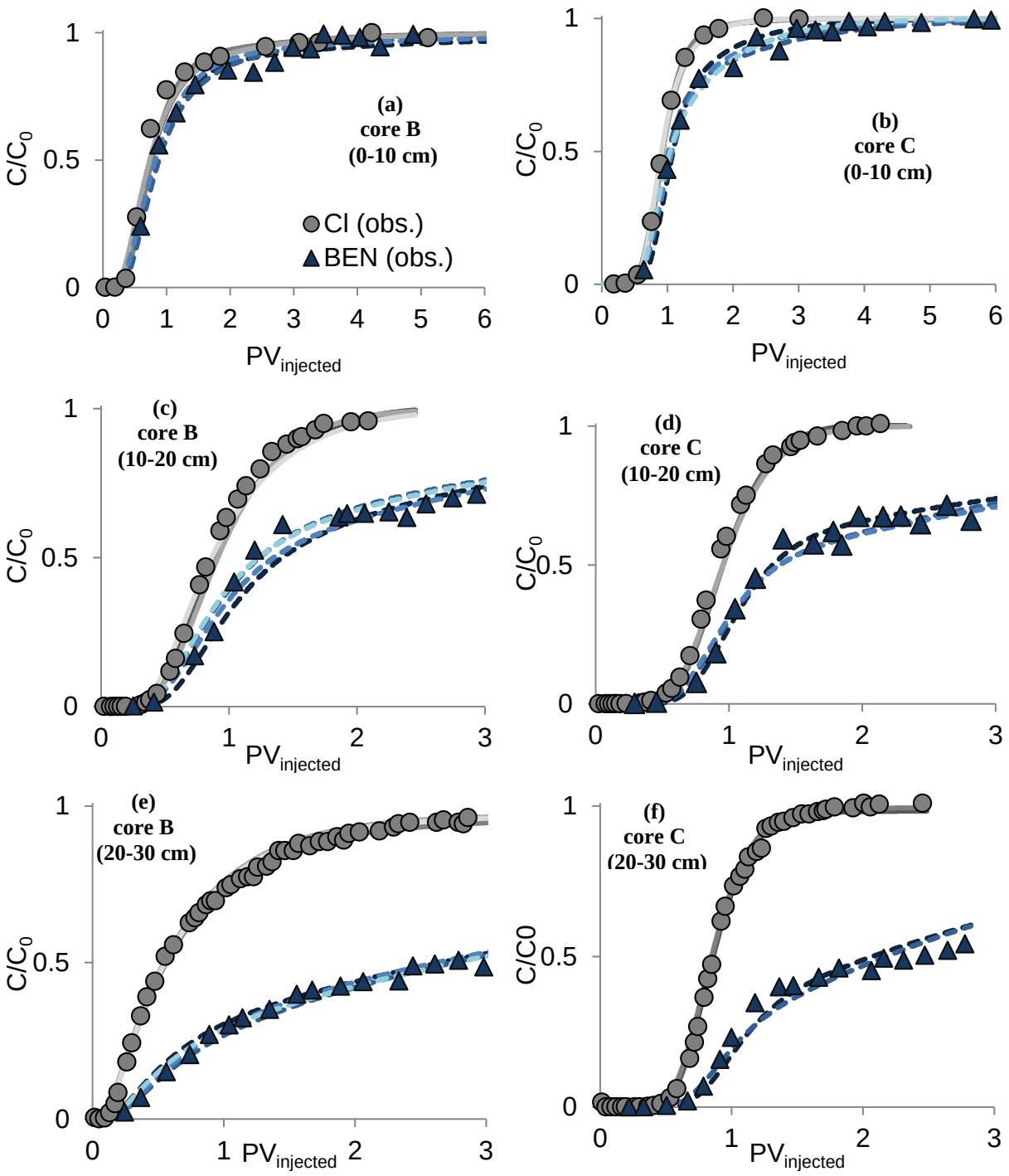

Figure 4.3- Observed (obs.) BTCs of chloride (Cl) and benzene (BEN). Observed (grey and blue points) and simulated (grey and blue lines) breakthrough for peat of core B (left) and core C (right) at 0-10 cm (a, b), 10-20 cm (c, d) and 20-30 cm (e, f) below ground surface

Table 4.4- Average (s.d.) soil properties in the experimental soil columns and summary of chloride and benzene errors in inverse modelling

core (depth)	No. of chosen realizations	Average chloride *RMSE*	Average benzene *RMSE*	$\phi_{active}/\phi_{total}$	α_{mim} (day^{-1})	λ(cm)	*frac*	α_{kin} (day^{-1})	K_d (cm^3/g)
B (0-10 cm)	3	0.04 (0.002)	0.04 (0.001)	0.81 (0.004)	18.8 (2.0)	2.2 (0.4)	0.26 (0.10)	18.7 (20.2)	7.7 (1.4)
B (10-20 cm)	4	0.03 (0.003)	0.04 (0.004)	0.82 (0.02)	150.3 (191.4)	1.4 (0.1)	0.09 (0.05)	4.3 (0.4)	33.5 (1.1)
B (20-30 cm)	4	0.02 (0.004)	0.02 (0.002)	0.71 (0.01)	1.7 (0.6)	11.4 (0.2)	0.18 (0.04)	4.5 (0.4)	51.9 (1.2)
C (0-10 cm)	4	0.01 (0.002)	0.03 (0.003)	0.92 (0.03)	65.6 (13.7)	0.50 (0.09)	0.16 (0.16)	33.8 (9.2)	12.3 (1.3)
C (10-20 cm)	3	0.03 (0.001)	0.04 (0.001)	0.83 (0.01)	955.0 (403.1)	0.66 (0.03)	0.05 (0.03)	3.9 (0.6)	37.8 (1.3)
C (20-30 cm)	2	0.02 (0.002)	0.04 (0.001)	0.88 (0.004)	1.0 (0.6)	0.56 (0.03)	0.09 (0.02)	5.0 (0.5)	58.0 (0.8)

4.3.4.2 First order adsorption kinetics rate (α_{kin})

The inverse simulation also provides first order kinetics rates (Table 4.4) that have never been reported for benzene adsorption onto peat; the first order adsorption rates ranged from ~3.9-33.8 day^{-1}. It was high at the surface (~18.7-33.8 day^{-1}), and less (3.9-5.0 day^{-1}) between 10-30 cm bgs. Such high adsorption rates at the surface shows that adsorption is almost instantaneous at the surface layer. However, for deeper peat kinetic rates show that adsorption equilibrium time for undisturbed peat might be around one day; for example, 95% of mass adsorption happens in 18.6 and 2.1 hours for adsorption rates of 3.9 day^{-1} and 33.8 day^{-1}, respectively. This shows that successful application of an equilibrium-based adsorption model in field-scale studies depends on the discharge rate of dissolved-phase plume and the contact time of contaminants with the peat matrix. If the discharge rate is high, causing limited contact time between dissolved contaminants and peat, the adsorption process will be rate-limited. As comparisons, the rate of benzene sorption in soils could be 60.5 day^{-1} (2.52 hr^{-1} in Brusseau and Rao 1989), and between 0.29-13.1 (0.012-0.544 hr^{-1} in Marqa et al. 1999), which shows that the sorption reaction of benzene onto peat is within range that previous studies have reported.

4.3.4.3 Fraction of instantaneous adsorption sites (*frac*)

The values of *frac* (fraction of instantaneous adsorption sites in both mobile and immobile zones) in Table 4.4 varied from 0.05 to 0.26. The fraction of instantaneous adsorption sites in adsorption of benzene onto mineral soils could be between 0.52-0.72 (Maraqa et al. 1999); in studies of other organic solutes, for example, *frac* could range between 0.42-0.61 (Brusseau et al. 1991) and 0.11-0.59 (Karickhoff and Morris 1985). This shows that only a small portion of adsorption sites are instantaneous and the majority are rate-limited. The *frac* parameter controls the breakthrough time of the low concentrations of contamination; the higher the *frac*, the later the front of the contamination plume reaches the observation point. Therefore, in media where *frac* is ~ 0.26, it is essential to use a two-site (TSFO) adsorption model or else the arrival time of the plume's front will be underestimated. In such cases, a single site rate-limited adsorption model might not fully describe the adsorption of organic contaminants onto peat.

4.3.4.4 Dispersivity (λ)

Dispersivity values range from 1.4-11.4 cm in core B, and from 0.5-0.66 cm for core C (Table 4.4). Excluding the dispersivity value for 20-30 cm of core B (11.4 cm), the remaining values are within the ranges determined in previous studies (e.g. Hoag and Price 1997). The variations of dispersivity were insignificant in core C. This could be due to the homogeneity of pore size distribution along the core C depth profile (Figure 4.4). Since the dispersivity is an expression of velocity variations which are function of pore size variations, the low variation in pore size distributions in core C produce small variations in peat dispersivity. On the other hand, the larger variations of pore size distributions in core B generated larger variations in peat dispersivity. These results suggest that peat dispersivity is a function of pore size distribution; the humification process (or other processes including root channeling) that cause variations of peat pore size distributions control the magnitude of longitudinal dispersivity.

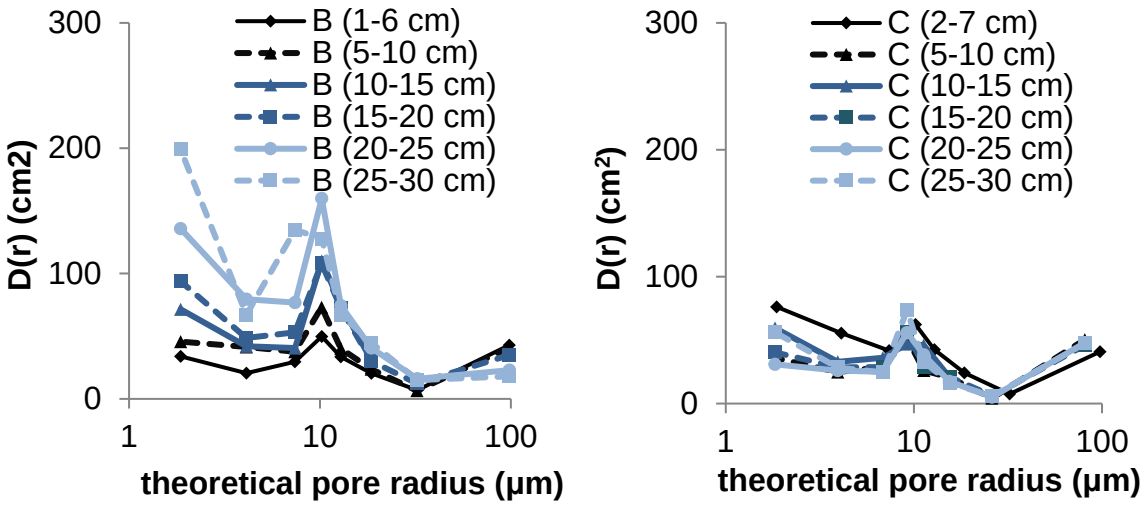

Figure 4.4- Variation of pore size distribution with depth in core B (left) and core C (right).

4.3.4.5 Linear adsorption coefficient (K_d)

For 0-10 cm peat the adsorption coefficients (K_d) obtained through inverse modelling (7.7-12.3 cm^3/g) were similar to the range of values determined with the batch experiments (7.9-10.75 cm^3/g). K_d values of both methods increased with depth; however, the values were not similar in deeper peat. At 10-20 cm bgs, K_d from batch experiments ranged from 18.6-18.8 cm^3/g while inverse modelling values at this depth were from 33.5-37.8 cm^3/g. At 20-30 cm bgs, K_d from batch experiments varied from 18.2-24.9 cm^3/g, while corresponding values from inverse modelling ranged from 51.9-58.0 cm^3/g. Differences between the adsorption parameters from inverse modelling and batch adsorption experiments have also been reported in other studies (e.g. Casey et al. 2003; De Wilde et al. 2009; Hanna et al. 2012). The differences could be due to the heterogeneity of peat chemical properties. However, it is more likely that DOC in pore water of the batch experiments negatively influenced the adsorption of organic solutes onto the soil matrix (Cram et al. 2004; Gschwend and Wu 1985), leading to reduced K_d (recall that the FTR columns were flushed, but not the peat used in batch experiments). Visually, the solution samples taken from reaction bottles of the deeper samples in the batch experiments appeared to have higher DOC (organic staining). Since the adsorption of organic solutes onto DOC and particulate organic carbons negatively affect the retardation of organic contaminants, the partitioning of organic

contaminants from aqueous phase onto them might be necessary to be considered in transport simulations. This requires characterizing the partitioning coefficients specific to this process (Chapter 2; Gharedaghloo and Price 2017).

4.3.5 Retardation factors

The retardation factor (R) was obtained by comparing the benzene BTC to that of chloride, specifically the ratio of breakthrough times, when breakthrough is defined as C/C_0=0.5. R increased with depth (e.g. from 1.2 to 2.8 at core C; Table 4.5), showing that benzene retardation is stronger in deeper peat. The retardation of solutes by adsorption is controlled by both bulk density and the adsorption coefficient. In this study, deeper peat generally had higher bulk density (Table 4.2) and a higher adsorption coefficient (Table 4.3 and Table 4.4) compared to shallow peat layers, resulting in higher solute retardation down the peat profile.

R is directly proportional to the ratio of adsorbed mass (m_{ad}) to non-adsorbed mass; thus, if adsorption is kinetically controlled, decreasing the discharge rate (q) enhances the duration of contact between solution and peat, and consequently increases m_{ad} (thus R). This means R increases with decreasing q. The equilibrium retardation factor (R_{eq}) is the retardation factor when q is sufficiently small to allow enough contact duration to ensure adsorption equilibrium. R_{eq} values were calculated using the adsorption partitioning coefficient (K_d) obtained with inverse modelling (Table 4.4) and using Equation 4.10.

$$R_{eq} = 1 + \frac{\rho_b \times K_d}{\phi_{total}} \qquad \textbf{Equation 4.10}$$

R is less than R_{eq} in all the columns (e.g. R=2.8 and R_{eq}=3.4 at 20-30 cm in core C) due to the non-equilibrium adsorption in FTR experiments. Similar to R, R_{eq} increased with depth from 1.3 to 6.1 at core B and from 1.3 to 3.4 at core C (Table 4.5). The increase means in the presence of chemical equilibrium, the deeper peat might retard the organic solutes more than the shallower peat. It must be noted that the typically slower discharge in deeper peat, compared to shallower peat, increases the likelihood of equilibrium retardation in deeper peat. These results showed that

irrespective of achieving chemical equilibrium the retardation was less in near-surface layers than at depth. The retardation factor of benzene in other aquifer material could range between 1.4-1.6 (Chen et al. 1992) or 1.36-2.32 (Marqa et al. 1999) which shows the similarities between retardation factors obtained for peat in this study with literature values for mineral aquifers.

Table 4.5- Retardation factor (R) and equilibrium retardation factor (R_{eq}) in the experimented soil columns

Core	Depth bgs	R	R_{eq}
core B	0-10 cm	1.2	1.3
	10-20 cm	1.4	2.5
	20-30 cm	5.2	6.1
core C	0-10 cm	1.2	1.3
	10-20cm	1.5	2.7
	20-30 cm	2.8	3.4

4.4 Summary and Conclusion

In high discharge events, the lack of chemical equilibrium between the adsorbed and solute phases results in less retardation of benzene. This enhances the risk of contamination in downstream water bodies. In contrast to chemical non-equilibrium, physical equilibrium between mobile and immobile water in peat pore space established quickly, causing a symmetrical BTC characteristic of a single-porosity medium. Solute dispersion and peat dispersivity are controlled by the variations of pore sizes; peat samples with similar pore size distributions might have similar dispersivity, even if they occur at different depths in the peat profile. Shallow peat layers typically have higher hydraulic conductivity compared to deeper peat. Therefore, under similar hydraulic gradient, water discharge, and as a consequence solute advection, will be more in shallow peat compared to deeper layers. The retardation of benzene was also enhanced with depth. Stronger transport coupled with weaker retardation in shallow peat, compared to deeper layers, will cause preferential migration of organic contaminants in shallow layers. This justifies using methods of restraining contamination redistribution in surface peat; this could include partial removal of the highly permeable upper peat layer in the hydrocarbon spill zone and its down-gradient area, lowering the water table, or establishing a physical or chemical barrier. It must be noted that the systematic heterogeneities in peatlands, e.g. layered nature of peat with significantly different

hydraulic conductivity between layers, still could cause a physical non-equilibrium (Hoag and Price 1995) and long tails in solute breakthrough at the field-scale. This means characterizing the hydraulic conductivity distribution in the peatland with a good resolution is essential for predicting a contaminant's fate and transport. In the field-scale problems, in addition to the sorption, other phenomena including biodegradation (Moore et al. 2002; Mallakin and Ward 1996) and volatilization (Moore et al. 1999) could limit the transport of a dissolved-phase plume. Indeed, further research, especially in field condition, are required to assess the cumulative effect of these processes on dissolved hydrocarbon's behavior. The field-scale studies would help characterizing scale-dependent parameters such as dispersivity (Neuman 1990). Also, the magnitude of the uptake of the dissolved hydrocarbons by the native plant species of peatlands should be quantified. These studies could determine the specific conditions in which natural attenuation scenarios are suitable to allow natural processes to immobilize and degrade a plume, compared to the current standard procedure of removing contaminated soils.

4.5 Acknowledgement

We would like to thank to Wetlands Hydrology Laboratory for their help and support. The research was funded by a NSERC Discovery Grant to Dr. Price.

5 Characterizing the immiscible transport properties of diesel and water in peat soil

5.1 Introduction

After a hydrocarbon spill onto a peatland, the hydrocarbon as a light non-aqueous phase liquid (NAPL) will spread in the aquifer and contaminate the down-gradient ecosystem. NAPL spreading velocity and extent in the contaminated aquifer will be controlled by multiphase flow properties of the aquifer material, including capillary pressure-saturation-relative permeability relations (P_c-S-k_r). The spatial distribution of NAPL plume controls the rate of volatilization, as well as dissolution of organic molecules in water, and determines the spatial distributions and temporal variations of dissolved contaminants down-gradient of the spill zone. It is important for environmental scientists to be able to forecast the distribution of the NAPL plume, but given the poor understanding of multiphase flow in peat, and the absence of parameters characterizing it, this cannot currently be done.

The P_c-S-k_r relation has been characterized for glass beads (e.g. Johnson et al. 1959), unconsolidated sand (e.g. Leverett and Lewis 1941) and sandstones (e.g. Caudle et al. 1951), but not for peat soils. Among the parameters of P_c-S-k_r relations, residual NAPL saturation (S_{Nr}) dominantly controls the extent of the free-phase plume. S_{Nr} is the NAPL saturation in which the relative permeability of NAPL, and consequently its mobility, tends to zero and NAPL stops moving. For a given volume of spilled NAPL, the higher the S_{Nr}, the smaller will be the final extent of a free-phase plume. In downward percolation of spilled NAPL, the magnitude of S_{Nr} determines the mass of NAPL left in the vadose zone and whether free NAPL reaches water table or not. This parameter has not been characterized in peat soils.

After reaching the water table (WT), Light NAPL (LNAPL) distributes above the water table and moves laterally down-gradient. In addition, WT fluctuations can displace the LNAPL (Oostrom et al. 2006) and enhance the lateral extent of the free-phase plume. The WT fluctuations could be frequent in peatlands due to the shallow WT in these aquifers where the thin unsaturated

zone has little capacity to buffer against atmospheric water fluxes. Related observations on the magnitude of the lateral migration of LNAPL above the WT and effect of WT fluctuations on NAPL redistribution have thus far not been documented for peatlands.

Although P_c-S-k_r relations have not been characterized for NAPL-water system in peat, they have been measured frequently for air-water system (e.g. Price et al. 2008; Price and Whittington 2010; McCarter and Price 2014). Due to the lower complexity of air-water measurements compared to NAPL-water measurements, as well as availability of P_c-S-k_r data of air-water systems, using air-water measurements to estimate NAPL-water relations could reduce the cost and characterization time. Notwithstanding the lack of a comparison between air-water and NAPL-water relations in peat soils, a comparison could indicate the similarities and differences and if air-water data are a reasonable proxy for NAPL-water simulations.

The aim of this study is 1) to characterize P_c-S-k_r relations and the residual NAPL saturation in peat soils in varying spill scenarios; 2) to observe the magnitude of the lateral migration of LNAPL above the WT and the effect of WT fluctuations on NAPL redistributions; and 3) to compare P_c-S-k_r relations of water-NAPL system to air-water relations to assess if air-water data provide reasonable estimates of NAPL-water relations. To fit this purpose, one- and two-dimensional peat column experiments were carried out. In these experiments, diesel was used as the NAPL, since it is one of the primary petroleum products transported and its spill, in addition to free-phase and dissolved-phase hydrocarbon plumes, can lead to remobilization of non-organic contaminants in peatlands (Deiss et al. 2004). The results of this study can be used by groundwater modellers and environmental scientists evaluating petroleum hydrocarbon spills in peatlands.

5.2 Methods

5.2.1 Contact angle and scaling capillary pressure relations

Air-water capillary pressure-saturation (P_c-S) relations have frequently been characterized and reported for different types of peat soils (Schwärzel et al. 2006; Price et al. 2008; McCarter et al. 2014) and could be used for a NAPL-contaminated peatland if they can be scaled to NAPL-air and

NAPL-water systems. Several studies have scaled P_c-S data between liquid-liquid and liquid-gas systems (e.g. Parker et al. 1987; Lenhard and Parker 1988). Scaling these data and relations requires knowledge of the interfacial tensions and contact angles of fluids present in the pore space (Demond and Roberts 1991; Bradford and Leij 1995). To investigate the validity of scaling in peat, corresponding P_c-S data and contact angles for different fluid combinations were measured. To measure the contact angles, air bubbles were released onto a peat surface in water or diesel saturated conditions, then the geometry of the bubbles (Figure 5.1) were analyzed to determine the contact angles. Details are available in chapter 2 and Gharedaghloo and Price (2017), who showed contact angle of water-NAPL system in water drainage and NAPL drainage conditions. Here, we report the contact angles of water-air, and NAPL-air (diesel-air) systems, for both the condition of air imbibition (water drainage and diesel drainage).

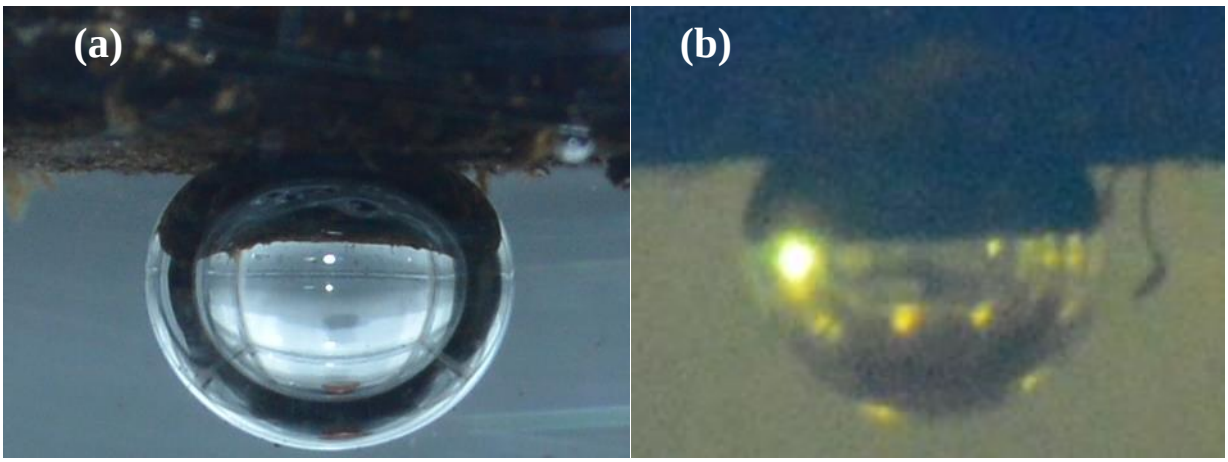

Figure 5.1- Air bubble on peat in the water saturated condition (a), and diesel saturated condition (b), illustrating the water-air and diesel-air contact angles in gas imbibition, respectively.

To obtain the capillary pressure-saturation relations in peat soil in a controlled and reproducible condition, gravity drainage column tests were carried out using milled peat. Milled peat was screened with 1 mm sieve to decreases the heterogeneities and to ascertain that peat particles are of similar size, so the pore size distributions between columns were similar. A column (Figure 5.2a) with separable segments was filled with milled peat. The dimensions of each segment were 5 cm length and 10 cm internal diameter. The peat in each segment was packed individually and with a given dry peat weight, before inserting into the column; this was done to seek homogeneous

bulk density, porosity, and pore size distribution along each column and between replicates. The packed peat column then was saturated with the desired liquid (water or diesel) in the upward direction through the bottom of the column to minimize air trapping. After saturation, the column was drained by opening its bottom valve leading to liquid drainage through bottom of the soil column and air imbibition through the top (Figure 5.2a). After 48 hours of drainage when the outflowing rate was zero the column was separated into segments starting from the top. The weight of a drained segment and the original dry weight of milled peat then were used to calculate the volume and the saturation of the liquid (water or diesel) in the segment. Repeating this for all segments, the variation of liquid saturation with height (Figure 5.2b) was obtained. The procedure was repeated in 4 replicates for water drainage and in 2 replicates for diesel drainage. Eventually, the diesel-air data were scaled and compared to water-air data using Equation 5.1, where σ_{aw} is air-water interfacial tension, σ_{ad} is air-diesel interfacial tension, α_{aw} is the water contact angle at the air-water interface on the peat surface, α_{ad} is the diesel contact angle at the air-diesel interface on peat surface, P_{cad} is capillary pressure in the diesel-air system at diesel saturation of S_d, and P_{caw} is capillary pressure in the water-air system at water saturation of S_w. In scaling, σ_{da} and σ_{wa}, respectively, were considered as 23.8 mN/m (Environment Canada 2018) and 72.0 mN/m (Lide 2012); the median diesel-air and water-air contact angles obtained in contact angle measurements were used in the scaling.

$$P_{caw}(S_w) = \frac{\sigma_{aw}\cos(\alpha_{aw})}{\sigma_{ad}\cos(\alpha_{ad})} P_{cad}(S_d) \qquad \textbf{Equation 5.1}$$

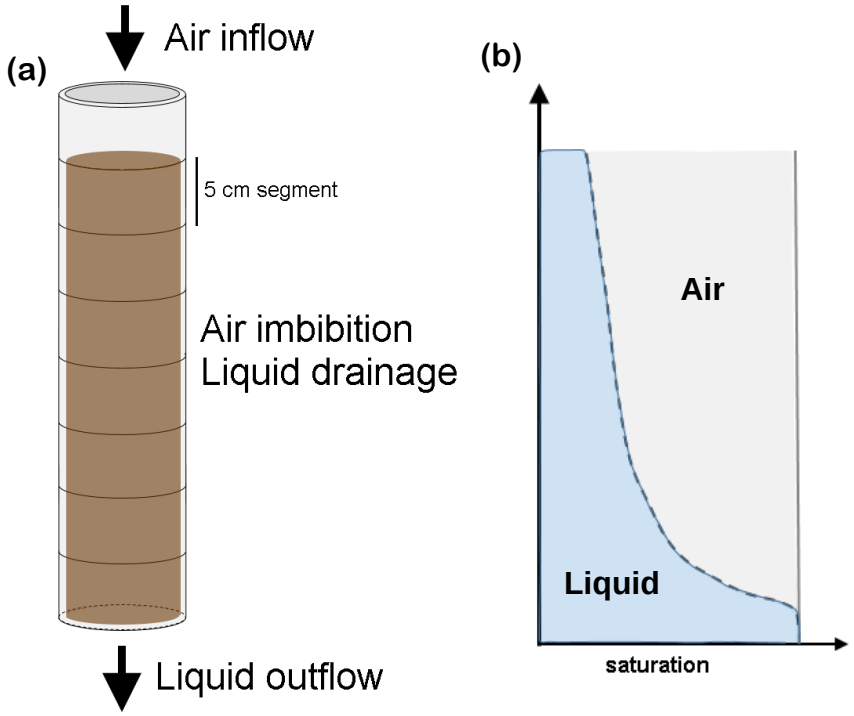

Figure 5.2- Air inflow through top and liquid outflow through bottom of the separable column causing liquid drainage and air imbibition along the soil column (a); idealized vertical distributions of liquid and air saturation along the column at the end of the experiment (b).

5.2.2 Unsteady state displacement column test

One dimensional studies of NAPL percolation into vertical soil columns (e.g. Lenhard et al. 1988; Thomson et al. 1992) have been carried out to assess the behavior of NAPL during imbibition into the soil pore. In addition, such vertical columns have been used to determine the relative permeability relations (Sahni et al. 1998; DiCarlo et al. 2000) and NAPL recovery (e.g. Kantzas et al. 1988) under gravity drainage conditions. Such vertical displacement tests could be representative of the condition that NAPL is spilled on water saturated soil surface (e.g. in a train derailment), after which NAPL spreads above the peat surface and percolates downward into the soil profile due to water table decline. Unsteady-state immiscible displacement tests were carried out in (unsegmented) vertical peat columns. The aim was to simulate the percolation of NAPL into the peat profile, to indicate the effects of peat properties on NAPL percolation rate and NAPL

trapping, and to quantify k_r of the diesel phase in peat columns under the gravity drainage condition.

Two types of peat (A and B) with different physical properties were used in these experiments. Peat A was extracted from a bog peatland in Quebec (47° 58' N, 69° 26' W) and peat B was from a bog peatland in Southern Ontario (43° 55' N, 80° 25' W), and the extracted peat monoliths were frozen after extraction. From each frozen peat monolith (peat A and B) three columns (A1, A2, A3, B1, B2, B3) with diameter of 5.1 cm and length between 30-36 cm were cut; one compacted peat column (A4) was also made using residue of peat A. The aim of using a compacted column was to compare the results of a highly disturbed (compacted) column and the intact columns. Each column was first saturated from the bottom with deionized water to minimize air trapping. Constant head permeability tests were carried out with deionized water on the columns to obtain their hydraulic conductivity and absolute permeability. Next, a 17.6-19.3 cm diesel column (varying between columns) was placed at the surface of water-saturated peat (Figure 5.3a). The bottom valve of the column was then opened allowing water to flow out the column and diesel to imbibe into it due to gravity (Figure 5.3b). Through diesel imbibition, diesel head above the peat surface declined continuously and equaled zero when the diesel-table was at the peat surface (Figure 5.3c) after which two-phase flow of diesel-water ended and air started imbibing into the pore space, forming a three-phase flow regime along the soil column. Through the experiment the cumulative produced volumes of water and diesel were recorded for two phase flow period and a part of the three-phase flow period (Figure 5.3d) to be used in relative permeability calculations. Gravity drainage was continued for ~48 hours until water and diesel outflow ceased.

In all columns of peat A, diesel breakthrough occurred before the two-phase flow period ended. However, diesel breakthrough at the outflow did not occur in column B1 at the end of the two-phase flow period, thus the diesel production trend was not recorded for this core. Again, for column B2, the initial height of diesel column was not sufficient to cause diesel breakthrough by the time the diesel level declined to the peat surface; so in this column, diesel was added gradually to the peat surface to maintain the diesel head at the peat surface and delay air imbibition until diesel production at the outflow started and continued for few minutes. To avoid such discrepancies, in column B3, the initial height of diesel column was increased to 25.3 cm to

ascertain diesel breakthrough and its production at the end of two-phase flow period of the experiment.

At the end of gravity drainage process, to determine the final distributions of water and diesel along the columns, each column was cut into ~5 cm segments, and the segments were squeezed with a hydraulic press (~120 atm) to extract the water and diesel. The deformable peat matrix provided good water and NAPL recovery from its pore spaces. However, since not all fluids were recovered by pressing, in-situ residual volumes and saturations of water and diesel were estimated (Appendix A) based on the extracted volumes of water and diesel and the air-dried weight of the peat. The air-dried weight was also used to calculate bulk density and porosity. Finally, the balance of residual diesel volume in peat columns was checked (Appendix B) to ascertain that no significant error was imposed.

The relative permeability of peat to diesel (kr_D) was estimated using the cumulative diesel percolation and production data. Diesel breakthrough at the column outflow indicated a continuous diesel phase along the column, which means the average relative permeability of diesel in the column could be calculated using diesel head data and its outflow rate. If at two times, t_1 and t_2 [T] diesel heads are h_1 and h_2 [L], respectively, and the average diesel outflow rate between t_1 and t_2 is Q_D [L^3T^{-1}], the average effective hydraulic conductivity of diesel (K_{effD}) between t_1 and t_2 is estimated using Darcy's law (Equation 5.2) for diesel such that

$$K_{effD} = \frac{Q_D L}{A \Delta h} \qquad \textbf{Equation 5.2}$$

where A is cross sectional area of the peat column [L^2], L is the length of the column [L], and Δh is the head difference between up-gradient (top of peat column) and down-gradient (bottom of peat column) [L], which is equal to $(h_1+h_2)/2$. Next, effective permeability of peat to diesel (k_{effD}) was obtained using

$$k_{effD} = \frac{K_{effD} \mu_D}{\rho_D g} \qquad \textbf{Equation 5.3}$$

where μ_D is diesel viscosity [$MT^{-1}L^{-1}$], ρ_D is diesel density [ML^{-3}], and g is acceleration constant [LT^{-2}]. Finally, kr_D was calculated as the ratio of k_{effD} and absolute permeability (k) of the peat column. The average water saturation (S_w) along the column between t_1 and t_2 was obtained using the cumulative water production data. If cumulative produced water volumes at t_1 and t_2 are V_{w1} and V_{w2}, the average cumulative water production between t_1 and t_2 ((V_{w1}+V_{w2})/2) demonstrates the drained volume, thus the drained porosity. Using the drained porosity and the total porosity of column, the average water saturation between t_1 and t_2 was calculated. Repeating these for every two adjacent measurements, the variations of diesel relative permeability with water saturation were obtained for each tested column. This relative permeability of diesel is for the water drainage condition.

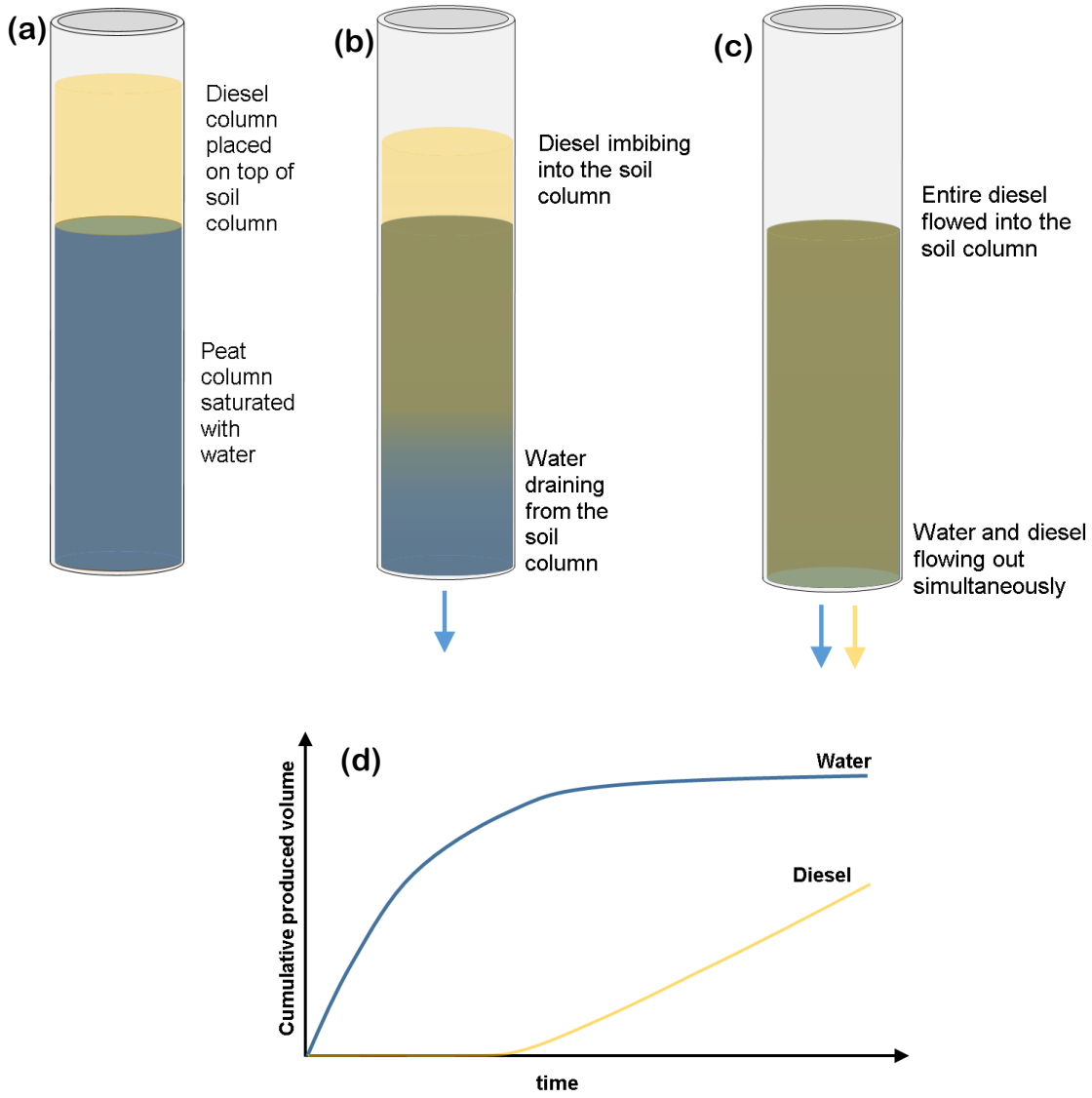

Figure 5.3- (a) peat column is saturated with water and a diesel head is placed above the peat surface; (b) outflow valve is opened, diesel imbibes into the soil column and water flows out through column bottom due to gravity drainage; (c) three-phase flow begins when no diesel head is left above soil surface; (d) idealized variations of cumulative produced water and diesel through the two-phase flow period of the experiment

5.2.3 Inverse modelling and estimating P_c-S-k_r functions

Capillary pressure and relative permeability functions have been estimated through inverse modelling in NAPL-water and air-water system (Chardaire-Riviere et al. 1992; Sigmund and McCaffery 1979; O'Carroll et al. 2005; Parker et al. 1985; Crescimanno and Iovino 1995). In these

studies, P_c-S-k_r functions of porous media were treated as fitting parameters and were adjusted to match observed data with numerical simulation results. In a similar approach, here, the two-phase flow periods of the immiscible displacement tests were used to estimate P_c-S-k_r functions of peat. The aim was to match the measured water and diesel cumulative outflows with a numerical model through adjusting peat P_c-S-k_r functions. Two different forms of P_c-S-k_r relations were used: 1) the Brooks and Corey's (1964) model, and 2) power law model (PLM) with no capillary pressure. Equation 5.4 to Equation 5.7 describe the P_c-S-k_r functions of Brooks and Corey's model (BCM) where P_{cth} is the threshold capillary pressure at which water drainage begins and diesel starts imbibing into the largest pore sizes corresponding to P_{cth}, S_e is the normalized water saturation, S_w is water saturation, S_{wirr} is the irreducible water saturation and is the water saturation at which water ceases flowing, λ is pore size distribution factor of the porous medium, k_{rw} is water relative permeability and k_{rN} is diesel (NAPL) relative permeability. λ controls the curvature of the k_r-S curves.

$$P_c = P_{cth} S_e^{-1/\lambda} \qquad \textbf{Equation 5.4}$$

$$S_e = \frac{S_w - S_{wirr}}{1 - S_{wirr}} \qquad \textbf{Equation 5.5}$$

$$k_{rw} = S_e^{\frac{2+3\lambda}{\lambda}} \qquad \textbf{Equation 5.6}$$

$$k_{rN} = (1 - S_e)^2 \left(1 - S_e^{2+\lambda/\lambda}\right) \qquad \textbf{Equation 5.7}$$

Equation 5.8 and Equation 5.9 describe the power law relative permeability relations, in which n_N and n_w, respectively, are the powers of diesel relative permeability and water relative permeability relations and determine the curvature of the relative permeability relations.

$$k_{rw} = S_e^{n_w} \qquad \textbf{Equation 5.8}$$

$$k_{rN} = (1 - S_e)^{n_N} \qquad \textbf{Equation 5.9}$$

To model the two-phase flow of water and NAPL in peat columns, the open-source MATLAB Reservoir Simulation Toolbox (MRST, 2017a) (Lie, 2016) was used. MRST solves the two-phase

flow equation (Equation 5.10) simultaneously for water and diesel, and calculates spatial distribution and temporal variations of saturations and fluxes along the peat columns.

$$\phi\rho_f \frac{\partial S_f}{\partial t} = \frac{\partial}{\partial z}\left(\rho_f \frac{kk_{rf}}{\mu_f}\left(\frac{\partial p_f}{\partial z} - \rho_f g \right)\right) + q_f \qquad \textbf{Equation 5.10}$$

In Equation 5.10, *f* is a pore fluid and represents water and diesel phases, S_f is the saturation of the fluid, p_f is the pressure of the fluid [$ML^{-1}T^{-2}$], k_{rf} is the relative permeability of the fluid, $\boldsymbol{k}$ is absolute permeability of peat [L^2], ϕ is porosity, ρ_f is density of the fluid [ML^{-3}], g is gravitational constant [LT^{-2}], z is the elevation [L] and q_f is a sink/source term [$ML^{-3}T^{-1}$]. A one-dimensional vertical model of each column with its corresponding permeability and porosity values was built in MRST. The upper boundary condition of the column was controlled by an imaginary diesel injection well in which the diesel injection rate (as the diesel percolation rate) varied with time. Temporal variations of diesel rate in the injection cell was obtained having the variations of diesel head with time. The boundary condition at the bottom of the column was a production well which operated with atmospheric bottom hole pressure (BHP) and was open to produce both water and diesel. Using the model the outflowing rates of water and diesel at each column's outflow were simulated. The density of diesel was measured as 0.83 g/mL and was used as input in the numerical models. Water density was assumed as 1g/mL and its dynamic viscosity was assigned as 1 mPa.s. The dynamic viscosity of diesel was assumed as 2 mPa.s at the laboratory condition (Environment Canada, 2018).

Two sets of estimating simulations, one with BCM and the other with PLM, were run for each column. In the estimating simulations with BCM, λ, S_{wirr}, and P_{cth} parameters were treated as the unknown parameters, and in the simulations with PLM, S_{wirr}, n_w, and n_N were the unknown parameters. For each column, MRST simulated the downward percolation of diesel into the peat column and calculated the variations water and diesel outflowing rates with time. Next the root-mean-square-error (*RMSE*) of diesel cumulative outflowing volume was calculated with

$$RMSE = \sqrt{\frac{\sum_{i=1}^{n}\left(y_i^{measured} - y_i^{simulated}\right)^2}{n}} \qquad \textbf{Equation 5.11}$$

where n is number of observed points, $y_i^{measured}$ is a value of observed cumulative diesel volume and $y_i^{simulated}$ is the corresponding value at in the simulated case. FMINCON minimizing function of MATLAB was used to minimize *RMSE* through adjusting and calibrating the unknown parameters. Finally, the realization with the lowest *RMSE* was selected as the model with representative model parameters.

Studies have raised concerns regarding uniqueness of the results obtained by this method (Kool et al. 1985; Eching and Hopmans 1993) meaning that there is a possibility that two or more sets of P_c-S-k_r data result in similar minimum objective functions. Eching and Hopmans (1993) recommended measuring pressure in the core to resolve the non-uniqueness issue; however there are other arguments that the including tensiometer data in inverse modelling are not necessary (O'Carroll et al. 2005). To avoid the possible problem of non-uniqueness, the calculated k_r-S data of diesel (discussed in previous section) was another check-point for the estimated diesel k_r–S relations.

5.2.4 Diesel spill in a two dimensional peat box model

Two-dimensional experimental soil boxes have been used to study the redistribution of NAPL in porous material (Høst-Madsen and Jensen 1992), the effect of water table variations on the behavior of NAPL (Oostrom et al. 2006), the effect of soil heterogeneity on NAPL redistribution (Illangasekare et al. 1995), and the recovery of petroleum contaminants through flooding them (Palomino and Grubb 2004). These 2-D flow cells allow control of the environmental condition and release of hydrocarbon between field-scale and core-scale studies. Using these box models, the redistribution of NAPLs can be studied where releasing a field-scale spill is not an option. Here, the peat box model was used to observe the redistribution of diesel in vadose zone of peat and to evaluate the effect of water table fluctuations on its remobilization.

An intact peat sample (50 cm x 50cm x 10 cm) was extracted from peatland B. Extraction was done in winter when the top 30 cm of the soil was frozen to minimize monolith disturbance. The peat monolith was placed in the main chamber of a peat box (Figure 5.4). A “well” at each side of

the box connected to the main chamber with screens allowed adjustment of the water table (WT) and visual monitoring of WT and free diesel thickness in the peat box during the experiment. The wells represented ditches that might be excavated around the spilled area to collect spilled liquids in a field-scale spill problem.

Monitoring NAPL percolation and spreading in pore space in laboratory-scale studies has been done visually (e.g. Van Geel and Sykes 1994; Palomino and Grubb 2004; Conrad et al. 2002), using X-ray (e.g. Fagerlund and 2007; Goldstein et al. 2007), dual gamma attenuation (e.g. Høst-Madsen and Jensen 1992), and electrical resistance (e.g. Pantazidou and Sitar 1993). Measuring the electrical resistance of porous media has been a tool for characterizing the variations of aqueous phase saturations in pore space in other earlier studies (e.g. Leverett 1939; Leverett and Lewis 1941; Morgan and Pirson 1964). Electrical resistance measurement was planned to be measured to monitor NAPL percolation during and following the diesel spill. The peat column was flushed with 50 litres of 100 mg/L sodium chloride solution for 2 weeks before the spill to place an electrically conductive aqueous fluid in peat pore space. A network of electrodes were embedded at the front and back of the 2D column (Figure 5.4). At the end of brine flushing WT level was set at 9.5 cm above the bottom of the peat (~40 cm below ground surface) and was monitored over the following 4 days to ascertain physical equilibrium established between air and water phases before the spill.

A network of 8 hydrophilic and 8 hydrophobic pressure transducers were embedded at the front face of the peat box (Figure 5.4) to respectively measure water and diesel pressures during the experiment. Preparing and treating the transducers are discussed in Appendix C. Primary measurements showed that the response time of a transducer was ~10 minutes which was not short enough to allow measuring fluid pressures with a high enough frequency during and following the shower spill. However, the transducers allowed monitoring the temporal variations of water pressure before the spill, and water and diesel pressures after the spill. This helped deciding whether a physical equilibrium was established between pore fluids, before and after spill, and following the rainfall events and water table fluctuations. Before and after each event, the pressure values were monitored; the absence of temporal variations of pressure in all the transducers was assumed to imply physical equilibrium.

To simulate the spill, diesel was released at a constant rate of 17.7 mL/min over the central 20 cm of the peat box (area of 200 cm^2). The diesel spill continued for 105 minutes, cumulatively releasing 1858 mL of diesel to the peat surface. The thickness of free NAPL above the WT at the side well and within the peat box was monitored following the spill. Starting 7 days after the spill, diesel was pumped out from the side wells. This was to simulate the lateral redistribution of NAPL in a field condition, to the surrounding area or to the excavated ditches. NAPL was collected continuously over the next 2 weeks until no free NAPL was evident at the side wells. The aim was to encourage lateral migration until the remaining free-phase diesel in pore spaces reached its residual saturation, whereupon it stops moving.

Next, two heavy rainfall events were simulated by releasing drips of deionized water across the peat surface through a network of tubes with 2.5 cm spacing. The aim of the simulated rainfall was to raise WT in the peat box and to observe the effect of WT fluctuations on diesel redistribution. For the first event the rate of water release was 34.7 mL/min, simulating a rainfall event with intensity of 4.2 cm/hour. WT level rose after the rainfall, and the system equilibrated in 24 hours, after which water was drained from the side wells to return WT to the pre-rainfall level. Another rainfall simulation with an intensity of 33.4 mL/min was done, and after 24 h WT was again returned to the pre-rainfall level. NAPL released after each rainfall event was collected from side wells. After the second rainfall the system was monitored for 1 week for possible flow of NAPL to the side wells and to ensure that system had reached equilibrium.

To determine the spatial distributions of NAPL after these experiments, the peat monolith was cut into segments. To avoid fluid loss during cutting, WT was lowered to the bottom of the peat prior to its removal, so that the fluids were under capillary pressure and would not leak out. The peat monolith was segmented into 25 10×10×10 cm cubes, which were then squeezed with a hydraulic press to collect the remaining diesel and water.

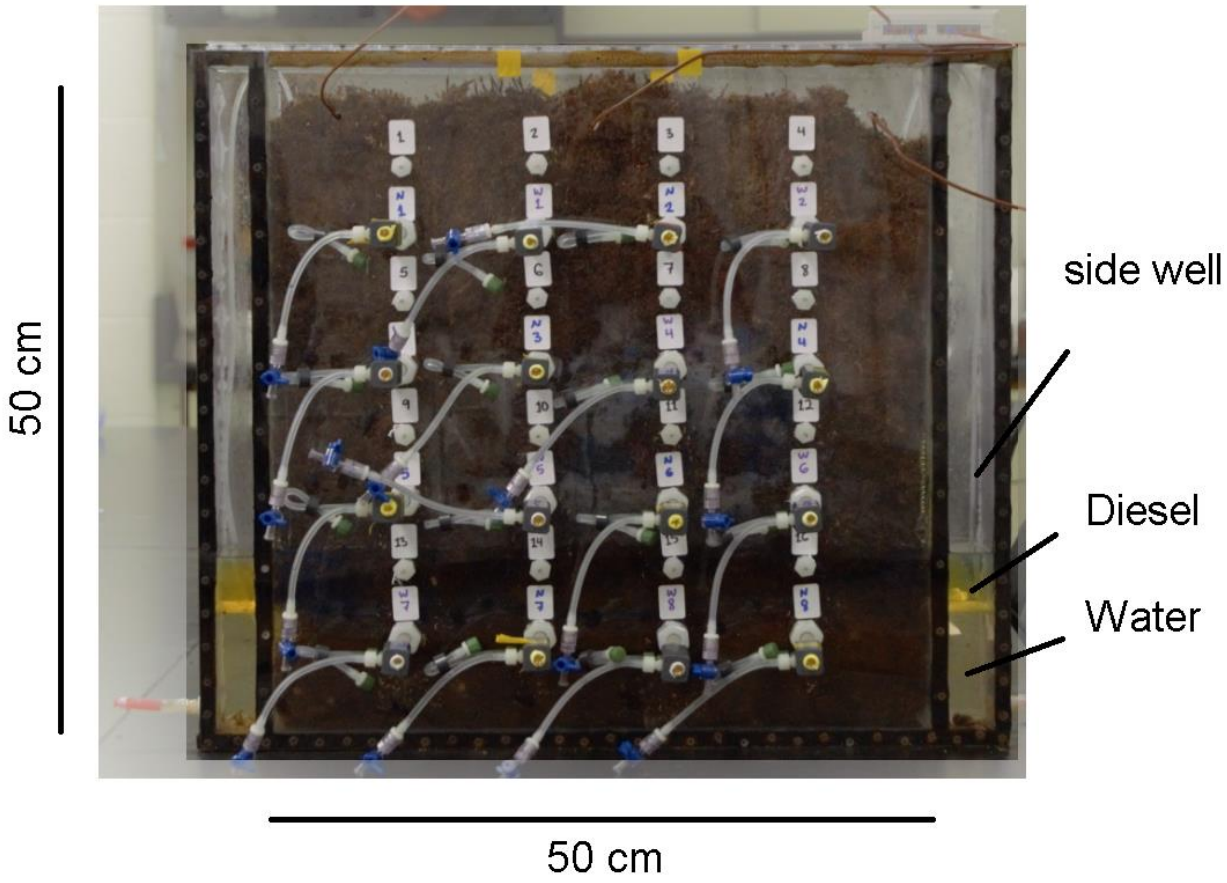

Figure 5.4- 2D peat box after the diesel spill; side well with diesel and water levels are evident; water and diesel pressure transducers with 10 cm spacing labelled N (for diesel) and W (for water). Hexagonal ports held electrodes enabling electrical resistance measurements through the experiment.

5.3 Results

5.3.1 Contact angle and air-liquid column tests

Respectively, 22 and 19 images were processed for water-air and diesel-air contact angles on peat. Water-air contact angles ranged from 39.7°-59.8° with a median of 51.7° (mean ± std.dev.=51.6° ± 4.5°). The diesel-air contact angles ranged from 45.9°-73.7° with a median of 61.2° (mean ± std.dev.=60.2° ± 7.6°). The median values of water and diesel contact angles were used in Equation 5.1 and in scaling the height-saturation data of the diesel to water-air system. Figure 5.5a illustrates the elevation-saturation data for the diesel-air and water-air (segmented) column tests, showing that at a given height above the water table or diesel table (pressure=1 atm)

the saturation of diesel is evidently less than water saturation (in the presence of air, hydrocarbon retention is less than water retention). In Figure 5.5b, capillary pressure-saturation data are calculated by converting the elevation to capillary pressure. Then, the capillary pressure-saturation data of the diesel-air system is scaled to that of the water-air system using Equation 5.1 (Figure 5.5c).

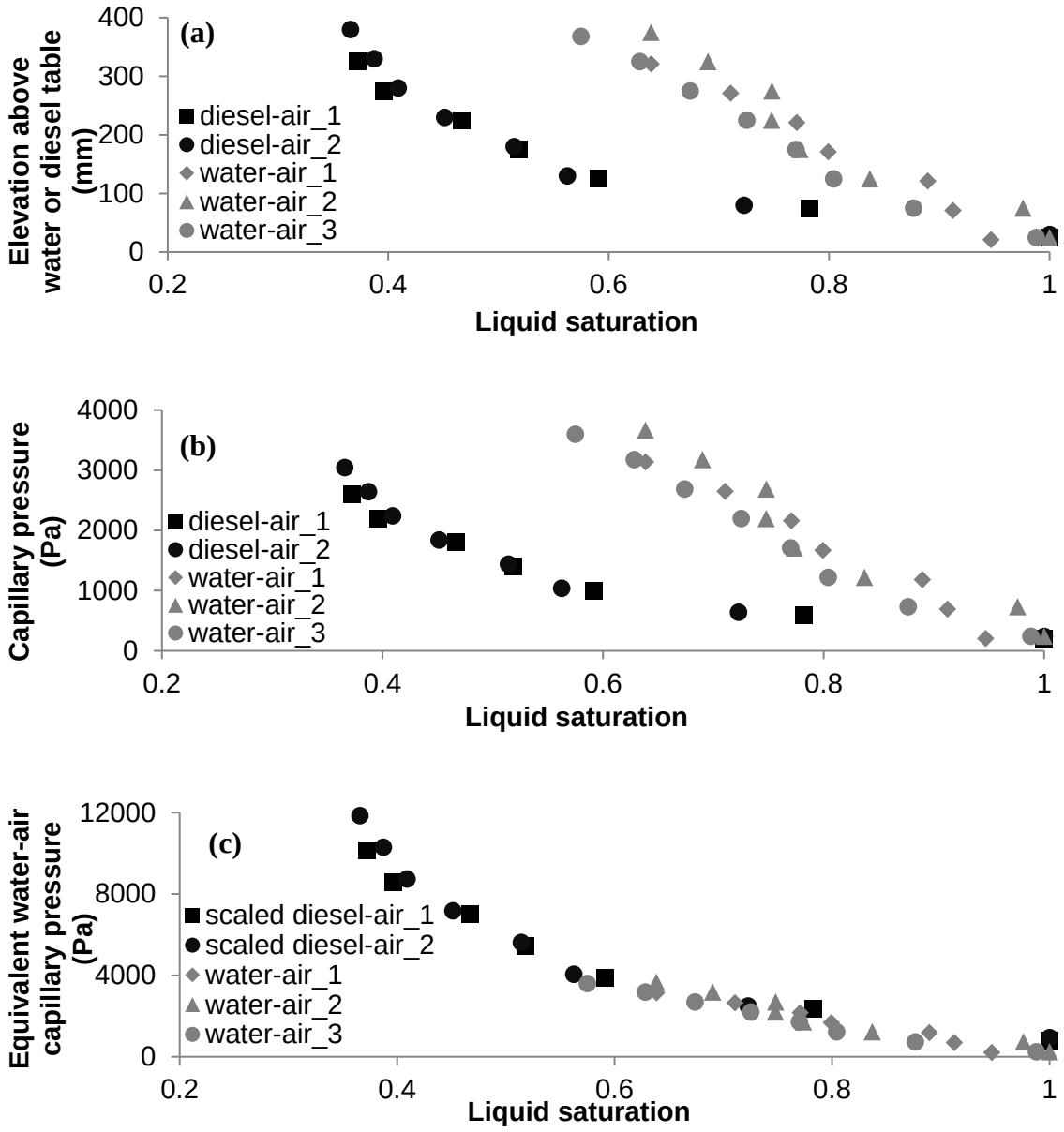

Figure 5.5- (a) unscaled height-saturation data for diesel-air and water-air column tests using milled peat; (b) unscaled capillary pressure-saturation relations for diesel-air and water-air drainage condition; (c) scaled diesel-air capillary pressure-saturation data (using Equation 5.1) compared to water-air capillary pressure-saturation data.

5.3.2 Vertical distributions of diesel and water

The physical properties of the tested 1D immiscible displacement columns (Table 5.1) shows that the porosity of peat A was evidently less than the porosity of peat B. The hydraulic conductivity of peat A was on average 5 times less than for peat B. The spatial variations of water and liquid (water+diesel) saturations along the columns at the end of immiscible displacement column experiments (Figure 5.6) show that due to capillarity, liquid and water saturations generally decreased with elevation above bottom of the columns; the increase is more evident in columns of peat A. The average water saturation remaining in columns of peat A is more than the average water saturation of the columns of peat B. In Figure 5.6, the area between water and liquid saturation curves corresponds to the diesel saturation showing that average diesel saturation along peat B is less than that in peat A, and on average is less than half the values of peat A (Table 5.1). This shows that residual diesel saturation in peat pore space is inversely correlated with its porosity and hydraulic conductivity. The results also show that although the peat column was compacted and highly disturbed in A4, its porosity, permeability, and residual diesel saturation were similar to those of A2 and A3.

Table 5.1- Physical properties of peat columns in unsteady state immiscible transport experiments; *porosity of A1 is the average of A2 and A3

column	Porosity (%)	Hydraulic Conductivity (m/s)	Absolute Permeability (m^2)	Residual diesel saturation (S_{Nr})
A1	92.8%*	1.0×10^{-4}	1.0×10^{-11}	-
A2	92.8%	1.1×10^{-4}	1.1×10^{-11}	17%
A3	92.7%	5.6×10^{-5}	5.6×10^{-12}	17%
A4	90.0%	3.4×10^{-5}	3.3×10^{-12}	12%
B1	97.1%	3.5×10^{-4}	3.4×10^{-11}	4%
B2	96.9%	4.0×10^{-4}	3.9×10^{-11}	5%
B3	96.2%	6.4×10^{-4}	6.3×10^{-11}	7%

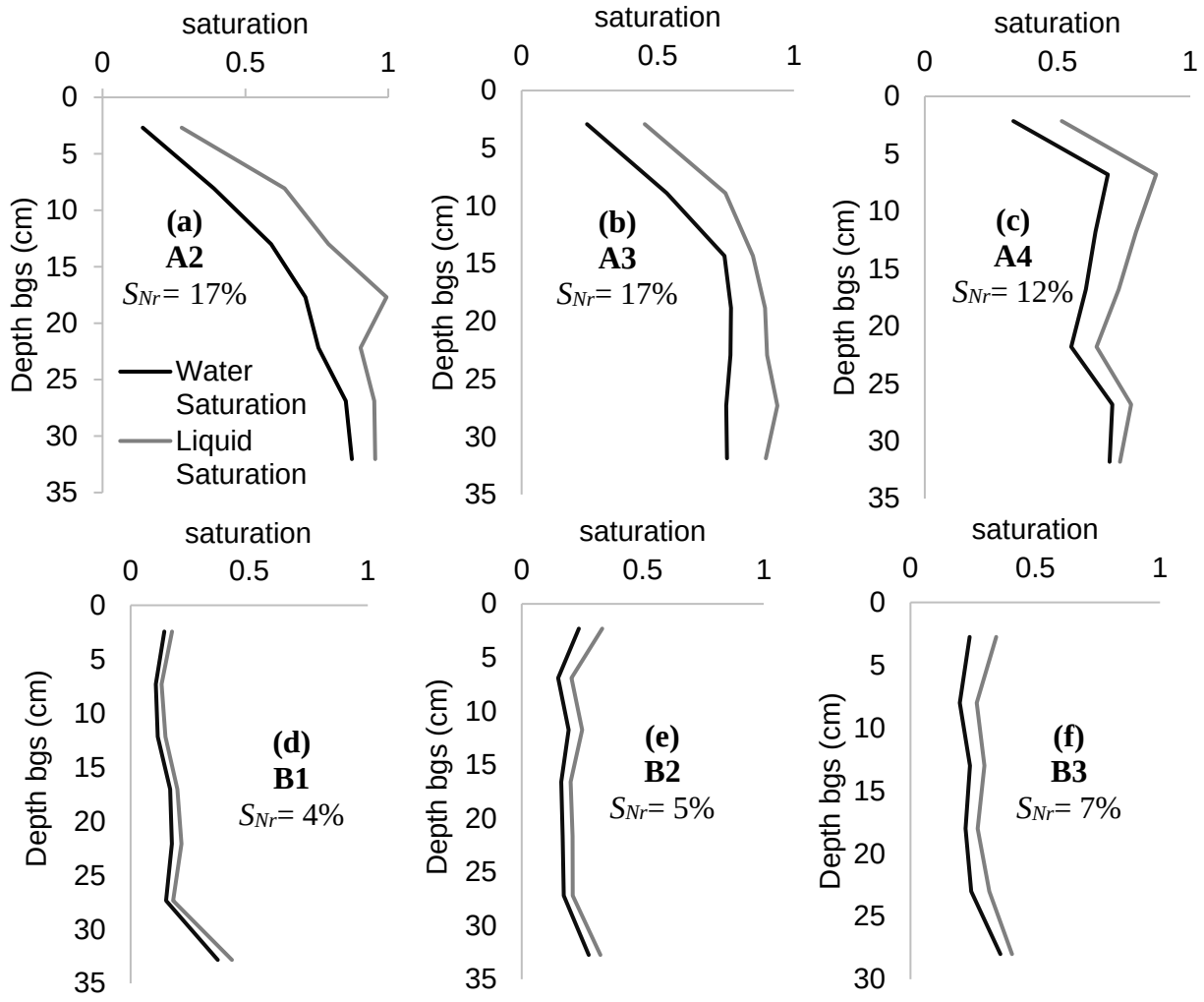

Figure 5.6- Variations of liquid saturation and water saturation with depth below ground surface (bgs) (top of each column) in the experimented columns of core A and core B; S_{Nr} is residual NAPL (diesel) saturation in the column.

5.3.3 Measured and estimated P_c-S-k_r relations

Each 1D immiscible displacement column test had a two-phase flow period, which started with diesel percolation into the pore space and ended when declining diesel head reached the peat surface, and a three-phase flow period as air imbibed into the peat column. The cumulative water and diesel production trends in the two-phase flow period of the immiscible displacement experiments were used in inverse modeling simulations. The range of the unknown parameters in

the inverse modelling simulations are presented in Table 5.2. Figure 5.7 illustrates the variations of measured and simulated cumulative production of water and diesel in the tested peat columns. The rate of diesel percolation into the pore space, which is the sum of the slopes of water and diesel production curves (in Figure 5.7), is evidently larger in peat B than in peat A. The diesel percolation rate correlates with hydraulic conductivity of peat columns.

Table 5.2- Ranges of uncertain/unknown parameters in random search simulations

	Brooks and Corey's Model (BCM)			**Power Law Model (PLM)**		
column	S_{wirr}	P_{cth} (Pa)	λ	S_{wirr}	n_w	n_N
A1	10-30%	20-100	0.1-7	45-55%	5-7	5-7
A2	10-70%	20-100	0.1-7	10-70%	2-7	2-7
A3	10-70%	20-100	0.1-7	10-70%	0.8-7	0.8-7
A4	60-75%	20-100	0.1-7	10-70%	0.8-7	0.8-7
B2	10-70%	20-100	0.1-7	25-50%	2-7	2-7
B3	10-70%	20-100	0.1-7	35-70%	2-7	2-7

The *RMSE* of all the columns are less than 6.1 mL (Table 5.3). The results show that both BCM and PLM relations can accurately describe diesel percolation and outflow rates in peat columns. Also, the water relative permeability curves obtained for a column by calibrating BCM (black lines in Figure 5.8) are in good agreement with corresponding curve estimated using PLM (black dashed lines in Figure 5.8).

Table 5.3- Estimated parameters of P_c-S-k_r relations

Brooks and Corey's Model (BCM)				
column	S_{wirr}	P_{cth}	λ	***RMSE*** **(mL)**
A1	29.9%	50.0	0.382	1.86
A2	45.8%	29.9	0.705	3.28
A3	47.5%	20.7	0.488	6.09
A4	61.2%	30.4	3.39	0.84
B2	10.6%	30.3	5.88	1.26
B3	26.0%	21.1	7.00	1.76
Power Law Model (PLM)				
column	S_{wirr}	n_w	n_N	***RMSE*** **(mL)**
A1	50.0%	5.83	5.46	3.71
A2	46.7%	5.61	2.00	3.04
A3	55.8%	5.07	2.00	5.83
A4	61.8%	3.39	2.30	0.79
B2	25.1%	2.01	2.82	1.39
B3	35.0%	2.52	4.59	0.738

The estimated BCM parameters show that for intact peat cores the estimated irreducible water saturation (S_{wirr}) ranges between 29.9-47.5% for peat A and between 10.6%-26.0% for peat B. In PLM model estimations, S_{wirr} ranges between 46.7-55.8% for peat A and between 25.1-35.0% for peat B. Independent of the P_c-S-k_r model used, S_{wirr} in peat A is higher than that in peat B. The curvature of water relative permeability (n_w) was similar between replicates of peat A (5.07-5.83), as well as between replicates of peat B (2.01-2.52).

S_{wirr} values obtained, respectively, using BCM and PLM simulations (Table 5.3) are similar in most columns, but differ in a few columns including A1 and B2. The difference is likely due to the limitations of BCM, which is unable to describe water and NAPL relative permeability curves with low curvatures. Details on the cause of differences are provided in Appendix D.

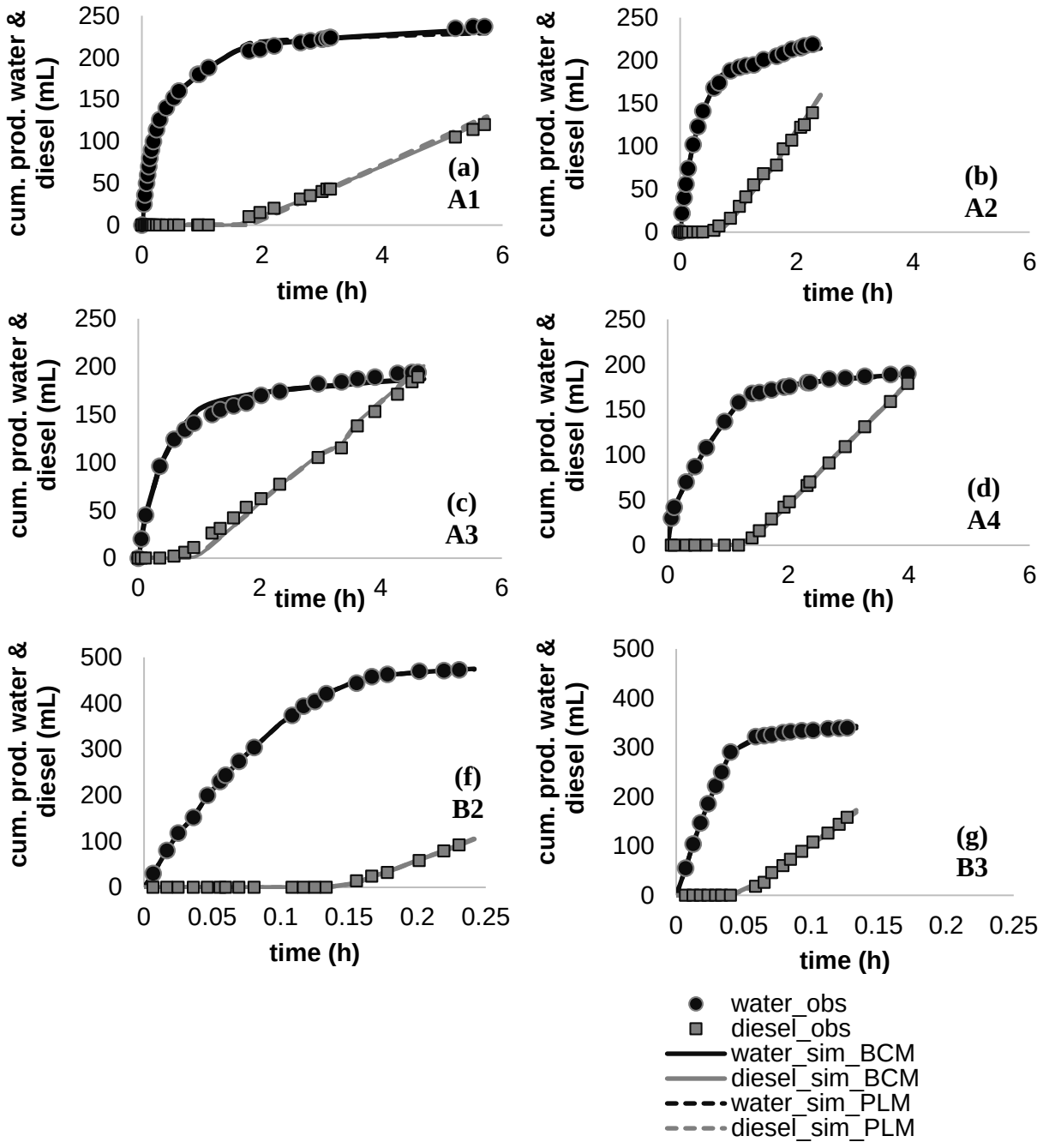

Figure 5.7- Measured and simulated cumulative production curves of water (black curves and circles) and diesel (grey curves and squares) in the experimened peat columns; note the different scales in the x- and y-axes of for the different peat types.

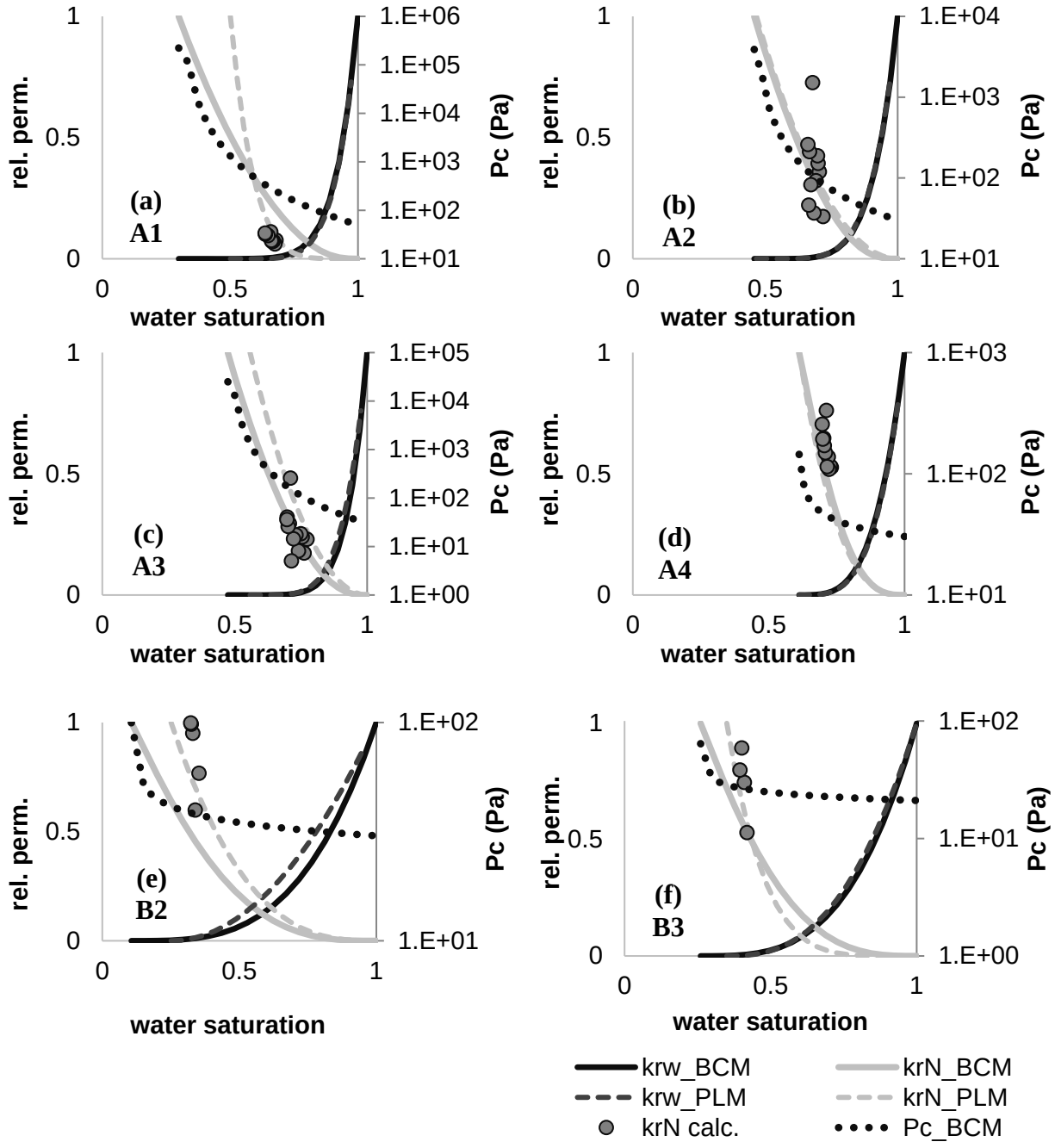

Figure 5.8- estimated water relative permeability (k_{rw}), diesel relative permeability (k_{rN}) and capillary pressure (Pc) curves using Brooks and Corey's model (BCM), and power-law model (PLM); grey circles illustrate diesel relative permeability measured using diesel outflow data.

5.3.4 Peat box

Twenty minutes after the spill started, traces of diesel were observed (visually) accumulating at the center of the peat box above the WT. Forty minutes after the spill began, diesel accumulation within peat and above the WT was observed. Approximately 4.7 hours after the spill began, the apparent diesel thickness above WT was ~6.5 cm in the main chamber, and diesel migrated to the side wells through the screens. Approximately 7.7 hours after the spill time, the diesel thickness at the left side well was 5.7 cm, and the apparent thickness of diesel layer within peat was 5.8 cm. The rate of change of diesel layer thickness slowed down after this time. After 21.7 hours the thickness of the diesel layer in the left well and within the peat box both were 6.1 cm. Two days after spill, the thicknesses of diesel were 6.2 cm and 6.1 cm in the left well and in peat, respectively. One week after spill the thicknesses were, respectively, 6.2 cm and 6.4 cm in the left well and in the peat box. During this one-week period diesel did not flow into the right well due to a clogged screen, so the clogging was removed allowing redistribution of diesel to a similar thickness in both side wells and in the main chamber. After 8 days the diesel that had collected above WT in the side wells was pumped out. This simulates lateral distribution of diesel in a natural peatland, or pumping diesel in collection ditches excavated around a spill zone. Approximately1525 mL of diesel were pumped out during the following two weeks period, representing ~82% of the 1858 mL of the spilled diesel, which had migrated laterally to the side wells after reaching the water table.

The first infiltration event, equivalent to ~5 cm of water over 1.3 hours, caused a WT rise of 6 cm. As the WT returned to its pre-rainfall level, 5 mL of diesel was released from the pore spaces to the side wells. The second rainfall was equivalent of 4.8 cm of water over 1.3 hours, causing a WT rise of 6.7 cm. No additional diesel flowed out as the WT returned to its pre-rainfall condition. At the end of experiment, dropping the WT to the bottom of the sample released 12 mL of diesel.

Figure 5.9 illustrates the spatial distributions of porosity, diesel saturation, and water saturation in the peat box at the end of the experiment. The porosity ranged from 92.4% to 98.0, and although scattered horizontally within a layer, generally declined with increasing depth and down the peat profile. On average the porosity in the right side of the chamber was less than in the center and left side of the monolith. Water retained by capillary forces was higher on the right side and with depth.

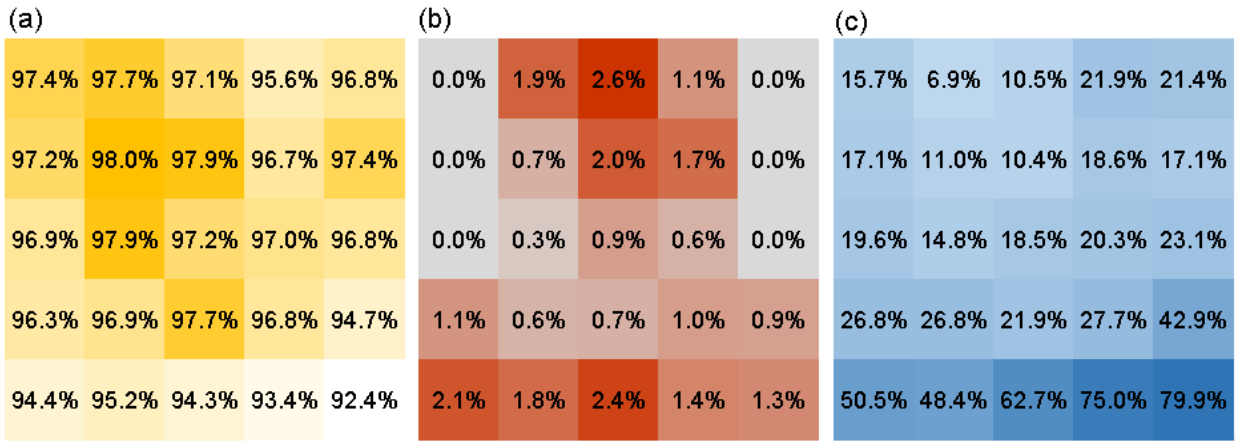

Figure 5.9- Spatial distribution of porosity in the peat box; value in each segment is (a) the porosity, (b) diesel saturation, and (c) water saturation of the segment; higher values in each figure are illustrated with more intense color.

The residual diesel saturation in the contaminated peat in the peat box experiment varied between 0.3% and 2.6%, with higher residual saturation in the central segments (0.7%-2.6%), reflecting the placement of the spill over the central 20 cm of the peat. No lateral dispersion of diesel into the side blocks at the top 30 cm of the peat occurred. The volume of diesel removed from the system due to lateral migration over the first 7 days, both simulated infiltration events, and final drainage was 1525, 5, and 12 mL, respectively. The volume of residual diesel in the drained monolith was 241 mL. Hence, of the 1860 mL spilled volume, 77 mL (~4% of initial spill volume) of diesel was unaccounted for, representing the mass balance error. The measured resistance values were inconsistent, experienced drift and a distinct diurnal oscillation and displayed no relation to diesel presence in pore space. Consequently, resistance values were considered spurious, and were rejected.

5.4 Discussion

Scaling measured diesel-air P_c-S data to water-air system successfully matched measured water-air P_c-S relations. This suggests water retention data available for different types of Canadian peat soils could be scaled to other fluid-fluid systems using representative interfacial

tensions and contact angles. In the case of a diesel spill onto a peatland, diesel-water and diesel-air capillary pressure data might be estimated using corresponding contact angles and the available water retention curves of the contaminated peat. In this study, diesel-air and water-air contact angles on peat were measured as 51.7° and 61.2° for liquid drainage conditions. Gharedaghloo and Price (2017) and chapter 2 have reported water contact angles on peat in presence of diesel during water drainage and water imbibition. If hydrocarbon liquid other than diesel is spilled on a peatland, similar methodology could be applied to determine corresponding contact angles and to scale the capillary pressure data using appropriate interfacial tensions.

In columns A1 and A4 the global minimum for a wide range of parameter uncertainty did not match the calculated diesel k_r data. Therefore, the upper and lower bounds of the uncertainty ranges of the parameters were limited to ensure k_r-S curve of diesel (grey lines in Figure 5.8) were close to the measured points (grey circles in Figure 5.8). This shows that the Brooks and Corey's (1964) model (Equation 5.4 to Equation 5.7) and the power law model (Equation 5.8 and Equation 5.9) can be used to model diesel flow and production in the column tests. While there are other relative permeability models (e.g. Chierici 1984; Huang et al. 1997), they have more parameters, which increases the risk of uncertainty and non-uniqueness in model parameterization.

Peat columns comprising peat from the same source had similar water relative permeability curves (Figure 5.10). The water relative permeability curves of peat A (black curves) and peat B (grey curves) form separate clusters illustrating their distinct water relative permeability trends. This similarity was reflected in similarity of relative permeability model parameters; for example the estimated n_w parameter of PLM ranged between 5.07-5.83 in A1-A3 columns of peat A and between 2.01-2.52 in columns of peat B (Table 5.3); in other example, the irreducible water saturation (S_{wirr}) of PLM ranged between 46.7-55.8% in A1-A3 columns of peat A and between 25.1-35.0% in B2-B3 columns of peat B showing similarities within a type of peat and differences between two experimented peat types. Price at al. (2008) presented unsaturated hydraulic conductivity (K_{unsat}) of water in peat B within peat samples taken between 0-25 cm below ground surface (bgs) at the same peatland. The calculated k_{rw} data from their study (grey circles in Figure 5.10) were in agreement with k_{rw} of peat B obtained in our study (grey lines in Figure 5.10). This suggests that in the absence of water relative permeability data for NAPL imbibition conditions,

the unsaturated hydraulic conductivity of peat that has been measured for water drainage condition could be a reasonable estimate of k_{rw}-S relation.

At a given water saturation, peat B has higher k_{rw} compared to peat A (Figure 5.8, Figure 5.10). The physical properties of the tested columns (Table 5.1) shows that peat A was more compacted and had smaller pore sizes compared to peat B. The amount of diesel saturation that reduces water relative permeability to $k_{rw} \leq 0.01$ is ~30% in peat A, while it is ~60-70% in peat B. This is likely due to a higher frequency of macro-pores and active pores in peat B compared to peat A, so that during diesel imbibition, a given saturation of diesel occupies a smaller fraction of active porosity of peat B compared to that of peat A. Consequently water flow is diminished less in peat B and the degree of k_{rw} reduction with increasing NAPL saturation is greater in peat A (Figure 5.10). Irreducible water saturation (S_{wirr}) of peat A (46.7-61.8%) was higher than that of peat B (25.1-35.0%) (Table 5.3). This is similar to the variations of residual water content in water-air system where reduction of peat hydraulic conductivity -which takes place typically down the peat profile and due to peat compaction and decomposition- is associated with increasing residual water content (Price and Whittington 2010; Goetz and Price 2015).

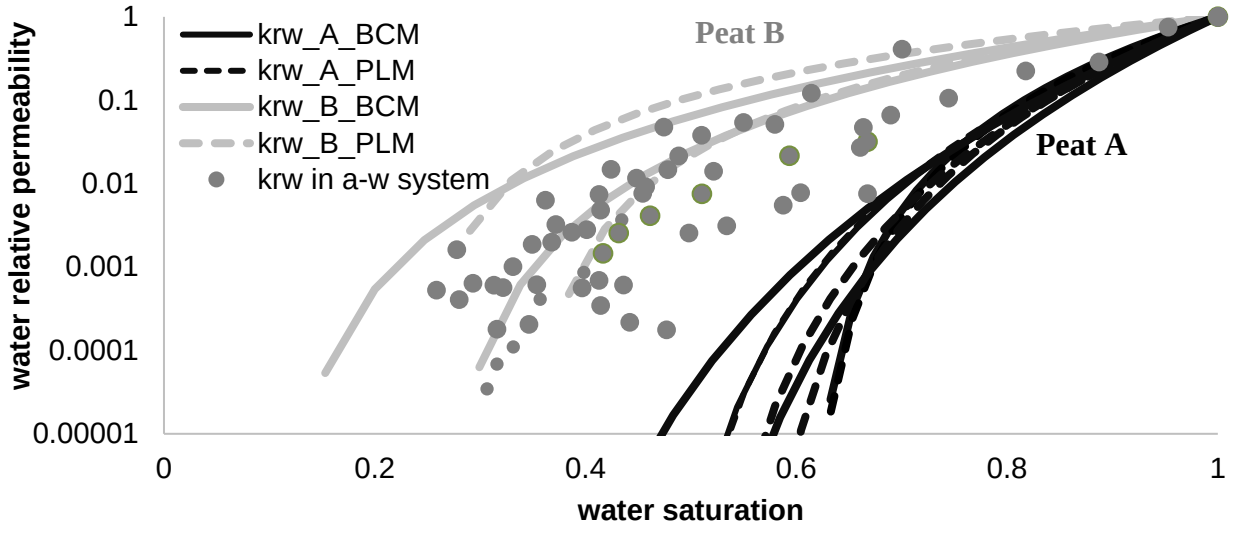

Figure 5.10- Estimated relative permeability curves from two-phase diesel-water flow (curves) for core A (black curves) (A1, A2, and A3 columns) and core B (grey curves) (B2 and B3 columns), and measured water relative permeability in water-air system (grey circles) from Price et al. (2008), taken from the same peatland.

The relative permeability relations and residual diesel saturation after gravity drainage of water and diesel were similar between intact columns of peat A (A1, A2, A3) and the compacted column (A4). This may have occurred due to the similar porosity and hydraulic conductivity of A4 peat to that of A1-A3. This means packing disturbed peat samples from a contaminated site to porosity and permeability values of the contaminated peat might be more representative of intact peat than using intact peat from a different peatland that may have completely different porosity and permeability.

In one dimensional immiscible displacement column tests, the residual saturation was higher in peat A compared to that in less dense peat B (Figure 5.6). Furthermore, the diesel percolation rate varied between peat types and was proportional to hydraulic conductivity. This, in association with the increase of residual diesel saturation with peat density, leads to faster percolation and higher risk of lateral diesel migration in peatlands with less dense peat. The results also suggest that, due to variation of peat density and hydraulic conductivity between hummocks and hollows, diesel percolation rate and the residual diesel saturation could vary substantially within a peatland. Due to shallower water table depth in hollows compared to hummocks, diesel migration to water table will likely happen earlier in hollows. This might lead to continuous NAPL phases and NAPL movement in the connected hollows, which is similar to the preferential migration of dissolved contaminants in the connected hollows of peatlands (Balliston 2017).

In the 1D column experiments, before air imbibition, macro-pores of the peat columns were drained and diesel replaced water in those pores. However, in the peat box experiment and during the spill, due to the rapid infiltration of diesel and limited rate of diesel spill, the vadose zone of the peat stayed partially unsaturated containing all three phases of water, diesel and air. Consequently, the maximum diesel saturation in 1D columns were higher than that in the vadose zone of the peat box. The residual NAPL saturation is positively correlated with maximum NAPL saturation before air imbibition (Van Geel and Roy 2002) which means higher residual saturation of diesel in the column experiments. This explains why the residual diesel saturation in peat B in the column experiments (4-7%) was higher than that in the same peat in the peat box experiment (0.3-2.6%.).

Nearly 77 mL the diesel was unaccounted for based on the mass balance; the difference could be due to diesel biodegradation, given the relatively warm column temperature (~21±2°C) that favours microbial biodegradation and considering that diesel microbial communities can actively degrade the petroleum hydrocarbons (Kelly-Hooper et al. 2013). However, the 77 mL of diesel is unlikely to have been broken down by microbial activity in such limited time (42 days). The other potential mass balance error could be due to retention of liquid hydrocarbons in the peat matrix even after air-drying and volatilization (Jarsjö et al. 1994). Finally, some methodological error associated with estimating the residual volume (Appendix A) likely contributed to the difference.

At diesel saturation of 1-S_{wirr}, diesel relative permeability tends to 1 meaning that diesel effective permeability becomes equal to absolute permeability of the peat column. Due to the large capillary pressure threshold of micro-pores, diesel does not percolate into the dead-end pores and the inactive porosity of peat, occupying only active porosity including macro-pores. Thus, if the diesel effective permeability equals the absolute permeability, 1-S_{wirr} is the portion of the porosity in which fluid flow takes places. This means 1-S_{wirr} corresponds to the active porosity, suggesting that the flooding of saturated peat with diesel might be a dynamic and flow-based method for characterizing active and inactive porosities of peat; so far the active porosity has been characterized with static and non-flow based methods (e.g. Hoag and Price 1997; Quinton et al. 2009; McCarter and Price, 2017; Rezanezhad et al. 2009, 2012).

In cases where spilled liquid is compositionally similar to diesel, the sum of water-NAPL (σ_{wN}) interfacial tension (28.9 mN/m for diesel-water from Environment Canada 2018) and NAPL-air (σ_{Na}) interfacial tension (23.8 mN/m for diesel-air from Environment Canada 2018) is less than water-air (σ_{wa}) interfacial tension (i.e. $\sigma_{wa}>\sigma_{wN}+\sigma_{Na}$). Physically this means a thin film of NAPL remains between the air and water phases in the contaminated pores, minimizing the surface energy of the system. Based on Chatzis et al. (1988) and Kantzas et al. (1988) the NAPL film spreading between water and air enhances NAPL drainage and reduces its retention. Sohrabi et al. (2000) demonstrated that in such condition an iterative imbibition of water phase and a gas phase (e.g. air) could reduce the NAPL retention and enhance its recovery from pore space. In a contaminated peatland, the iterative imbibition of water and air could take place due to frequent rainfall events and the consequent water and air invasions to the NAPL contaminated zone. In the peat box

experiment, 5 mL of diesel were released after the first rainfall and during the WT drawdown, which could be due to the iterative water and gas invasion. In a field condition the iterative invasion of water and air can potentially remobilize residual NAPL from the contaminated zone. This suggests that manipulated fluctuations of the water table might be an appropriate strategy for reducing residual NAPL in the spill zone of a contaminated peatland.

5.5 Conclusion

For the first time, relative permeability of a NAPL in peat pore space was estimated and P_c-S-k_r model parameters were characterized. The estimated relative permeability of water was in good agreement with measured value of Price et al. (2008) suggesting that relative permeability of peat to water in an air-water system might be a reasonable estimate for its relative permeability to water in NAPL-water flow. The estimated relative permeability of diesel was also in good agreement with the measured values of this study. The relative permeability are needed by environmental scientists and groundwater modellers to estimate NAPL migration in contaminated peatlands after an oil spill.

The diesel percolation rate and its retardation in the vadose zone of the peat layer was shown to be a function of peat pore structure. The percolation rate increased in peat with lower bulk density, while residual diesel saturation increased with bulk density. The residual diesel saturation in peat varied between 0.3-17% depending on the spill scenario and physical properties of the peat. The variation of residual diesel saturation with water table depth in a given peat implies that the residual diesel saturation depends on moisture regime and thus potentially on the time of the year in which the spill occurs. In the case of a hydrocarbon spill onto a peatland, these results could be used to determine if the downward percolating free-phase NAPL will be retained by peat in the vadose zone, or if the volume of free-phase hydrocarbon is large enough to pass the vadose zone and arrive at the water table.

In the peat box experiment and when water table was ~40 cm below ground surface, more than 80% of the spilled diesel reached water table and migrated laterally to the side wells. In a shallower water table condition, the total volume of residual diesel left in the narrower vadose zone would

be less compared to deep water table conditions, so the fraction of spilled diesel migrating to the side wells would be greater. In a natural peatland setting, excavating ditches at the down-gradient face of the free-phase plume's edge might be an efficient option for recovering spilled LNAPL. If the volume of spilled NAPL is large enough for it to pass through the vadose zone and reach the water table, the ditches could collect the mobile portion of the spilled NAPL. The results also suggest that water table fluctuations could remobilize NAPL present in peat vadose zone meaning that artificially fluctuating the water table in the source zone could reduce the residual NAPL in the vadose zone.

5.6 Appendix A: Estimating diesel and water volumes in contaminated peat

A traditional method for obtaining residual NAPL saturation is retort distillation, in which the NAPL-containing sample is placed in a chamber and the temperature is raised to >500°C to evaporate water and NAPL from the core. Then, the released vapours are condensed giving the initial water and NAPL mass in the sample (API, 1998). However, this method cannot be employed for peat soils since at temperatures of ~500°C the peat sample would burn away. A potential alternative method would be to place the sample containing NAPL and water in a Dean-Stark apparatus from which the water is removed by distillation and the NAPL is extracted through with a solvent (e.g. toluene) (API, 1998). However, this method would dissolve the natural hydrocarbons and waxes present in the peat matrix and cause error. A method that was sufficiently simple and could be repeated for heavy masses of contaminated peat and a large number of contaminated samples is needed. A cylindrical apparatus with an outflow was constructed using a hydraulic press, whereby the liquids are released from an outflow valve. To determine diesel and water volumes remaining in the pore space, peat was squeezed with hydraulic press up to a pressure of ~120 atm. Compacting peat removed in average 73% of pore fluids in each column test; the rest of the liquids remained in the compacted peat. To overcome this issue, it was assumed that the volumetric ratio of liquids that flowed out of peat while pressing was the same as the ratio of their in-situ saturations. Using the primary weight of the peat containing water and diesel, the dry weight of peat after drying the compacted peat for 7 days, and the volumetric ratios of liquids in the sample (from the compression), in-situ volumes and saturations of water and diesel were estimated for

contaminated samples. To test the accuracy of this method, 20 grams of milled peat were mixed with known volumes of diesel and water at varying ratios. The mixtures were then pressed, and then using the approach noted above the volume of diesel and water in the mixture was estimated. Figure 5.A.1 compares the actual and estimated volumes of liquids in the evaluation tests showing that the estimating method does not overestimate or underestimate the water and diesel volumes in peat samples, and the error associated with estimations is negligible. It should be noted that this method is specific to peat soils and when NAPL saturation is high enough to flow out of the pore space. The advantage of this method is its simplicity and potential for use in the field. The disadvantage is that it might perform poorly at low and non-mobile ranges of contamination concentrations.

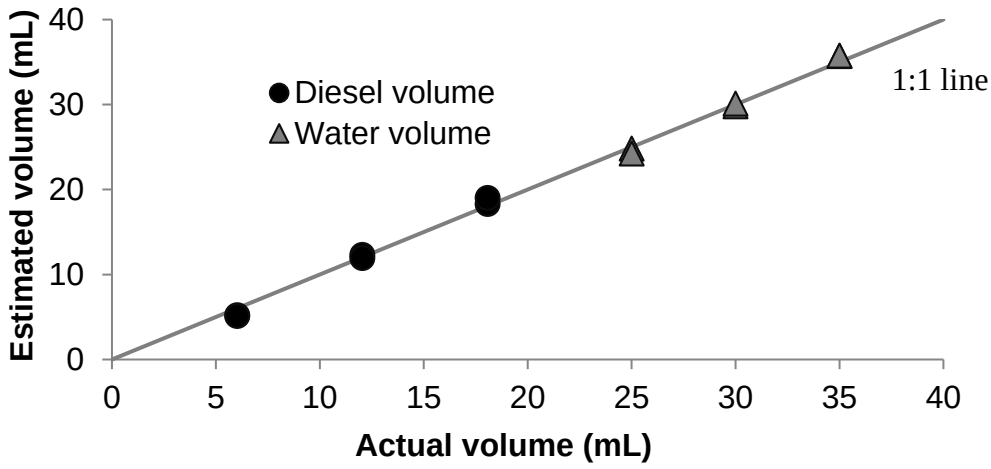

Figure 5.A.1- Actual and estimated volumes of water and diesel in peat pressing tests

5.7 Appendix B: mass balance in one dimensional peat column experiments

Using the assumption discussed in Appendix A, peat segments from column tests were pressed and the extracted volumes of each phase and the total liquid weight of each segment were used to estimate in-situ volumes of water and diesel along each column. Table 5.B.1 shows the error in diesel mass balance is under 5 mL (up to 1.3% of spilled diesel volume). This means the estimated volumes of diesel inside columns are similar to actual values and the estimations did not introduce large errors in estimated diesel volumes of each column.

Table 5.B.1- Summary of mass balance of diesel in the peat column experiments; where $V_{spilled}$ is volume of diesel initially placed above the water saturated peat column, $V_{outflow}$ is volume of diesel that flowed out of the column bottom by the end of the experiment, V_{column} is the estimated volume of diesel remaining inside the column; $Error_{volume}$ is the volumetric error of diesel mass that is missing due to assumptions, and *Error* is the percentage of missing to total volume.

Column	$V_{spilled}$ (mL)	$V_{outflow}$ (mL)	V_{column} (mL)	$Error_{volume}$ (mL) ($V_{spilled}$-$V_{outflow}$-V_{column})	*Error* ($Error_{volume}/V_{spilled}$)×100%
A2	367	256	112	-1	-0.3%
A3	395	283	107	5	+1.3%
A4	368	297	75	-4	-0.9%
B1	356	329	26	1	+0.3%
B2	578	536	37	5	+0.9%
B3	513	475	40	2	+0.4%

5.8 Appendix C. Preparing pressure transducers

Hydrophobic porous ceramic are required to measure NAPL pressure in the system. Several studies have chemically treated porous ceramics to change their wetting tendency and to obtain hydrophobic ceramics to facilitate measurement of NAPL pressure with transducers. Lenhard and Parker (1988) used chlorotrimethysila and Ahmed and Van Geel (2009) used octadecyltrichlorosilane as the chemicals for treating the porous ceramics. A similar chemical, Dichlorodimethylsilane (Sigma-Aldrich) was used in this study. Clean dry porous ceramic cups (Soilmoisture Equipment Corp, USA) were placed in 50:50 (vol/vol) mixture of Dichlorodimethylsilane and benzene (EMD Millipore, GR grade, purity>99%) for 1 week. The bottle containing mixture and the porous cups was shaken once every 24 hours to promote the chemical reaction between Dichlorodimethylsilane and ceramic cups. After 1 week the ceramics were dried in the fume hood for 24 hours, and then were placed in kerosene for 24 hours to remove residual free Dichlorodimethylsilane from ceramic cups (suggested by Ahmed and Van Geel 2009). Then, the treated ceramic cups were used in assembling the NAPL pressure transducers. Untreated porous ceramic cups were used in assembling water pressure transducers. The NAPL and water transducers were filled respectively with diesel and water; the filling process and air removal process was done iteratively to leave no air bubbles in main chamber of the transducers. Finally, the transducers were inserted into the peat body in a way that each porous cup was 5 cm

within the peat body. Out of 8 NAPL (diesel) and 8 water pressure transducers, 6 NAPL and 6 water pressure transducers were above the initial water table, and two of each type were below the initial water table.

5.9 Appendix D: Causes of the differences in the estimated S_{wirr} between BCM and PLM models

For λ ranging between 0.1-7 the power of k_{rw} curve varies in 3.3-23; therefore, if the power of k_{rw} relation of the media is less than 3.3 (i.e. the k_{rw} curve has low curvature), the BCM model will fail to describe the k_r-S relation of water in the medium. In this case, the optimization function that is minimizing the error between observed and simulated production curves cannot match the production curves by adjusting λ, and instead, will adjust S_{wirr} (to less realistic values) to produce required k_{rw} values in mid ranges of water saturations. On the other hand, PLM does not contain the curvature limitation and can describe and produce low curvature k_r-S relations with power less than 3.3. In addition, water and NAPL relative permeability relations in BCM are correlated by λ. Based on the equation of k_{rN} in BCM (Equation 5.7), the curvature of k_{rN} relation has a higher and a lower limit, which can add to the risk of unrealistic S_{wirr} in the BCM model in the optimization process. The ability of the PLM model in producing k_r-S curvatures that are out of the bounds of BCM could explain why the RMSE from PLM simulations is generally less that of BCM results (Table 5.3). The inability of BCM model in producing low curvatures in relative permeability curves and the co-dependence of water and NAPL k_r-S relations in this model could be the reasons that S_{wirr} determined from BCM is less than that from the PLM. It must be noted that irrespective of the difference between values of S_{wirr} in these models, the k_r-S curves obtained from PLM and BCM simulations, especially those of water, are very similar graphically (Figure 5.8). In summary, BCM limitations in producing low curvatures in the relative permeability relation may render it less accurate than PLM.

6 Conclusion and Recommendations

This thesis is one of very few studies with specific focus on hydrocarbon fate and transport in peat and considering specific properties of peat and peatlands. Multiphase flow characteristics of peat including its wetting tendencies in the presence of water, diesel, and air, and its relative permeability-saturation relations were investigated (Chapter 5). The contact angle measurements demonstrated strong hysteresis in peat wetting preferences, and showing that peat surface is both hydrophilic and hydrophobic depending on the water drainage or imbibition scenarios (Chapter 2). For the first time, the water contact angle on peat surface in water drainage and air imbibition condition was estimated as 51.7° (Chapter 5). This contact angle can be used to estimate the corresponding pore radius size of a specific matric potential when analyzing peat water retention data. Relative permeability-saturation (k_r-S) relations were estimated for two types of peat with different bulk densities and hydraulic conductivities. The estimated k_r-S relations showed that the irreducible water saturation increases with peat bulk density (Chapter 5), which was analogous to the increase of residual water content with peat bulk density in air-water retention analyses. In the experiments, the higher the bulk density of peat, the more was the curvature of water k_r-S relations. This means the reduction of water relative permeability due to the percolation of a given volume of diesel is more intense in the denser peat. The residual diesel saturation was measured in peat using different peat types and in different moisture conditions. It was observed that the residual diesel saturation were positively correlated with peat bulk density (Chapter 5). Furthermore, the residual diesel saturation for a given type of peat varied depending on the spill scenario and the maximum diesel saturation before air imbibition; the residual diesel saturation was directly proportional to the maximum NAPL saturation in pore space which is in agreement with observations of previous studies done in inorganic porous media.

Diesel percolation rate due to water table drawdown was directly proportional to the hydraulic conductivity of peat (Chapter 5). In the experiment simulating a diesel spill, for a spilled diesel thickness of ~9.6 cm, more than 80% of the spilled liquid passed the vadose zone, reached the water table and left the soil column through lateral migration, leaving <2.6% of diesel saturation in the contaminated section of the vadose zone. This suggests that excavating ditches at the perimeter of the spill zone could potentially collect a large portion of the spilled NAPL (Chapter

5). Indeed, similar studies on other types of peat, with different water table depths, and other NAPLs such as bitumen or gasoline could provide a more comprehensive evidence on the efficiency of excavated ditches.

Observations of dissolved contaminant adsorption and miscible transport experiments showed that the fate and transport of dissolved hydrocarbons is controlled by the variation of peat matrix chemistry and its pore network. In these experiments, the adsorption of benzene and toluene varied with peat depth (Chapter 3). Based on the results, the adsorption of each of these compounds was not affected by presence of the other (Chapter 3). The lack of competition in the adsorption of these contaminants suggested that individual partitioning coefficients could be used in multi-solute transport problems. The results also demonstrated that toluene K_{OC} in peat was less than the average previously reported value which means using non-peat-specific values might underestimate the velocity of dissolved-phase plumes and contaminant breakthrough time in the surrounding observation points (Chapter 3). Measuring adsorption coefficient of other organic contaminants such as poly-aromatic hydrocarbons (PAHs) and in a wider range of peat types (woody peat or sedge peat) and deeper peat layers (deeper than 40 cm) would fill the data gap and help with the assessment of dissolved-contaminant behavior in peatlands more realistically.

The active macro-pores and inactive dead-end pores present in peat pore network constitute a systematic dual-porosity pore structure, where solute advection takes place through the active porosity. Estimating the rate of mass transfer between active and inactive porosities showed that even with high water discharge rates, the transfer rate between active and inactive porosities is potentially high enough to promote physical equilibrium between active and inactive pores (Chapter 4). The symmetrical breakthrough curves associated with the physical equilibrium suggests that the type of peat that is systematically a dual porosity medium might still behave as a single-porosity medium at the core-scale (Chapter 4). However, it must be noted that the field-scale heterogeneities including the systematic variation of peat hydraulic conductivity with depth could still cause a non-Fickian transport and long tails in the breakthrough of conservative tracers. The asymmetry in the breakthrough of dissolved benzene indicated a chemical non-equilibrium in the adsorption of benzene (Chapter 4). A reduction of the contaminant's retardation factor was an

implication of the chemical non-equilibrium, which implies a higher risk of the pollution of surrounding systems in high water discharge periods of the year.

Conceptually, both free-phase and dissolved-phase plumes could potentially spread in shallow peat layers that have high hydraulic conductivity and larger pore sizes. The larger horizontal permeability coupled with less pore entry pressure in the shallow peat horizons compared to deeper peat might cause preferential lateral distribution of NAPL at the shallower and more conductive peat layers (Chapter 2). On the other hand, the retardation factors of dissolved organic contaminants increases with peat depth, while peat hydraulic conductivity typically decreases down the peat profile (e.g. Hoag and Price 1995, Quinton et al. 2008); the cumulative effect of these variations is a less spreading velocity of dissolved contaminants in deeper peat horizons compared to the shallower one (Chapter 4). Both free-phase and dissolved-phase will reach a maximum extent and stop growing afterward. The maximum extent of free-phase plume is reached when NAPL saturation reaches its residual NAPL saturation value, whereupon the free-phase plume stops moving (Chapter 2). The maximum extend of dissolved-phase plumes is determined as a cumulative effect of dissolution, advection, and fate (i.e. adsorption, biodegradation, volatilization, and other transformations), thus depends on the individual rate of each (Chapter 2).

So far, there has been no documented application of well-established treatment techniques such as pump and treat, air-sparging, soil vapor extraction, chemical oxidation, etc. in treatment of hydrocarbon contaminated peatlands. Meanwhile, there is a concern of unwanted additional disturbance of the peat layers such as stripping, which destroys the ecological function of the system. Our laboratory-scale observations suggests that the excavation of collection ditches at the perimeter of the spill zone might be an efficient way for removing the mobile fraction of the spilled light NAPLs (Chapter 5). Excavating the ditches does not require removal or disturbance of entire contaminated peat, which is the current primary practice after a spill (Chapter 2), and can be done with light excavating tools that reduce compaction or disturbance of peat layer. Our observations also suggest that manipulating the water table could remobilize the residual free hydrocarbons and promote the removal of entrapped free-phase hydrocarbons in field settings. As the mobile fraction of free-phase hydrocarbons are removed, natural attenuation processes such as adsorption of dissolved contaminants (Chapters 3 and 4), biodegradation of remaining free-phase and dissolved-

phase contaminants (Moore et al. 2002; Kelly-Hooper et al. 2013), could limit the extent of the contaminant plume (Chapter 2) and remove contamination mass. Although very limited field-scale studies have explored natural attenuation processes in peatlands (Moore et al. 2002), the efficiency and success of these processes in limiting contaminating plumes' extent in mineral aquifers has been proven in a large number of cases studies (e.g. Rice et al. 1995; Newell and Connor 1998), which suggests that after removing the mobile fraction of free-phase hydrocarbons from contaminated peatlands, it might worth trying monitored natural attenuation as a remediation strategy. Monitoring the contaminated peatlands under natural attenuation would provide empirical evidence on the degree of the efficiency of natural attenuation in peatlands and would help assess whether the strategy is suitable for peatlands.

The insights gained from this study may help peatland scientists, environmentalists, and groundwater modellers in predicting the behavior of petroleum hydrocarbon contaminants in peat and peatlands and in assessing the risks of these contamination. However several questions remain unanswered and further work is required to be done to fill the knowledge gap. Additional research could be conducted 1) to examine the functionality of P_c-S-k_r relations with the botanical origin of peat soil, as well as to peat depth, 2) to characterize the variations of adsorption and retardation with depth in peat of a wider range of peatlands (fen, swamp, etc), and 3) to investigate NAPL biodegradation and the impact of its biodegradation on the peat decomposition rate. In addition, and more importantly, it is recommended to study the natural attenuation of hydrocarbon contaminants in a peatland setting at the field-scale. This would enhance our understanding of the sustainability of peatlands after a contamination and their capability in retaining the contaminants and potentially resolving the issue.

7 References

Abdul, A. S., Gibson, T. L., & Rai, D. N. (1990). Use of humic acid solution to remove organic contaminants from hydrogeologic systems. *Environmental science & technology*, *24*(3), 328-333.

Adamson, A.W., & Gast, A.P. (1967). Physical chemistry of surfaces. Interscience New York.

Adebajo, M. O., Frost, R. L., Kloprogge, J. T., Carmody, O., & Kokot, S. (2003). Porous materials for oil spill cleanup: a review of synthesis and absorbing properties. *Journal of Porous materials*, *10*(3), 159-170. doi:10.1023/A:1027484117065.

Ahmed, M. E., & Van Geel, P. J. (2009). Potential concerns related to using octadecyltrichlorosilane (OTS) in rendering soils and porous ceramics hydrophobic. *Journal of contaminant hydrology*, 110(1-2), 22-33.

Alberta Energy Regulator (2017a). Investigation Summary Report 2015-004: Murphy Oil Company Ltd.; Licence No. P44181-016. Available from http://www1.aer.ca/compliancedashboard/investigations/2015004_ISR_MurphyOil_20170303.pdf [accessed 6 July 2017].

Alberta Energy Regulator (2017b). https://www.aer.ca/documents/news-releases/NR-2017-12.pdf. Retrieved on May 20th, 2018.

Al-Futaisi, A., & Patzek, T. W. (2004). Secondary imbibition in NAPL-invaded mixed-wet sediments. *Journal of contaminant hydrology*, *74*(1-4), 61-81. doi:10.1016/j.jconhyd.2004.02.005.

Andersen, R., Chapman, S. J., & Artz, R. R. E. (2013). Microbial communities in natural and disturbed peatlands: a review. *Soil Biology and Biochemistry*, *57*, 979-994. doi:10.1016/j.soilbio.2012.10.003.

Anderson, W.G. (1986a). Wettability Literature Survey- Part 1: Rock/Oil/Brine Interactions and the Effects of Core Handling on Wettability. *Journal of Petroleum Technology*. 38(10): 1125–1144. doi:10.2118/13932-pa.

Anderson, W.G. (1986b). Wettability Literature Survey- Part 2: Wettability Measurement. *Journal of Petroleum Technology*. 38(11): 1246–1262. doi:10.2118/13933-PA.

Andriesse, J.P. (1988). Nature and management of tropical peat soils. FAO Soils Bulletin. No. 59. Food and Agriculture Organization of the United Nations, Rome

API, Recommended Practices for Core Analysis, 2nd Edition, February 1998.

Appelo, C.A.J., & Postma, D. 2006. Geochemistry, Groundwater and Pollution. CRC press.

Bachmann, J., Ellies, A., & Hartge, K. H. (2000a). Development and application of a new sessile drop contact angle method to assess soil water repellency. *Journal of Hydrology*, *231*, 66-75. doi:10.1016/S0022-1694(00)00184-0.

Bachmann, J., Horton, R., Van Der Ploeg, R. R., & Woche, S. (2000b). Modified sessile drop method for assessing initial soil–water contact angle of sandy soil Journal Paper No. J-18480 of the Iowa Agriculture and Home Economics Experiment Stn., Ames, Iowa, Project No. 3262, and supported in part by Hatch Act and State of Iowa. *Soil Science Society of America Journal*, *64*(2), 564-567. doi:10.2136/sssaj2000.642564x.

Baird, A. J. (1997). Field estimation of macropore functioning and surface hydraulic conductivity in a fen peat. *Hydrological Processes*, *11*(3), 287-295. doi:10.1002/(SICI)1099-1085(19970315)11:3<287::AID-HYP443>3.0.CO;2-L.

Balliston, N. (2017). Saturated and vadose zone fate and transport of a continuously released tracer in a sub-arctic bog peatland. Masters thesis, University of Waterloo, UWSpace. http://hdl.handle.net/10012/11333.

Barker, J. P., Patrick, G. C., & Major, D. (1987). Natural attenuation of aromatic hydrocarbons in a shallow sand aquifer. *Groundwater Monitoring & Remediation*, *7*(1), 64-71. doi:10.1111/j.1745-6592.1987.tb01063.x.

Barry, D. A. (2009). Effect of nonuniform boundary conditions on steady flow in saturated homogeneous cylindrical soil columns. *Advances in water resources*, *32*(4), 522-531. doi:10.1016/j.advwatres.2009.01.003.

Bekins, B. A., Godsy, E. M., & Warren, E. (1999). Distribution of microbial physiologic types in an aquifer contaminated by crude oil. *Microbial Ecology*, *37*(4), 263-275. doi:10.1007/s002489900149

Bennett, P. C., Siegel, D. E., Baedecker, M. J., & Hult, M. F. (1993). Crude oil in a shallow sand and gravel aquifer—I. Hydrogeology and inorganic geochemistry. *Applied Geochemistry*, *8*(6), 529-549. doi: 10.1016/0883-2927(93)90012-6.

Boelter, D. H. (1965). Hydraulic conductivity of peats. *Soil Science*, *100*(4), 227-231.doi:10.1097/00010694-196510000-00001.

Bozkurt, S., Lucisano, M., Moreno, L., & Neretnieks, I. (2001). Peat as a potential analogue for the long-term evolution in landfills. *Earth-Science Reviews*, *53*(1-2), 95-147. doi:10.1016/s0012-8252(00)00036-2.

Bradford, S. A., & Abriola, L. M. (2001). Dissolution of residual tetrachloroethylene in fractional wettability porous media: Incorporation of interfacial area estimates. *Water Resources Research*, *37*(5), 1183-1195. doi:10.1029/2000WR900374.

Bradford, S. A., & Leij, F. J. (1995). Wettability effects on scaling two-and three-fluid capillary pressure-saturation relations. *Environmental science & technology*, 29(6), 1446-1455.doi:10.1021/es00006a004

Brewster, M. L., Annan, A. P., Greenhouse, J. P., Kueper, B. H., Olhoeft, G. R., Redman, J. D., & Sander, K. A. (1995). Observed migration of a controlled DNAPL release by geophysical methods. *Groundwater*, *33*(6), 977-987. doi:10.1111/j.1745-6584.1995.tb00043.x.

Brooks, P. W., Fowler, M. G., & Macqueen, R. W. (1988). Biological marker and conventional organic geochemistry of oil sands/heavy oils, Western Canada Basin. *Organic geochemistry*, *12*(6), 519-538.

Brooks, R., & Corey, T. (1964). Hydraulic Properties of Porous Media. Hydrology Papers, Colorado State University, 24.

Brooks, R. H., & Corey, A. T. (1964). Hydraulic properties of porous media and their relation to drainage design. *Transactions of the ASAE*, *7*(1), 26-0028.

Brusseau, M. L., & Rao, P. S. C. (1989). The influence of sorbate-organic matter interactions on sorption nonequilibrium. *Chemosphere*, *18*(9-10), 1691-1706. doi:10.1016/0045-6535(89)90453-0.

Brusseau, M. L., Jessup, R. E., & Rao, P. S. C. (1991a). Nonequilibrium sorption of organic chemicals: Elucidation of rate-limiting processes. *Environmental Science & Technology*, *25*(1), 134-142. doi:10.1021/es00013a015.

Brusseau, M. L., Larsen, T., & Christensen, T. H. (1991b). Rate-limited sorption and nonequilibrium transport of organic chemicals in low organic carbon aquifer materials. *Water Resources Research*, *27*(6), 1137-1145. doi:10.1029/91wr00503.

Burdine, N. (1953). Relative permeability calculations from pore size distribution data. *Journal of Petroleum Technology*, *5*(03), 71-78. doi:10.2118/225-g.

Calvet, R. (1989). Adsorption of organic chemicals in soils. *Environmental health perspectives*, *83*, 145. doi:10.2307/3430653.

Cameron, D. R., & Klute, A. (1977). Convective-dispersive solute transport with a combined equilibrium and kinetic adsorption model. *Water Resources Research*, *13*(1), 183-188. doi:10.1029/wr013i001p00183.

Carey, S. K., Quinton, W. L., & Goeller, N. T. (2007). Field and laboratory estimates of pore size properties and hydraulic characteristics for subarctic organic soils. *Hydrological Processes: An International Journal*, *21*(19), 2560-2571. doi:10.1002/hyp.6795.

Carpenter, J. H. (1966). New measurements of oxygen solubility in pure and natural water. *Limnology and oceanography*, *11*(2), 264-277.

Casey, F. X., Larsen, G. L., Hakk, H., & Šimůnek, J. (2003). Fate and transport of 17β-estradiol in soil− water systems. *Environmental science & technology*, *37*(11), 2400-2409.doi:10.1021/es026153z.

Casey, F. X., Ong, S. K., & Horton, R. (2000). Degradation and transformation of trichloroethylene in miscible-displacement experiments through zerovalent metals. *Environmental science & technology*, *34*(23), 5023-5029. doi:10.1021/es001185c.

Caudle, B. H., Slobod, R. L. and Brownscombe, E. R. (1951). Further developments in the laboratory determination of relative permeability. *Journal of Petroleum Technology*, 3(05), 145-150. doi:10.2118/951145-g.

Chapelle, F. H., & Lovley, D. R. (1990). Rates of microbial metabolism in deep coastal plain aquifers. *Applied and Environmental Microbiology*, *56*(6), 1865-1874.

Chaplin, B.P., Delin, G.N., Baker, R.J., & Lahvis, M.A. (2002). Long-term evolution of biodegradation and volatilization rates in a crude oil-contaminated aquifer. *Bioremediation Journal* 6(3), 237–255. doi:10.1080/10889860290777594.

Chardaire-Riviere, C., Chavent, G., Jaffre, J., Liu, J. and Bourbiaux, B. J. (1992). Simultaneous Estimation of Relative Permeabilities and Capillary Pressure. *Society of Petroleum Engineers Formation Evaluation*, 7(04), 283–289. doi:10.2118/19680-pa.

Chason, D. B., & Siegel, D. I. (1986). Hydraulic conductivity and related physical properties of peat, Lost River Peatland, northern Minnesota. *Soil Science*, *142*(2), 91-99. doi:10.1097/00010694-198608000-00005.

Chatzis, I., Kantzas, A., & Dullien, F. A. L. (1988). On the investigation of gravity-assisted inert gas injection using micromodels, long Berea sandstone cores, and computer-assisted tomography. In *Society of Petroleum Engineers Annual Technical Conference and Exhibition*. doi:10.2118/18284-ms.

Chen, Y. M., Abriola, L. M., Alvarez, P. J., Anid, P. J., & Vogel, T. M. (1992). Modeling transport and biodegradation of benzene and toluene in sandy aquifer material: Comparisons with experimental measurements. *Water Resources Research*, *28*(7), 1833-1847.

Chierici, G. L. (1984). Novel relations for drainage and imbibition relative permeabilities. *Society of Petroleum Engineers Journal*, 24(03), 275-276. doi: 10.2118/10165-pa.

Chiou, C. T., Porter, P. E., & Schmedding, D. W. (1983). Partition equilibriums of nonionic organic compounds between soil organic matter and water. *Environmental Science & Technology*, *17*(4), 227-231.

Clement, T. P., Sun, Y., Hooker, B. S., & Petersen, J. N. (1998). Modeling multispecies reactive transport in ground water. *Groundwater Monitoring & Remediation*, *18*(2), 79-92.doi:10.1111/j.1745-6592.1998.tb00618.x.

Clymo, R., Turunen, J., & Tolonen, K. (1998). Carbon Accumulation in Peatland. Oikos: 81(2), 368-388. doi:10.2307/3547057.

Cohen, A. D., Rollins, M. S., Zunic, W. M., & Durig, J. R. (1991). Effects of chemical and physical differences in peats on their ability to extract hydrocarbons from water. *Water research*, 25(9), 1047-1060.

Collins, C.M. (1983). Long-term active layer effects of crude oil spilled in interior Alaska. In Permafrost, Fourth International Conference Proceedings, National Academy Press, Washington, DC. CONF. pp. 175–179.

Conrad, S. H., Glass, R. J., & Peplinski, W. J. (2002). Bench-scale visualization of DNAPL remediation processes in analog heterogeneous aquifers: surfactant floods and in situ oxidation using permanganate. *Journal of Contaminant Hydrology*, 58(1-2), 13-49. doi:10.1016/s0169-7722(02)00024-4.

Costa, A. S., Romão, L. P. C., Araújo, B. R., Lucas, S. C. O., Maciel, S. T. A., Wisniewski, A., & Alexandre, M. D. R. (2012). Environmental strategies to remove volatile aromatic fractions (BTEX) from petroleum industry wastewater using biomass. *Bioresource Technology* 105, 31-39.

Cozzarelli, I. M., Bekins, B. A., Baedecker, M. J., Aiken, G. R., Eganhouse, R. P., & Tuccillo, M. E. (2001). Progression of natural attenuation processes at a crude-oil spill site: I. Geochemical evolution of the plume. *Journal of Contaminant Hydrology*, 53(3-4), 369-385.

Cram, S., Siebe, C., Ortíz-Salinas, R., & Herre, A. (2004). Mobility and Persistence of petroleum hydrocarbons in peat soils of southeastern Mexico. *Soil & Sediment Contamination*, 13(5), 341-360. doi:10.1080/10588330490500392.

Crescimanno, G. and Iovino, M. (1995). Parameter estimation by inverse method based on one-step and multi-step outflow experiments. *Geoderma*, 68(4), 257-277. doi:10.1016/0016-7061(95)00049-8.

Da Silva, M. L., & Alvarez, P. J. (2002). Effects of ethanol versus MTBE on benzene, toluene, ethylbenzene, and xylene natural attenuation in aquifer columns. *Journal of Environmental Engineering*, *128*(9), 862-867.

Dane, J. H., Hofstee, C., & Corey, A. T. (1998). Simultaneous measurement of capillary pressure, saturation, and effective permeability of immiscible liquids in porous media. *Water Resources Research*, *34*(12), 3687-3692. doi:10.1029/1998WR900026.

Dane, J.H., Oostrom, M., and Missildine, B.C. (1992). An improved method for the determination of capillary pressure-saturation curves involving TCE, water and air. *Journal of Contaminant Hydrology*, 11(1–2), 69–81. doi:10.1016/0169-7722(92)90034-C.

Danesh, A. (1998). PVT and phase behaviour of petroleum reservoir fluids. Elsevier.

De Wilde, T., Mertens, J., Šimunek, J., Sniegowksi, K., Ryckeboer, J., Jaeken, P., ... & Spanoghe, P. (2009). Characterizing pesticide sorption and degradation in microscale biopurification systems using column displacement experiments. *Environmental pollution*, *157*(2), 463-473. doi:10.1016/j.envpol.2008.09.008.

Deiss, J., Byers, C., Clover, D., D'Amore, D., Love, A., Menzies, M. A., ... & Walter, M. T. (2004). Transport of lead and diesel fuel through a peat soil near Juneau, AK: a pilot study. *Journal of contaminant hydrology*, 74(1-4), 1-18. doi:10.1016/j.jconhyd.2004.02.003.

Delicato, D. (1996). Physical-chemical properties and sorption characteristics of peat. Doctoral thesis, School of Chemical Sciences, Dublin City University, Dublin, Ireland.

Demond, A. H., & Roberts, P. V. (1991). Effect of interfacial forces on two-phase capillary pressure—saturation relationships. *Water Resources Research*, 27(3), 423-437.doi:10.1029/90wr02408

Demond, A.H., & Roberts, P. V. (1993). Estimation of two-phase relative permeability relationships for organic liquid contaminants. *Water Resources Research*, 29(4), 1081–1090. doi:10.1029/92WR02987.

Demond, A. H., Rathfelder, K., & Abriola, L. M. (1996). Simulation of organic liquid flow in porous media using estimated and measured transport properties. *Journal of contaminant hydrology*, *22*(3-4), 223-239.doi:10.1016/0169-7722(95)00091-7.

Dewulf, J., Van Langenhove, H., & Graré, S. (1999). Sediment/water and octanol/water equilibrium partitioning of volatile organic compounds: temperature dependence in the 2–25 C range. *Water Research.* 33, 2424-2436.

DiCarlo, D. A., A. Sahni, and M. J. Blunt (2000), Three-Phase Relative Permeability of Water-Wet, Oil-Wet and Mixed-Wet Sandpacks. *Society of Petroleum Engineers Journal*, 5(01), pp.82–91. Available at: doi:10.2118/60767-pa.

Dickinson, C. H., & Maggs, G. H. (1974). Aspects of the decomposition of *Sphagnum* leaves in an ombrophilous mire. *New Phytologist*, *73*(6), 1249-1257. Dillard, L. A., Essaid, H. I., & Blunt, M. J. (2001). A functional relation for field-scale nonaqueous phase liquid dissolution developed using a pore network model. *Journal of contaminant hydrology*, *48*(1-2), 89-119. doi:10.1016/S0169-7722(00)00171-6.

Donaldson, E. C., Thomas, R. D., & Lorenz, P. B. (1969). Wettability determination and its effect on recovery efficiency. *Society of Petroleum Engineers Journal*, *9*(01), 13-20. doi:10.2118/2338-PA.

Donaldson, E. C., & Thomas, R. D. (1971, January). Microscopic observations of oil displacement in water-wet and oil-wet systems. In *Fall Meeting of the Society of Petroleum Engineers of AIME*. Society of Petroleum Engineers. doi:10.2118/3555-MS.

Dontsova, K. M., Pennington, J. C., Hayes, C., Šimunek, J., & Williford, C. W. (2009). Dissolution and transport of 2, 4-DNT and 2, 6-DNT from M1 propellant in soil. *Chemosphere*, 77, 597-603. doi:10.1016/j.chemosphere.2009.05.039.

Eching, S. O., & Hopmans, J. W. (1993). Optimization of hydraulic functions from transient outflow and soil water pressure data. *Soil Science Society of America Journal*, 57(5), 1167-1175. doi:10.2136/sssaj1993.03615995005700050001x.

Eganhouse, R. P., Dorsey, T. F., Phinney, C. S., & Westcott, A. M. (1996). Processes affecting the fate of monoaromatic hydrocarbons in an aquifer contaminated by crude oil. *Environmental Science & Technology*, 30(11), 3304-3312.

Energy Resources Conservation Board. (2011). ERCB Investigation Report: Plains Midstream Canada ULC, NPS 20 Rainbow Pipeline Failure, April 28, 2011. Available from https://www.aer.ca/documents/reports/IR_20130226-PlainsMidstream.pdf [accessed 17 July 2017].

Environment Canada, Benzene in Canadian Gasoline: Effect of the Benzene in Gasoline Regulations. https://www.ec.gc.ca/doc/energie-energy/1088/ben/tables-eng.htm; retrieved at 19th January 2018.

Environment Canada, www.etc-cte.ec.gc.ca/databases/oilproperties/pdf/web_diesel_fuel_oil_(canada).pdf, retrieved: 18th June 2018.

Environmental Protection Agency (1996). Soil screening guidance: user's guide: Washington, D.C., U.S. Environmental Protection Agency, Office of Solid Waste and Emergency Response Publication 9355.4-23.

Essaid, H. I., Bekins, B. A., Herkelrath, W. N., & Delin, G. N. (2011). Crude oil at the Bemidji site: 25 years of monitoring, modeling, and understanding. *Groundwater*, *49*(5), 706-726. doi:10.1111/j.1745-6584.2009.00654.x.

Essaid, H.I., Bekins, B.A., & Cozzarelli, I.M. (2015). Organic contaminant transport and fate in the subsurface: Evolution of knowledge and understanding. *Water Resources Research*, 51(7): 4861–4902. doi:10.1002/2015WR017121.

Everett, K. R. (1978). Some effects of oil on the physical and chemical characteristics of wet tundra soils. *Arctic*, 260-276. doi:10.14430/arctic2657.

Fagerlund, F., Illangasekare, T. H., & Niemi, A. (2007). Nonaqueous-phase liquid infiltration and immobilization in heterogeneous media: 1. Experimental methods and two-layered reference case. *Vadose Zone Journal*, 6(3), 471-482. doi:10.2136/vzj2006.0171.

Fatt, I., & Klikoff Jr, W. A. 1959. Effect of fractional wettability on multiphase flow through porous media. *Journal of Petroleum Technology*, 11(10), 71-76. doi:10.2118/1275-g.

Faust, C. R. (1985). Transport of immiscible fluids within and below the unsaturated zone: A numerical model. *Water Resources Research*, 21(4), 587-596. doi:10.1029/WR021i004p00587.

Fetter, C. W. (2000). Applied hydrogeology. Prentice hall.

Fitzhenry, L. C., R. M. Bacon, & J. M. Gronseth. (1992). Reservoir/well repair and environmental impact management of surface discharge at Cold Lake. *Journal of Petroleum Technology*, 44(05), 618-622. doi:10.2118/21521-pa.

Freeman, C., Evans, C.D., Monteith, D.T., Reynolds, B., & Fenner, N. 2001. Export of organic carbon from peat soils. *Nature*, 412(6849), 785. doi:10.1038/35090628.

Fry, V. A., Istok, J. D., Semprini, L., O'Reilly, K. T., & Buscheck, T. E. (1995). Retardation of dissolved oxygen due to a trapped gas phase in porous media. *Groundwater* 33(3), 391-398. doi:10.1111/j.1745-6584.1995.tb00295.x.

Garbarini, D. R., & Lion, L. W. (1985). Evaluation of sorptive partitioning of nonionic pollutants in closed systems by headspace analysis. *Environmental science & technology*, *19*(11), 1122-1128.Garbarini, D. R., & Lion, L. W. (1986). Influence of the nature of soil organics on the sorption of toluene and trichloroethylene. *Environmental science & technology*, *20*(12), 1263-1269.Garrett, R. M., Pickering, I. J., Haith, C. E., & Prince, R. C. (1998). Photooxidation of crude oils. *Environmental Science & Technology*, *32*(23), 3719-3723. Gaudet, J. P., Jegat, H., Vachaud, G., & Wierenga, P. J. (1977). Solute Transfer, with Exchange between Mobile and Stagnant Water, through Unsaturated Sand. *Soil Science Society of America Journal*, *41*(4), 665-671. doi:10.2136/sssaj1977.03615995004100040009x.

Geller, J. T., & Hunt, J. R. (1993). Mass transfer from nonaqueous phase organic liquids in water-saturated porous media. *Water resources research*, *29*(4), 833-845. doi:10.1029/92WR02581.

Ghaly, R. A., Pyke, J. B., Ghaly, A. E., & Ugursal, V. I. (1999). Remediation of diesel-oil-contaminated soil using peat. *Energy sources*, *21*(9), 785-799. doi:10.1080/00908319950014344.

Gharedaghloo, B., Price, J. S. (2015). Characterization of multiphase flow in peat. In International Association of Hydrogeologists–Canadian National Chapter (IAH-CNC) 2015 Waterloo Conference.

Gharedaghloo, B., & Price, J. (2017). Fate and Transport of free-phase and dissolved-phase hydrocarbons in peat and peatlands: Developing a conceptual model. *Environmental Reviews*.

Gidley, P. T., Kwon, S., Yakirevich, A., Magar, V. S., & Ghosh, U. (2012). Advection dominated transport of polycyclic aromatic hydrocarbons in amended sediment caps. *Environmental science & technology*, *46*(9), 5032-5039. doi:10.1021/es202910c.

Gillham, R. W., Sudicky, E. A., Cherry, J. A., & Frind, E. O. (1984). An advection-diffusion concept for solute transport in heterogeneous unconsolidated geological deposits. *Water Resources Research*, *20*(3), 369-378. doi:10.1029/WR020i003p00369.

Goetz, J. D., & Price, J. S. (2015). Role of morphological structure and layering of *Sphagnum* and Tomenthypnum mosses on moss productivity and evaporation rates. *Canadian Journal of Soil Science*, 95(2), 109-124. doi:10.4141/cjss-2014-092.

Goldstein, L., Prasher, S. O., & Ghoshal, S. (2007). Three-dimensional visualization and quantification of non-aqueous phase liquid volumes in natural porous media using a medical X-ray Computed Tomography scanner. *Journal of Contaminant Hydrology*, 93(1-4), 96-110. doi:10.1016/j.jconhyd.2007.01.013.

Golubev, V., & Whittington, P. (2018). Effects of volume change on the unsaturated hydraulic conductivity of *Sphagnum* moss. *Journal of Hydrology*, *559*, 884-894. doi:10.1016/j.jhydrol.2018.02.083.

Grant, C.D., and Groenevelt, P.H. (1993). Air permeability. In Soil Sampling and Methods of Analysis. Edited by M.R. Carter. Lewis Publishers, Boca Raton, FL. pp. 645–650.

Gschwend, P. M., & Wu, S. (1985). On the constancy of sediment-water partition coefficients of hydrophobic organic pollutants. *Environmental Science & Technology*, *19*(1), 90-96. doi:10.1021/es00131a011.

Guerin, T. F., Horner, S., McGovern, T., & Davey, B. (2002). An application of permeable reactive barrier technology to petroleum hydrocarbon contaminated groundwater. *Water Research*, *36*(1), 15-24. doi:10.1016/s0043-1354(01)00233-0.

Guignard, C., Lemée, L., & Amblès, A. (2000). Structural characterization of humic substances from an acidic peat using thermochemolysis techniques. *Agronomie*, *20*(5), 465-475. doi:10.1051/agro:2000142.

Hanna, K., Lassabatere, L., & Bechet, B. (2012). Transport of two naphthoic acids and salicylic acid in soil: experimental study and empirical modeling. *Water research*, *46*(14), 4457-4467. doi:10.1016/j.watres.2012.04.037.

Harvey, R. W., George, L. H., Smith, R. L., & LeBlanc, D. R. (1989). Transport of microspheres and indigenous bacteria through a sandy aquifer: results of natural-and forced-gradient tracer experiments. *Environmental Science & Technology*, *23*(1), 51-56. doi: 10.1021/es00178a005.

Hassett, J. P., & Anderson, M. A. (1982). Effects of dissolved organic matter on adsorption of hydrophobic organic compounds by river-and sewage-borne particles. *Water Research*, *16*(5), 681-686. doi:10.1016/0043-1354(82)90091-4.

Hatfield, K., Ziegler, J., & Burris, D. R. (1993). Transport in porous media containing residual hydrocarbon. II: Experiments. *Journal of Environmental Engineering*, *119*(3), 559-575.doi:10.1061/(asce)0733-9372(1993)119:3(559).

Hoag, R. S., & Price, J. S. (1995). A field-scale, natural gradient solute transport experiment in peat at a Newfoundland blanket bog. *Journal of Hydrology*, *172*(1-4), 171-184.doi:10.1016/0022-1694(95)02696-M.

Hoag, R. S., & Price, J. S. (1997). The effects of matrix diffusion on solute transport and retardation in undisturbed peat in laboratory columns. *Journal of Contaminant Hydrology*, 28(3), 193-205. doi:10.1016/s0169-7722(96)00085-x.

Hobbs, N. B. (1986). Mire morphology and the properties and behaviour of some British and foreign peats. *Quarterly Journal of Engineering Geology and Hydrogeology*, *19*(1), 7-80. doi:10.1016/0148-9062(86)90667-4.

Hofstee, C., Dane, J. H., & Hill, W. E. (1997). Three-fluid retention in porous media involving water, PCE and air. *Journal of contaminant hydrology*, *25*(3-4), 235-247. doi:10.1016/s0169-7722(96)00035-6.

Holden, J. (2005). Peatland hydrology and carbon release: why small-scale process matters. *Philosophical Transactions of the Royal Society of London A: Mathematical, Physical and Engineering Sciences*, *363*(1837), 2891-2913.doi:10.1098/rsta.2005.1671.

Høst-Madsen, J. and Jensen, K. H. (1992). Laboratory and numerical investigations of immiscible multiphase flow in soil. *Journal of hydrology*, 135(1-4), 13-52. doi:10.1016/0022-1694(92)90079-b.

Huang, D. D., Honarpour, M. M., & Al-Hussainy, R. (1997, September). An improved model for relative permeability and capillary pressure incorporating wettability. In SCA (Vol. 9718, pp. 7-10).

Huang, W., Peng, P. A., Yu, Z., & Fu, J. (2003). Effects of organic matter heterogeneity on sorption and desorption of organic contaminants by soils and sediments. *Applied Geochemistry*, *18*(7), 955-972.

Illangasekare, T. H., Armbruster III, E. J. and Yates, D. N. (1995). Non-aqueous-phase fluids in heterogeneous aquifers—experimental study. *Journal of Environmental Engineering*, 121(8), 571-579. doi:10.1061/(asce)0733-9372(1995)121:8(571).

Imhoff, P. T., Frizzell, A., & Miller, C. T. (1997). Evaluation of thermal effects on the dissolution of a nonaqueous phase liquid in porous media. *Environmental science & technology*, *31*(6), 1615-1622. doi:10.2172/1036838.

Ingram, H. A. P. (1978). Soil layers in mires: function and terminology. *Journal of Soil Science*, *29*(2), 224-227. doi:10.1111/j.1365-2389.1978.tb02053.x.

Ingram, H.A.P. (1983). Hydrology. In Ecosystems of the World, vol. 4A, Mires: Swamp, Bog, Fen and Moor. Edited by A.J.P. Gore. Elsevier Scientific Publishing Company, New York. pp. 67–158.

Ishihara, Y., Shimojima, E., & Harada, H. (1992). Water vapor transfer beneath bare soil where evaporation is influenced by a turbulent surface wind. *Journal of Hydrology*, *131*(1-4), 63-104. doi:10.1016/0022-1694(92)90213-f.

Jacobsen, O. H., Leij, F. J., & van Genuchten, M. T. (1992). Parameter determination for chloride and tritium transport in undisturbed lysimeters during steady flow. *Hydrology Research*, *23*(2), 89-104. Available from http://hr.iwaponline.com/content/23/2/89 [accessed 28 December 2016]

Jarsjö, J., Destouni, G., & Yaron, B. (1994). Retention and volatilisation of kerosene: Laboratory experiments on glacial and post-glacial soils. *Journal of contaminant hydrology*, 17(2), 167-185. 167–185. doi:10.1016/0169-7722(94)90020-5.

Jindrova, E., Chocova, M., Demnerova, K., & Brenner, V. (2002). Bacterial aerobic degradation of benzene, toluene, ethylbenzene and xylene. *Folia microbiologica*, *47*(2), 83-93.

Joekar-Niasar, V., Hassanizadeh, S. M., & Leijnse, A. (2008). Insights into the relationships among capillary pressure, saturation, interfacial area and relative permeability using pore-network modeling. *Transport in Porous Media*, *74*(2), 201-219. doi:10.1007/s11242-007-9191-7.

Johnson, E. F., Bossler, D. P. & Bossler, V. O. (1959). Calculation of relative permeability from displacement experiments. Society of Petroleum Engineers.

Johnson, L.A. (1980). The fate and effect of crude oil spilled on subarctic permafrost terrain in interior Alaska. Corvallis Environmental Research Laboratory, Office of Research and Development, US Environmental Protection Agency.

Jol, H. M., & Smith, D. G. (1995). Ground penetrating radar surveys of peatlands for oilfield pipelines in Canada. *Journal of Applied Geophysics*, *34*(2), 109-123. doi:10.1016/0926-9851(95)00018-6.

Kantzas, A., Chatzis, I. and Dullien, F. A. L. (1988). Enhanced Oil Recovery by Inert Gas Injection. *Society of Petroleum Engineers Enhanced Oil Recovery Symposium*. doi:10.2118/17379-ms.

Kao, C. M., & Prosser, J. (2001). Evaluation of natural attenuation rate at a gasoline spill site. *Journal of Hazardous Materials*, 82(3), 275-289.

Kao, C. M., & Wang, C. C. (2000). Control of BTEX migration by intrinsic bioremediation at a gasoline spill site. *Water Research*, *34*(13), 3413-3423.

Karickhoff, S. W. (1981). Semi-empirical estimation of sorption of hydrophobic pollutants on natural sediments and soils. *Chemosphere*, *10*(8), 833-846. Karickhoff, S. W., Brown, D. S., & Scott, T. A. (1979). Sorption of hydrophobic pollutants on natural sediments. *Water research*, *13*(3), 241-248. Karickhoff, S. W., & Morris, K. R. (1985). Sorption dynamics of hydrophobic pollutants in sediment suspensions. *Environmental Toxicology and Chemistry*, *4*(4), 469-479. doi:10.1002/etc.5620040407.

Karickhoff, S. W. (1984). Organic pollutant sorption in aquatic systems. *Journal of hydraulic engineering*, *110*(6), 707-735. doi:10.1061/(asce)0733-9429(1984)110:6(707)

Kelly-Hooper, F., Farwell, A. J., Pike, G., Kennedy, J., Wang, Z., Grunsky, E. C., & Dixon, D. G. (2013). Is it clean or contaminated soil? Using petrogenic versus biogenic GC-FID chromatogram patterns to mathematically resolve false petroleum hydrocarbon detections in clean organic soils: A crude oil–spiked peat microcosm experiment. *Environmental toxicology and chemistry*, 32(10), 2197-2206. doi:10.1002/etc.2285.

Kershaw, G.P. (1990). Movement of crude oil in an experimental spill on the SEEDS simulated pipeline right-of-way, Fort Norman, NWT. *Arctic, 43(2)*, 176–183. doi:10.14430/arctic1608.

Ketcheson, S. J., & Price, J. S. (2016). Comparison of the hydrological role of two reclaimed slopes of different ages in the Athabasca oil sands region, Alberta, Canada. *Canadian Geotechnical Journal*, *53*(9), 1533-1546. doi:10.1139/cgj-2015-0391.

Kile, D. E., Chiou, C. T., Zhou, H., Li, H., & Xu, O. (1995). Partition of nonpolar organic pollutants from water to soil and sediment organic matters. *Environmental science & technology*, *29*(5), 1401-1406. doi:10.1021/es00005a037.

Kim, J., & Corapcioglu, M. Y. (2003). Modeling dissolution and volatilization of LNAPL sources migrating on the groundwater table. *Journal of contaminant hydrology*, *65*(1-2), 137-158. doi:10.1016/s0169-7722(02)00105-5.

Klingenfuß, C., Roßkopf, N., Walter, J., Heller, C., & Zeitz, J. (2014). Soil organic matter to soil organic carbon ratios of peatland soil substrates. *Geoderma*, 235: 410-417.

Knutson, C. E., Werth, C. J., & Valocchi, A. J. (2001). Pore-scale modeling of dissolution from variably distributed nonaqueous phase liquid blobs. *Water Resources Research, 37*(12), 2951-2963. doi:10.1029/2001WR000587.

Kögel-Knabner, I., & Totsche, K. U. (1998). Influence of dissolved and colloidal phase humic substances on the transport of hydrophobic organic contaminants in soils. *Physics and Chemistry of the Earth*, *23*(2), 179-185. doi:10.1016/S0079-1946(98)00010-X.

Kool, J. B., Parker, J. C., & Van Genuchten, M. T. (1985). Determining Soil Hydraulic Properties from One-step Outflow Experiments by Parameter Estimation: I. Theory and Numerical Studies 1. *Soil Science Society of America Journal*, 49(6), 1348-1354. doi:10.2136/sssaj1985.03615995004900060004x.

Kwok, D. Y., & Neumann, A. W. (1999). Contact angle measurement and contact angle interpretation. *Advances in colloid and interface science*, *81*(3), 167-249. doi:10.1016/s0001-8686(98)00087-6.

Lahvis, M. A., Baehr, A. L., & Baker, R. J. (1999). Quantification of aerobic biodegradation and volatilization rates of gasoline hydrocarbons near the water table under natural attenuation conditions. *Water Resources Research*, 35(3), 753-765.

Lai, D. Y. F. (2009). Methane dynamics in northern peatlands: a review. *Pedosphere*, *19*(4), 409-421.doi:10.1016/S1002-0160(09)00003-4.

Landva, A. O., & Pheeney, P. E. (1980). Peat fabric and structure. *Canadian Geotechnical Journal*, *17*(3), 416-435. doi:10.1139/t80-048.

Lee, J. F., Crum, J. R., & Boyd, S. A. (1989). Enhanced retention of organic contaminants by soils exchanged with organic cations. *Environmental Science & Technology*, *23*(11), 1365-1372.

Leelamanie, D. A. L., Karube, J., & Yoshida, A. (2008). Characterizing water repellency indices: Contact angle and water drop penetration time of hydrophobized sand. *Soil Science & Plant Nutrition*, *54*(2), 179-187. doi:10.1111/j.1747-0765.2007.00232.x.

Lenhard, R. J. & Parker, J. C. (1988). Experimental validation of the theory of extending two-phase saturation-pressure relations to three-fluid phase systems for monotonic drainage paths. *Water Resources Research*, 24(3), 373-380. doi:10.1029/wr024i003p00373.

Lenhard, R. J., Dane, J. H., Parker, J. C., & Kaluarachchi, J. J. (1988). Measurement and simulation of one-dimensional transient three-phase flow for monotonic liquid drainage. *Water Resources Research*, 24(6), 853-863. doi:10.1029/wr024i006p00853.

Lenhard, R. J. (1992). Measurement and modeling of three-phase saturation-pressure hysteresis. *Journal of Contaminant Hydrology*, *9*(3), 243-269.doi:10.1016/0169-7722(92)90007-2.

Parker, J. C., & Lenhard, R. J. (1987). A model for hysteretic constitutive relations governing multiphase flow: 1. Saturation-pressure relations. *Water Resources Research*, *23*(12), 2187-2196. doi:10.1029/wr023i012p02197.

Leverett, M. C. (1939). Flow of oil-water mixtures through unconsolidated sands. *Transactions of the AIME, 132(01)*, 149-171. doi:10.2118/939149-g.

Leverett, M., & Lewis, W. B. (1941). Steady flow of gas-oil-water mixtures through unconsolidated sands. *Transactions of the AIME, 142(01)*, 107-116. doi:10.2118/941107-g.

Lide, D. R. (2012). CRC handbook of chemistry and physics.

Lie, K. A. (2016). An Introduction to Reservoir Simulation Using MATLAB: User guide for the Matlab Reservoir Simulation Toolbox (MRST). SINTEF ICT.

Limpens, J., Berendse, F., Blodau, C., Canadell, J.G., Freeman, C., Holden, J., Roulet, N., Rydin, H., & Schaepman-Strub, G. (2008). Peatlands and the carbon cycle: from local processes to global implications–a synthesis. *Biogeosciences, 5,*: 1475–1491. doi:10.5194/bg-5-1475-2008.

Luxmoore, R. J. (1981). Micro-, meso-, and macroporosity of soil. *Soil Science Society of America Journal*, *45*(3), 671-672.doi:10.2136/sssaj1981.03615995004500030051x.

Mackay, D. M., Freyberg, D. L., Roberts, P. V., & Cherry, J. A. (1986). A natural gradient experiment on solute transport in a sand aquifer: 1. Approach and overview of plume movement. *Water Resources Research*, *22*(13), 2017-2029.doi:10.1029/wr022i013p02017.

Mackay, D., Shiu, W. Y., & Ma, K. C. (1997). Illustrated handbook of physical-chemical properties of environmental fate for organic chemicals. *CRC press*.

Mackay, D. M., De Sieyes, N. R., Einarson, M. D., Feris, K. P., Pappas, A. A., Wood, I. A., ... & Wilson, J. T. (2006). Impact of ethanol on the natural attenuation of benzene, toluene, and o-xylene in a normally sulfate-reducing aquifer. *Environmental Science & Technology*, *40*(19), 6123-6130. Magee, B. R., Lion, L. W., & Lemley, A. T. (1991). Transport of dissolved organic macromolecules and their effect on the transport of phenanthrene in porous media. *Environmental Science & Technology*, *25*(2), 323-331. doi:10.1021/es00014a017.

Magee, B. R., Lion, L. W., & Lemley, A. T. (1991). Transport of dissolved organic macromolecules and their effect on the transport of phenanthrene in porous media. *Environmental Science & Technology*, *25*(2), 323-331.

Mallakin, A., & Ward, O. P. (1996). Degradation of BTEX compounds in liquid media and in peat biofilters. *Journal of Industrial Microbiology*, *16*(5), 309-318.doi:10.1007/bf01570040.

Maraqa, M. A., Wallace, R. B., & Voice, T. C. (1999). Effects of residence time and degree of water saturation on sorption nonequilibrium parameters. *Journal of contaminant hydrology*, *36*(1-2), 53-72. doi:10.1016/s0169-7722(98)00144-2.

Mark, N., Arthur, J., Dontsova, K., Brusseau, M., Taylor, S., & Šimůnek, J. (2017). Column transport studies of 3-nitro-1, 2, 4-triazol-5-one (NTO) in soils. *Chemosphere*, *171*, 427-434. doi:10.1016/j.chemosphere.2016.12.067.

Marshall, T. J. (1958). A relation between permeability and size distribution of pores. *Journal of Soil Science*, *9*(1), 1-8. doi: 10.1111/j.1365-2389.1958.tb01892.x.

Martin-Hayden, J. M., & Robbins, G. A. (1997). Plume distortion and apparent attenuation due to concentration averaging in monitoring wells. *Groundwater*, *35*(2), 339-346. doi:10.1111/j.1745-6584.1997.tb00091.x.

McAuliffe, C. (1966). Solubility in water of paraffin, cycloparaffin, olefin, acetylene, cycloolefin, and aromatic hydrocarbons1. *The Journal of Physical Chemistry*, *70*(4), 1267-1275.McCaffery, F. G., & Mungan, N. (1970). Contact angle and interfacial tension studies of some hydrocarbon-water-solid systems. *Journal of Canadian Petroleum Technology*, *9*(03).doi:10.2118/70-03-04.

McCarter, C. P., & Price, J. S. (2014). Ecohydrology of *Sphagnum* moss hummocks: mechanisms of capitula water supply and simulated effects of evaporation. *Ecohydrology*, 7(1), 33-44. doi:10.1002/eco.1313.

McCarter, C. P., & Price, J. S. (2017). The transport dynamics of chloride and sodium in a ladder fen during a continuous wastewater polishing experiment. *Journal of Hydrology*, 549, 558-570. doi:10.1016/j.jhydrol.2017.04.033.

McGill, W.B., and Nyborg, M. (1973). Reclamation of forested soils damaged by oil spills. Results of preliminary studies. Canadian Forestry Service, Northern Forest Research Centre, Edmonton, Alberta. 28 p.

Mercer, J. W., & Cohen, R. M. (1990). A review of immiscible fluids in the subsurface: properties, models, characterization and remediation. *Journal of Contaminant Hydrology, 6*(2), 107-163. doi:10.1016/0169-7722(90)90043-G.

Michel, J. C., Rivière, L. M., & Bellon-Fontaine, M. N. (2001). Measurement of the wettability of organic materials in relation to water content by the capillary rise method. *European journal of soil science*, 52(3), 459-467. doi:10.1046/j.1365-2389.2001.00392.x.

Michel, J. C. (2009). Influence of clay addition on physical properties and wettability of peat-growing media. *HortScience, 44*(6), 1694-1697. Available from http://hortsci.ashspublications.org/content/44/6/1694.full [accessed 28 December 2016].

Miller, C. T., Poirier-McNeil, M. M., & Mayer, A. S. (1990). Dissolution of trapped nonaqueous phase liquids: Mass transfer characteristics. *Water Resources Research, 26*(11), 2783-2796.doi:10.1029/WR026i011p02783.

Miller, M. A., & Ramey Jr, H. J. (1985). Effect of temperature on oil/water relative permeabilities of unconsolidated and consolidated sands. *Society of Petroleum Engineers Journal, 25*(06), 945-953.doi:10.2118/12116-pa.

Moore, B. J., Hardisty, P. E., Thompson, R. G., & Esselinckx, B. (1999). Fate of hydrocarbon contaminants in natural wetlands. *Journal of Canadian Petroleum Technology, 38*(13).doi:10.2118/99-13-32.

Moore, B. J., Headley, J. V., Dupont, R. R., Doucette, W. D., & Armstrong, J. E. (2002). Abatement of gas-condensate hydrocarbons in a natural wetland. *Journal of Environmental Science and Health, Part A*, 37(4), 425-438.

Moore, J. P., & Phillips, C. R. (1975). Adsorption of crude oil on arctic terrain. *Chemosphere, 4*(4), 215-220. doi:10.1016/0045-6535(75)90065-x.

Moore, J. P., Phillips, C. R., & Tombalakian, A. S. (1976). Adsorption of binary liquid-phase hydrocarbon mixtures on arctic terrain. *The Canadian Journal of Chemical Engineering, 54*(1-2), 75-80.doi:10.1002/cjce.5450540111.

Morgan, W. B., & Pirson, S. J. (1964, January). The effect of fractional wettability on the Archie saturation exponent. In Society of Petrophysicists and Well-Log Analysts 5th Annual Logging Symposium.

MRST: The MATLAB Reservoir Simulation Toolbox. www.sintef.no/MRST (2017a).

Mungan, N., & Moore, E. J. (1968). Certain wettability effects on electrical resistivity in porous media. *Journal of Canadian Petroleum Technology, 7(01),* 20-25. doi:10.2118/68-01-04.

National Wetlands Working Group. 1988. Wetlands of Canada. Canada Committee on Ecological Land Classification and Environment Canada. Ecological Land Classification Series, No. 24, 454p.

National Wetlands Working Group. 1997. The Canadian Wetland Classification System, 2nd ed. University of Waterloo, Waterloo, Ontario. In National Wetlands Working Group. Wetlands Research Branch, University of Waterloo. pp. 1-68.

Nesbitt, H. W., Fedo, C. M., & Young, G. M. (1997). Quartz and feldspar stability, steady and non-steady-state weathering, and petrogenesis of siliciclastic sands and muds. *The Journal of Geology*, *105*(2), 173-192. doi:10.1086/515908.

Neuman, S. P. (1990). Universal scaling of hydraulic conductivities and dispersivities in geologic media. *Water Resources Research*, *26*(8), 1749-1758. doi:10.1029/wr026i008p01749.

Newell, C.J., Acree, S.D., Ross, R.R., and Huling, S.G. 1995. Ground water issue: Light nonaqueous phase liquids. EPA/540/S-95/500. US Environmental Protection Agency, Washington DC.

Nimmo, J. R. (1992). Semiempirical model of soil water hysteresis. *Soil Science Society of America Journal*, *56*(6), 1723-1730. doi:10.2136/sssaj1992.03615995005600060011x.

O Kane, J. P. (2005). Hysteresis in hydrology. *Acta Geophysica Polonica*, *53*(4), 373.

O'Carroll, D. M., Phelan, T. J. and Abriola, L. M. (2005). Exploring dynamic effects in capillary pressure in multistep outflow experiments. *Water Resources Research*, 41(11). doi:10.1029/2005wr004010.

Odermatt, J. R. (1994). Natural chromatographic separation of benzene, toluene, ethylbenzene and xylenes (BTEX compounds) in a gasoline contaminated ground water aquifer. *Organic Geochemistry*, *21*(10-11), 1141-1150.

Oostrom, M., Hofstee, C. and Wietsma, T. W. (2006). Behavior of a viscous LNAPL under variable water table conditions. *Soil & Sediment Contamination*, 15(6), 543-564. doi:10.1080/15320380600958976.

Owens, W. W., & Archer, D. (1971). The effect of rock wettability on oil-water relative permeability relationships. *Journal of Petroleum Technology*, *23*(07), 873-878.doi:10.2118/3034-pa.

Palomino, A. M. & Grubb, D. G. (2004). Recovery of dodecane, octane and toluene spills in sandpacks using ethanol. *Journal of Hazardous Materials*, 110(1-3), 39-51. doi:10.1016/j.jhazmat.2004.02.035.

Pantazidou, M., & Sitar, N. (1993). Emplacement of nonaqueous liquids in the vadose zone. *Water Resources Research*, 29(3), 705-722. doi:10.1029/92wr02450.

Parker, J. C., Kool, J. B. and Van Genuchten, M. T. (1985). Determining Soil Hydraulic Properties from One-step Outflow Experiments by Parameter Estimation: II. Experimental Studies 1. *Soil Science Society of America Journal*, 49(6), 1354-1359. doi:10.2136/sssaj1985.03615995004900060005x.

Parker, J. C., Lenhard, R. J., & Kuppusamy, T. (1987). A parametric model for constitutive properties governing multiphase flow in porous media. *Water Resources Research*, 23(4), 618-624. doi:10.1029/wr023i004p00618.

Parker, J. C. (2003). Physical processes affecting natural depletion of volatile chemicals in soil and groundwater. *Vadose Zone Journal*, *2*(2), 222-230.. doi:10.2113/2.2.222.

Pignatello, J. J., & Xing, B. (1995). Mechanisms of slow sorption of organic chemicals to natural particles. *Environmental Science & Technology*, *30*(1), 1-11. doi:10.1021/es940683g.

Pinder, G. F., & Abriola, L. M. (1986). On the simulation of nonaqueous phase organic compounds in the subsurface. *Water Resources Research, 22*(9S). doi:10.1029/wr022i09sp0109s.

Poston, S. W., Ysrael, S., Hossain, A. K. M. S., & Montgomery III, E. F. (1970). The effect of temperature on irreducible water saturation and relative permeability of unconsolidated sands. *Society of Petroleum Engineers Journal*, *10*(02), 171-180. doi:10.2118/1897-pa.

Powers, S. E., Anckner, W. H., & Seacord, T. F. (1996). Wettability of NAPL-contaminated sands. *Journal of Environmental Engineering*, *122*(10), 889-896. doi:10.1061/(asce)0733-9372(1996)122:10(889).

Price, J. S. (2003). Role and character of seasonal peat soil deformation on the hydrology of undisturbed and cutover peatlands. *Water Resources Research*, *39*(9). doi:10.1029/2002WR001302

Price, J. S., & Whittington, P. N. (2010). Water flow in *Sphagnum* hummocks: Mesocosm measurements and modelling. *Journal of Hydrology*, 381(3-4), 333-340. doi:10.1016/j.jhydrol.2009.12.006.

Price, J. S., Whittington, P. N., Elrick, D. E., Strack, M., Brunet, N., & Faux, E. (2008). A Method to Determine Unsaturated Hydraulic Conductivity in Living and Undecomposed Moss. *Soil Science Society of America Journal*, 72(2), 487. doi:10.2136/sssaj2007.0111n.

Price, J. S., & Maloney, D. A. (1994). Hydrology of a patterned bog-fen complex in southeastern Labrador, Canada. *Hydrology Research*, *25*(5), 313-330.http://hr.iwaponline.com/content/25/5/313 [accessed 28 December 2016).

Priddle, M. W., & Jackson, R. E. (1991). Laboratory column measurement of VOC retardation factors and comparison with field values. *Groundwater*, *29*(2), 260-266. Quinton, W. L., Elliot, T., Price, J. S., Rezanezhad, F., & Heck, R. (2009). Measuring physical and hydraulic properties of peat from X-ray tomography. *Geoderma*, 153(1-2), 269-277. doi:10.1016/j.geoderma.2009.08.010.

Quinton, W. L., Hayashi, M., & Carey, S. K. (2008). Peat hydraulic conductivity in cold regions and its relation to pore size and geometry. *Hydrological Processes: An International Journal*, *22*(15), 2829-2837.doi:10.1002/hyp.7027.

Rael, J., Shelton, S., & Dayaye, R. (1995). Permeable barriers to remove benzene: candidate media evaluation. *Journal of Environmental Engineering*, *121*(5), 411-415.

Reeve, A. S., Siegel, D. I., & Glaser, P. H. (2001). Simulating dispersive mixing in large peatlands. *Journal of Hydrology*, *242*(1-2), 103-114. doi:10.1016/s0022-1694(00)00386-3.

Rezanezhad, F., Andersen, R., Pouliot, R., Price, J. S., Rochefort, L., & Graf, M. D. (2012). How fen vegetation structure affects the transport of oil sands process-affected waters. *Wetlands*, *32*(3), 557-570. doi:10.1007/s13157-012-0290-z.

Rezanezhad, F., Price, J. S., & Craig, J. R. (2012). The effects of dual porosity on transport and retardation in peat: A laboratory experiment. *Canadian Journal of Soil Science*, 92(5), 723-732. doi:10.4141/cjss2011-050.

Rezanezhad, F., Quinton, W. L., Price, J. S., Elrick, D., Elliot, T. R., & Heck, R. J. (2009). Examining the effect of pore size distribution and shape on flow through unsaturated peat using computed tomography. *Hydrology and Earth System Sciences*, 13(10), 1993–2002. doi:10.5194/hess-13-1993-2009

Rezanezhad, F., Quinton, W. L., Price, J. S., Elliot, T. R., Elrick, D., & Shook, K. R. (2010). Influence of pore size and geometry on peat unsaturated hydraulic conductivity computed from 3D computed tomography image analysis. *Hydrological processes*, *24*(21), 2983-2994. doi:10.1002/hyp.7709.

Rezanezhad, F., Price, J. S., Quinton, W. L., Lennartz, B., Milojevic, T., & Van Cappellen, P. (2016). Structure of peat soils and implications for water storage, flow and solute transport: A review update for geochemists. *Chemical Geology*, *429*, 75-84.

Rice, D. W., Grose, R. D., Michaelsen, J. C., Dooher, B. P., MacQueen, D. H., Cullen, S. J., ... & Marino, M. A. (1995). California leaking underground fuel tank (LUFT) historical case analyses. *California State Water Resources Control Board.*

Ritter, H. L., & Drake, L. C. (1945). Pressure porosimeter and determination of complete macropore-size distributions. Pressure porosimeter and determination of complete macropore-size distributions. *Industrial & Engineering Chemistry Analytical Edition*, *17*(12), 782-786.doi:10.1021/i560148a013.

Roberts, P. V., Goltz, M. N., & Mackay, D. M. (1986). A natural gradient experiment on solute transport in a sand aquifer: 3. Retardation estimates and mass balances for organic solutes. *Water Resources Research*, *22*(13), 2047-2058. doi:10.1029/wr022i013p02047.

Rochefort, L., Strack, M., Poulin, M., Price, J.S., and Lavoie, C. 2012. Northern Peatlands. In Wetland Habitats of North America: Ecology and Conservation Concerns. Edited by D.P. Batzer and A.H. Baldwin. University of California Press, Berkeley and Los Angeles, California. pp. 119–134.

Rogers, R. D., McFarlane, J. C., & Cross, A. J. (1980). Adsorption and desorption of benzene in two soils and montmorillonite clay. *Environmental science & technology*, *14*(4), 457-460. Rubio, A. D., Zalts, A., & El Hasi, C. D. (2008). Numerical solution of the advection–reaction–diffusion equation at different scales. *Environmental Modelling & Software*, *23*(1), 90-95. doi: 10.1016/j.envsoft.2007.05.009.

Rutherford, D. W., Chiou, C. T., & Kile, D. E. (1992). Influence of soil organic matter composition on the partition of organic compounds. *Environmental science & technology*, *26*(2), 336-340.doi:10.1021/es00026a014.

Sahni, A., Burger, J., & Blunt, M. (1998). Measurement of three phase relative permeability during gravity drainage using CT. In SPE/DOE Improved Oil Recovery Symposium. *Society of Petroleum Engineers*. doi:10.2118/39655-ms.

Salminen, J. M., Tuomi, P. M., Suortti, A. M., & Jørgensen, K. S. (2004). Potential for aerobic and anaerobic biodegradation of petroleum hydrocarbons in boreal subsurface. *Biodegradation*, *15*(1), 29-39. doi:10.1023/B:BIOD.0000009954.21526.e8.

Schlotzhauer, S. M., & Price, J. S. (1999). Soil water flow dynamics in a managed cutover peat field, Quebec: Field and laboratory investigations. *Water Resources Research*, *35*(12), 3675-3683. doi:10.1029/1999wr900126.

Schwarzenbach, R. P., & Westall, J. (1981). Transport of nonpolar organic compounds from surface water to groundwater. Laboratory sorption studies. *Environmental Science & Technology*, *15*(11), 1360-1367. doi:10.1021/es00093a009.

Seagren, E. A., & Becker, J. G. (2002). Review of natural attenuation of BTEX and MTBE in groundwater. *Practice periodical of hazardous, toxic, and radioactive waste management*, *6*(3), 156-172.

Seip, H. M., Alstad, J., Carlberg, G. E., Martinsen, K., & Skaane, R. (1986). Measurement of mobility of organic compounds in soils. Science of Total Environment *50*, 87-101.

Selucky, M. L., Chu, Y., Ruo, T., & Strausz, O. P. (1977). Chemical composition of Athabasca bitumen. *Fuel*, *56*(4), 369-381.Selucky, M. L., Chu, Y., Ruo, T. C., & Strausz, O. P. (1978). Chemical composition of Cold Lake bitumen. *Fuel*, *57*(1), 9-16. Shang, J., Flury, M., Harsh, J. B., & Zollars, R. L. (2008). Comparison of different methods to measure contact angles of soil colloids. *Journal of colloid and interface science*, *328*(2), 299-307.doi:10.1016/j.jcis.2008.09.039.

Siegel, D. I., & Glaser, P. H. (1987). Groundwater flow in a bog-fen complex, Lost River Peatland, northern Minnesota. *The Journal of Ecology*, 743-754.. doi:10.2307/226020.

Sigmund, P. M. & McCaffery, F. G. (1979). An Improved Unsteady-State Procedure for Determining the Relative-Permeability Characteristics of Heterogeneous Porous Media (includes associated papers 8028 and 8777). *Society of Petroleum Engineers Journal*, *19*(01), 15–28. doi:10.2118/6720-pa.

Simunek, J., Van Genuchten, M. T., Sejna, M. 2005. The HYDRUS-1D software package for simulating the one-dimensional movement of water, heat, and multiple solutes in variably-saturated media. University of California-Riverside Research Reports, 3, 1-240.

Smith, D. G., Bryson, C., Thompson, E. M., & Young, E. G. (1958). Chemical composition of the peat bogs of the maritime provinces. *Canadian Journal of Soil Science*, *38*(2), 122-129.doi:10.4141/cjss58-019.

Smith, L. C., MacDonald, G. M., Velichko, A. A., Beilman, D. W., Borisova, O. K., Frey, K. E., ... & Sheng, Y. (2004). Siberian peatlands a net carbon sink and global methane source since the early Holocene. *Science*, *303*(5656), 353-356. doi:10.1126/science.1090553.

Soga, K., Page, J. W. E., & Illangasekare, T. H. (2004). A review of NAPL source zone remediation efficiency and the mass flux approach. *Journal of Hazardous Materials*, 110(1-3), 13-27.

Sohrabi, M., Henderson, G. D., Tehrani, D. H., & Danesh, A. (2000). Visualisation of Oil Recovery by Water Alternating Gas (WAG) Injection Using High Pressure Micromodels - Water-Wet System. *SPE Annual Technical Conference and Exhibition*. doi:10.2118/63000-ms.

Stuart, B. J., Bowlen, G. F., & Kosson, D. S. (1991). Competivive sorption of benzene, toluene and the xylenes onto soil. *Environmental progress*, *10*(2), 104-109. Suarez, M. P., & Rifai, H. S. (1999). Biodegradation rates for fuel hydrocarbons and chlorinated solvents in groundwater. *Bioremediation Journal*, *3*(4), 337-362.doi:10.1080/10889869991219433.

Tallis, J. H. (1998). Growth and degradation of British and Irish blanket mires. *Environmental Reviews*, *6*(2), 81-122.doi:10.1139/er-6-2-81.

Tatalovich, M. E., Lee, K. Y., & Chrysikopoulos, C. V. (2000). Modeling the transport of contaminants originating from the dissolution of DNAPL pools in aquifers in the presence of dissolved humic substances. *Transport in Porous Media*, *38*(1-2), 93-115. doi:10.1023/A:1006674114600.

Thomson, N. R., Graham, D. N., & Farquhar, G. J. (1992). One-dimensional immiscible displacement experiments. *Journal of contaminant hydrology*, 10(3), 197-223.doi:10.1016/0169-7722(92)90061-i.

Thomson, N. R., Sykes, J. F., & Van Vliet, D. (1997). A numerical investigation into factors affecting gas and aqueous phase plumes in the subsurface. *Journal of Contaminant Hydrology*, *28*(1-2), 39-70. doi:10.1016/s0169-7722(96)00044-7.

Transportation Safety Board of Canada. (2004). Railway Investigation report R03T0064. Available from www.tsb.gc.ca/eng/rapports-reports/rail/2003/r03t0064/r03t0064.pdf [accessed 4 January 2017].

Transportation Safety Board of Canada. (2006). Railway Investigation Update R04Q0040. Available from http://www.tsb.gc.ca/eng/rapports-reports/rail/2004/r04q0040/r04q0040.asp [accessed 4 January 2017].

Transportation Safety Board of Canada. (2007). Pipeline Investigation Report P05H0044. Available from www.tsb.gc.ca/eng/rapports-reports/pipeline/2005/p05h0044/p05h0044.asp [accessed 4 January 2017].

Valat, B., Jouany, C., & Riviere, L. M. (1991). Characterization of the wetting properties of air-dried peats and composts. *Soil Science*, *152*(2), 100-107. doi:10.1097/00010694-199108000-00006.

Van Dijke, M. I. J., McDougall, S. R., & Sorbie, K. S. (2001). Three-phase capillary pressure and relative permeability relationships in mixed-wet systems. *Transport in Porous Media*, *44*(1), 1-32. doi:10.1023/A:1010773606657.

Van Geel, P. J., & Roy, S. D. (2002). A proposed model to include a residual NAPL saturation in a hysteretic capillary pressure–saturation relationship. *Journal of contaminant hydrology*, 58(1-2), 79-110. doi:10.1016/s0169-7722(02)00012-8.

Van Geel, P. J., & Sykes, J. F. (1994). Laboratory and model simulations of a LNAPL spill in a variably-saturated sand, 1. Laboratory experiment and image analysis techniques. *Journal of Contaminant Hydrology*, 17(1), 1-25. doi:10.1016/0169-7722(94)90075-2.

Van Genuchten, M. T., & Wagenet, R. J. (1989). Two-site/two-region models for pesticide transport and degradation: Theoretical development and analytical solutions. *Soil Science Society of America Journal*, *53*(5), 1303-1310. doi:10.2136/sssaj1989.03615995005300050001x.

Van Genuchten, M. T., & Wierenga, P. J. (1976). Mass transfer studies in sorbing porous media I. Analytical solutions 1. *Soil Science Society of America Journal*, *40*(4), 473-480. doi:10.2136/sssaj1976.03615995004000040011x.

Vitagliano, V., & Lyons, P. A. (1956). Diffusion coefficients for aqueous solutions of sodium chloride and barium chloride. *Journal of the American Chemical Society*, *78*(8), 1549-1552. doi:10.1021/ja01589a011.

Vitt, D. H., Halsey, L. A., Bauer, I. E., & Campbell, C. (2000). Spatial and temporal trends in carbon storage of peatlands of continental western Canada through the Holocene. *Canadian Journal of Earth Sciences*, 37(5), 683-693.

Vowles, P. D., & Mantoura, R. F. C. (1987). Sediment-water partition coefficients and HPLC retention factors of aromatic hydrocarbons. *Chemosphere*, *16*(1), 109-116. Waksman, S. A., & Smith, H. W. (1934). Transformation of the Methoxyl Group in Lignin in the Process of Decomposition of Organic Residues by Microörganisms1. *Journal of the American Chemical Society*, *56*(5), 1225-1229.

Walton, B. T., Hendricks, M. S., Anderson, T. A., Griest, W. H., Merriweather, R., Beauchamp, J. J., & Francis, C. W. (1992). Soil sorption of volatile and semivolatile organic compounds in a mixture. *Journal of environmental quality*, *21*(4), 552-558. Weber, T. K., Iden, S. C., & Durner, W. (2017). Unsaturated hydraulic properties of *Sphagnum* moss and peat reveal trimodal pore-size distributions. *Water Resources Research*, *53*(1), 415-434.doi: 10.1002/2016WR019707.

Westlake, D. W. S., Jobson, A., Phillippe, R., & Cook, F. D. (1974). Biodegradability and crude oil composition. *Canadian Journal of Microbiology*, *20*(7), 915-928. Whittington, P. N., & Price, J. S. (2006). The effects of water table draw-down (as a surrogate for climate change) on the hydrology of a fen peatland, Canada. *Hydrological Processes*, *20*(17), 3589-3600. doi:10.1002/hyp.6376.

Wilkins, M. D., Abriola, L. M., & Pennell, K. D. (1995). An experimental investigation of rate-limited nonaqueous phase liquid volatilization in unsaturated porous media: Steady state mass transfer. *Water Resources Research*, *31*(9), 2159-2172.doi:10.1029/95wr01677.

Williams, S. D., Ladd, D. E., & Farmer, J. J. (2006). *Fate and transport of petroleum hydrocarbons in soil and ground water at Big South Fork National River and Recreation Area, Tennessee and Kentucky, 2002-2003*. US Department of the Interior, US Geological Survey.

Witherspoon, P. A., & Bonoli, L. (1969). Correlation of diffusion coefficients for paraffin, aromatic, and cycloparaffin hydrocarbons in water. *Industrial & Engineering Chemistry Fundamentals*, *8*(3), 589-591. doi:10.1021/i160031a038.

Wolff, R. G. (1982). *Physical properties of rocks; porosity, permeability, distribution coefficients, and dispersivity* (No. 82-166). US Geological Survey,.

World Health Organization. (2004). *Guidelines for drinking-water quality: recommendations* (Vol. 1). World Health Organization.

Xing, B. (1998). Reaction of toluene with soil organic matter. *Journal of Environmental Science & Health Part B*, *33*(3), 293-305. Xing, B., McGill, W. B., & Dudas, M. J. (1994). Cross-correlation of polarity curves to predict partition coefficients of nonionic organic contaminants. *Environmental science & technology*, *28*(11), 1929-1933. Yang, C., Wang, Z., Yang, Z., Hollebone, B., Brown, C. E., Landriault, M., & Fieldhouse, B. (2011). Chemical fingerprints of Alberta oil sands and related petroleum products. *Environmental Forensics*, *12*(2), 173-188. Yerushalmi, L., Manuel, M. F., & Guiot, S. R. (1999). Biodegradation of gasoline and BTEX in a microaerophilic biobarrier. *Biodegradation*, *10*(5), 341-352.

Yonebayashi, K., Pechayapisit, J., Vijarnsorn, P., Zahari, A. B., & Kyuma, K. (1994). Chemical alterations of tropical peat soils determined by Waksman's proximate analysis and properties of humic acids. *Soil Science and Plant Nutrition*, *40*(3), 435-444. doi:10.1080/00380768.1994.10413321.

Yuan, Y., & Lee, T.R. (2013). Contact Angle and Wetting Properties. In Surface Science Techniques. Edited by G. Bracco and B. Holst. Springer Berlin Heidelberg, Berlin, Heidelberg. pp. 3–34. doi:10.1007/978-3-642-34243-1_1.

Zaccone, C., Miano, T. M., & Shotyk, W. (2007). Qualitative comparison between raw peat and related humic acids in an ombrotrophic bog profile. *Organic Geochemistry*, *38*(1), 151-160. doi:10.1016/j.orggeochem.2006.06.023.

Zoltai, S.C., & Kershaw, G.P. (1995). Large volume oil spill on land surface. The Vozey Oil Field, Russia. In 18th Arctic and Marine Oil Spill Program (AMOP) Technical Seminar Environmental Protection Service. Technology Development Directorate, Environment Canada, Ottawa. ON. June 14 - 16, 1995, Edmonton Alberta. Vol 2. pp. 1177-1186.

Zoltai, S.C., & Vitt, D.H. (1995). Canadian wetlands: Environmental gradients and classification. In Classification and Inventory of the World's Wetlands. Edited by C.M. Finlayson and A.G. van der Valk. Springer Netherlands, Dordrecht. pp. 131–137. doi:10.1007/978-94-011-0427-2_11.

Zytner, R. G. (1994). Sorption of benzene, toluene, ethylbenzene and xylenes to various media. *Journal of Hazardous Materials*, *38*(1), 113-126.doi:10.1016/0304-3894(94)00027-1.

Zytner, R., Biswas, N., & Bewtra, J. K. (1989). Adsorption and desorption of perchloroethylene in soils, peat moss, and granular activated carbon. *Canadian Journal of Civil Engineering*, *16*(6), 798-806. doi:10.1139/l89-123.